To the Graduate Council:

I am submitting herewith a dissertation written by Ali Hedayatpour entitled "Transient Two-Phase Flow of Cryogenic Fluid in A Vertical Transfer Line During the Cooldown Process." I have examined the final copy of this dissertation for form and content and recommend that it be accepted in partial fulfillment of the requirements for the degree of Doctor of Philosophy with a major in Mechanical Engineering.

Basil N. Antar, Major Professor

We have read this dissertation
and recommend its acceptance:

Accepted for the Council:

Vice Provost
and Dean of the Graduate School

TRANSIENT TWO-PHASE FLOW OF CRYOGENIC FLUID IN A VERTICAL TRANSFER LINE DURING THE COOLDOWN PROCESS

A Dissertation

Presented for the

Doctor of Philosophy

Degree

The University of Tennessee, Knoxville

Ali Hedayatpour

August 1990

Dedicated to My Family for Their Love and Support

ACKNOWLEDGMENTS

The author is greatly indebted to his major advisor, Dr. Basil Antar, who introduced the area of two-phase flow and numerical heat transfer, as well as the physical understanding of the subject. His supervision and guidance at every stage made this work possible.

The author wishes to express his gratitude to Dr. Frank Collins, Dr. Firouz Sharokhi and Dr. Robert Young, whose academic work benefited the author in the course of this study. In addition, the author would like to thank the Center for Advanced Space Propulsion, particularly Dr. George Garrison, director of the center, for providing financial support throughout this work.

Also, the author would like to thank Dr. M. Kawaji of The University of Toronto for helpful discussions and valuable suggestions.

The author acknowledges his appreciation to the staff of The UTSI library, particularly Mrs. Mary Lo and Mrs. Margorie Joseph, for their assistance.

The author would also like to thank Mrs. Linda Williams for her immeasurable effort and assistance with typing of this work.

The author wishes to recognize and express his gratitude to all former teachers, especially the first teacher, his late father, for inspiration and encouragement to learn.

The author would like to thank his mother, sisters, and brother for their love, support, and prayers throughout graduate school.

To his wife Marsha, goes a special thanks and gratitude for her assistance in proof reading of the rough draft manuscript. She was the source of support, encouragement and patience throughout the author's years in school. Without her this work could not have been completed.

ABSTRACT

The analytical and numerical modeling for prediction of the thermo-fluid parameters of the cooldown process of a vertical tube carrying cryogenic liquid are presented.

Formulation of the problem is based on the flow patterns observed in the experimental studies. In this model the flow field consists of four distinct regions of fully liquid, inverted annular film boiling, dispersed flow film boiling, and fully vapor. For the fully liquid and fully vapor regions, the one-dimensional form of the mass, momentum, and energy conservation equations are used. For the two-phase regions, the volume-averaged, one-dimensional two-fluid model conservation equations are applied. In addition, a one-dimensional energy equation is formulated to determine the tube wall history.

The numerical approximations are based on the finite difference technique. Calculation for inverted annular flow are based on a semi-implicit model while computations for the wall, fully liquid, and dispersed flow regions are performed explicitly. Comparison of calculated results with experimental data for water and liquid nitrogen are presented.

TABLE OF CONTENTS

LIST OF FIGURES

NOMENCLATURE

A = cross sectional area of the flow channel (ft^2)

A_D = projected area of a drop

A_i''' = interfacial area per unit volume

A_w = cross sectional area of the flow channel

C_D = drag coefficient

c_p = specific heat capacity ($btu/^oFlb$)

c_{p_l} = specific heat capacity of liquid

c_{p_v} = specific heat capacity of vapor

c_{p_w} = specific heat capacity of flow channel wall

C_2 = heat transfer coefficient parameter

D = diameter of the flow channel (ft)

D_d = droplet diameter

D_H = hydraulic diameter

D_i = inner diameter of the tubular flow channel

D_{max} = maximum droplet diameter

D_o = outer diameter of the flow channel

D_{max}^e = maximum entrainable diameter of drops

D_{max}^s = maximum stable diameter of drops

D_t = inside diameter of the flow channel

D_{20} = area-averaged, population-mean diameter of drops

D_{30} = volume-averaged, population-mean diameter of drops

D_{32} = Sauter mean diameter of a droplet population

F_D = drag force defined by equation (2-80)

F_{ij} = view factor for radiation model

F_{red} = interfacial friction reduction factor

F_1 = liquid heating flux parameter for inverted annular flow model

F_2 = droplet heating flux parameter for dispersed flow model

$G_l = \rho_l \alpha_l u_l$

$G_v = \rho_v \alpha_v u_v$

$H_l = \rho_l \alpha_l h_l$

$H_v = \rho_v \alpha_v h_v$

j_0 = Bessel function of the first kind of zeroth order

j_1 = Bessel function of the first kind of first order

$M_l = \rho_l \alpha_l$

$M_v = \rho_v \alpha_v$

N_d = number density of drops

Nu = Nusselt number

Nu_1, Nu_2 = Nusselt number for heat transfer between parallel plates

Nu^* = Nusselt number for only one side heated or cooled and other side insulated

P_i = inner perimeter of tubular flow channel (ft)

p_l = pressure of the liquid phase (lbf/in^2)

Δp_{li} = difference between the interfacial pressure and the liquid pressure

Δp_{lv} = difference between the vapor and the liquid pressure

Pr = Prandtl number

Δp_{st} = pressure increase due to surface tension

p_v = vapor pressure

Δp_{vi} = difference between the interfacial pressure and the vapor pressure

Δp_{vt} = pressure increase due to vapor thrust

P_w = wetted perimeter of the flow channel

R = radius of the flow channel (ft)

R_r = radius of curvature in the transverse section

R_z = radius of curvature in the axial section

R_l = radius of the liquid column

Re = Reynolds number

R_d = mean diameter of droplet population

R_d, R_v, R_w = parameters for the radiation model

T = temperature (^oF)

T_v = vapor temperature

T_l = vapor temperature

T_o = average temperature of liquid at the quench front or initial temperature of drops at generation

T_{sat} = saturation temperature

T_v = vapor temperature

T_w = wall temperature

u_d = droplet velocity

u_v = vapor velocity

u = velocity (ft/sec)

u_l = liquid velocity

u_i = interface velocity

u_{max} = maximum velocity

V = volume fraction of drop size distribution

V_v = vapor velocity in the direction normal to the liquid-vapor interface

V_{thr} = velocity contributing to the vapor thrust

w = drop size distribution parameter defined by equation (2-66)

We = Weber number

We_c = critical Weber number

z = axial coordinate

z^+ = dimensionless parameter defined by equation (2-32)

z_o = distance from the test section inlet to the point of zero coolant quality

Δz = unit axial length or distance between axial nodes

a = drop size distribution parameter

a_v = absorption coefficient of vapor

a_l = absorption coefficient of liquid

f = friction factor

f_i = interfacial friction factor

g = local acceleration of gravity

h = enthalpy (btu/lb)

h_c = convective heat transfer coefficient

h_{fg} = latent heat of vaporization

h_v = vapor enthalpy

$h_{v,sat}$ = saturation enthalpy of vapor

h_l = liquid enthalpy

$h_{l,sat}$ = saturation enthalpy of liquid

h_{nb} = heat transfer coefficient for nucleate boiling $(btu/ft^2 - F^o - sec)$

h_v = vapor enthalpy

h_{wd} = heat transfer coefficient for wall-drop interaction heat transfer

k_f = thermal conductivity evaluated at the film temperature $(btu/ft - F^o - sec)$

k_v = thermal conductivity of vapor

k_l = thermal conductivity of liquid

k_w = thermal conductivity of wall

m_l''' = interfacial mass transfer rate $(lbm/sec - ft^3)$

n = number fraction of drop size distribution

q'' = heat flux (btu/ft^2)

q''' = heat transfer rate per unit volume (btu/ft^3)

q''_{evap} = vaporization heat flux

q''_{lH} = droplet heating flux

q''_{vd} = vapor to drop convective heat flux

q''_{d} = heat flux received by drops

$q''_{vd}{}^{r}$ = vapor to drop radiation heat flux

q''_{CHF} = critical heat flux

q''_{l} = total heat flux received by liquid

q''_{lH} = liquid heating flux

q''_{rad} = wall to liquid radiation heat flux

q''_{vl} = vapor to liquid convective heat flux

q''_{v} = heat flux received by vapor

q''_{w} = wall to fluid heat flux

q''_{wd} = heat flux due to wall-drop interaction

$q''_{wd}{}^{r}$ = wall to drop radiation heat flux

q''_{wv} = wall to vapor convective heat flux

$q''_{wv}{}^{r}$ = wall to vapor radiation heat flux

r = radial coordinate

t = time (sec)

Δt = time step size

y = parameter used in log-normal distribution function defined by equation (2-66)

Greek Letters

Θ = dimensionless temperature

Θ_{av} = dimensionless average temperature

α = volume fraction

α_v = volume fraction of vapor

α_l = volume fraction of liquid

β = drop size distribution parameter

β_n = roots of Bessel function

γ = fraction of heat used to generate vapor below the quench front

δ = vapor film thickness (ft)

ϵ_l = liquid emissivity

ϵ_v = vapor emissivity

ϵ_w = wall emissivity

η_l^e = unnormalized volume fraction of entrainable drops

η_l^* = normalization factor for the drop size distribution

μ_v = vapor viscosity $(lb/ft - sec)$

μ_l = liquid viscosity

ρ_v = vapor density (lb/ft^3)

ρ_l = liquid density

ρ_w = density of the flow channel

σ = surface tension coefficient (lb/sec^2)

σ^r = Stefan-Boltzmann constant

τ''' = shear stress per unit volume

τ_d''' = vapor-drop shear per unit volume

τ_i''' = interfacial shear per unit volume

τ_{wv}''' = wall-vapor shear per unit volume

Ω = influence coefficient for heat transfer between parallel plates

Subscript

z = axial direction

$conv$ = convection

c = convection

$evap$ = evaporization

i = vapor-liquid interface

j = axial node

l = liquid

r = radial direction

sat = saturation

v = vapor

w = wall

Superscripts

N = time step

n = iteration step

$''$ = quantity per unit area

$'''$ = quantity per unit volume

CHAPTER I

INTRODUCTION

In the future, cryogenic refueling of spase-based vehicles and satellites is one of the important operations for long term space missions. To minimize losses during refueling, the temperature of the transfer line must be lowered to a point at which the cryogen passing through stays in the liquid phase.

When cryogenic liquid enters into the transfer line, the cooldown process starts with the production of vapor, two-phase flow, and reduction of the line temperature. This process continues until the line temperature drops to the boiling temperature of the liquid. During the process, the flow regimes inside the line change continuously with time; and consequently, the heat transfer and fluid flow characteristics are strongly time dependent.

In order to develop and design the transfer line and storage systems, parameters such as the duration of cooldown and the amount of the coolant must be known. To achieve this, a comprehensive study of the cooldown process in 1 g and in microgravity is necessary. The present work deals with the 1 g environment. The following sections review the experimental and theoretical investigations of the cooldown and related two-phase flows, particularly when the liquid passes through a vertical tube.

1.1 Cooldown Studies

Cooldown studies on cryogenic transfer lines have been conducted that consider different aspects of the process such as estimation of cooldown time, amount of coolant, and physical characteristics of the flow.

Burke et al [1] studied the problem of pressurized line cooldown, both exper-

imentally and analytically. They constructed a small pressurized transfer system to investigate the physical process involved in line cooldown and to determine the effects of various system variables on line cooldown time. An analysis was developed from thermodynamic principles so that the test data could be correlated and the range of their experimental results extended. The transfer line, was fabricated from stainless steel tube (2 inch OD, 0.065 inch wall thickness). Liquid nitrogen was used as a test fluid. The effect of the following four variables were studied:

1) Total pressure at the line entrance

2) Line heat leak

3) Line pressure drop

4) Line mass

The driving pressures ranged from 40 to 80 psi. The following variables were measured during the test:

1) Fluid static pressures along the length of the line and differential pressures across line components

2) Line wall and fluid temperature along the length of the line

3) Inlet liquid flow to the line, and gas and liquid flow out of the line.

The proposed physical model of the pressurized cooldown process based on the observations was as follows: When the line inlet valve was opened, a liquid front quickly advanced into the line. This front initially overshot its "equilibrium" position, and pressure surges resulted. The front then proceeded in a relatively uniform manner down the line at a controlled rate. The arrival of single-phase liquid at the end of the line corresponded closely with the attainment of equilibrium wall temperature. This physical model served as a guide in the development of an analytical solution of line cooldown time. It should be emphasized that the above model can be applied most accurately to rather long, thin-wall, transfer lines. The

above method assumed an infinite heat transfer coefficient between the fluid and tube wall, and hence tended to overestimate the percentage cooldown. The analysis was applied to a 175 foot test configuration. The effect of ambient heat leak, which was a time function, was seen to be more pronounced at low storage tank pressures where the cooldown time was relatively long.

Jacobs [2] estimated the amounts of cryogenic liquid required to cool cryogenic equipment to its operating condition. The purpose of Jacob's study was :

1) to derive relations for making these estimates

2) to compute the cooldown requirements for commonly used liquid (helium, hydrogen, nitrogen, and oxygen) with some commonly used materials (stainless steel, copper, and aluminum)

(3) to present the results of the computations in a readily usable graphical form.

He considered two liquid requirements:

1) The minimum liquid requirement - the liquid required to cool a system to its operating condition if all of the refrigeration available in the liquid was utilized.

2) The maximum liquid requirement - the liquid required to cool a system to its operating condition if only the refrigeration available in the latent heat of vaporization of the liquid was utilized.

Drake et al [3] developed a simplified line cooldown model which permitted them to predict line cooldown time. The assumption was that cooldown has occurred when saturated liquid reaches the end of the line. The fluid properties of the liquid in the line was obtained by averaging the properties at the line inlet and outlet. The average mass flow rate was estimated from compressible flow theory, provided the major flow restrictions in the system were located near the end of the line. For this case, the combined line and flow restrictions could be replaced

by an equivalent single flow restriction. Ambient heat flux during cooldown was a function of the variation in the pipe wall temperature. To simplify the evaluation of this factor, which was generally small compared to the exit gas heat flux, they assumed that during cooldown the average ambient heat flux equaled one-half the total heat flux after cooldown. They applied this model to the vertical line configuration. In order to use this model, one must know the average pressure differential across the line during cooldown.

A later analysis by Steward [4] comprises studies of surging in transfer lines. This method enables calculation of cooldown time of vacuum insulated lines using an iterative method. Steward conducted a series of experiments with instrumented transfer lines and analyzed the cooldown process in some detail. His previous analysis [5], based on a simplified model, predicted the nitrogen pressure surges observed early in the experimental program; however, an analysis was required which would more accurately represent the physical process. The detailed computational system was supplemented by a highly simplified method for estimating cooldown time. To obtain the inlet liquid condition designated as "subcooled", the tests were started within several seconds after pressurization. Tests were made with constant inlet pressure and temperature. The inlet flow rate, stream temperatures, and pressures were recorded continuously from the time the valve was first opened until the transfer line reached stable operating temperature. The primary assumptions in developing the equations were; 1) the single phase fluid or homogenous two-phase mixture; 2) thermal and mechanical equilibrium between liquid and vapor; 3) one-dimensional flow.

The fluid mechanics of the approximate model was further simplified by assuming that all of the heat transfer, rather than being distributed down the pipe, took place only at the interface. In addition, it was assumed that there was a dis-

continuity in the density, velocity, temperature at that point, and that the vapor stream was adiabatic. These assumptions probably limited the model to relatively long pipes. This model supplied a heat transfer area which is simply taken to be the area of warm pipe in contact with liquid, (plus the added amount due to entrainment of liquid downstream with the vapor). Other assumptions of the approximate model were as follows; 1) the horizontal transfer line was of constant cross-section area, with an initial temperature; 2) Quasi-steady-state Fanno flow for the vapor stream. The modes of heat transfer considered were: 1) forced-convection heat transfer to non boiling subcooled liquid; 2) nucleate boiling of saturated liquid; 3) surface boiling of subcooled liquid; 4) film boiling of saturated liquid; 5) forced-convection heat transfer to vapor.

Both the experiment and the computer program showed that a small amount of precooling could cause larger peaks. The model produced smaller surges with shorter periods for liquid hydrogen than for liquid nitrogen. The agreement obtained using this model would seem to indicate that driving pressure, inlet liquid temperature, fluid, pipe length and diameter, and pipe precooling were some of the most important considerations. On the other hand, pipe wall thickness, heat capacity, or external heat peak were not believed to have a great effect on the peak surge because of the fact that very little change in the pipe temperature occurred in the few seconds of one surge, although they could contribute to the total cooldown time. The effect of transfer line diameter was not clear. As mentioned earlier, the model is probably limited to long pipes.

Based on Steward's results, one of the most effective means of reducing surging during the cooldown would be warming of the liquid supply nearly to the saturation point at the driving pressure. In addition, experimental and computational results suggested that the following factors could be expected to bring about or aggravate

surging in long cryogenic transfer lines; 1) a high degree of subcooling of the inlet liquid; 2) long transfer lines.

Bronson, et al [6] observed a "cold front" type of cooldown in their transfer system used for supplying liquid hydrogen to nuclear rocket engines. One of the main concerns in this horizontal system of 8 and 10 inch diameter stainless steel tubes was that stratified flow should not be allowed to develop. That is, flow conditions must not be such that the liquid could flow along the bottom of the pipe with relatively warm gas above.

For the case of the short transfer lines, Sirinivasan [7] suggested an analytical model with two-phase flow persisting over the entire length of the tube during cooldown. Chi [8] carried out an experimental study on the cooldown of aluminum test sections by liquid hydrogen. The test section consisted of several 26-in. aluminum tubes of 0.5, 1, and 2 in. OD with 3/16 in. ID. The data showed that film boiling occurred approximately 90 percent of the cooldown time. The dominant mechanism of observed two-phase flow was mist flow. A cooldown model was proposed and equations were derived for the prediction of cooldown wall and fluid temperatures at any time and location. The calculated wall temperature histories correlated reasonably well with experimental data.

1.2 Two-phase Flow

Two-phase flow is characterized by the existence of interfaces between phases and discontinuities of properties associated with them. The gas and liquid phase may have different geometrical configurations when flowing simultaneously. Such configurations are usually termed two-phase flow pattern or flow regimes. The internal structures of flow are classified by two-phase flow regimes. Various transfer mechanisms between the mixture and wall, as well as between phases strongly

depend on these two-flow regimes. This leads to the use of regime dependent constitutive equations and correlations together with appropriate flow regime transition criteria.

A change of flow pattern usually means a change in the mode of transport of momentum or heat. Therefore, the pattern is a very important subject of study and a great deal of work has been done to determine characteristics of various patterns and the boundaries between the regimes.

A variety of flow patterns, ranging from vapor bubbles in a continuous liquid medium to liquid droplets in a continuous vapor medium, occur with saturated boiling in forced flow. These flow patterns are distinguished either by fundamental differences in the transfer process (phenomenological description) or by characteristic geometric distributions of various phases (visual description). The visual description does not always have associated with it a change in the basic transfer mechanism of momentum, heat, or matter, and vice versa. Moreover, the transition region from one flow pattern to the next is often unstable, making precise definition of the range of the patterns difficult. Factors which can affect the beginning of a flow pattern regime are: (1) inlet conditions, (2) pipe dimensions geometry and inclination, (3) flow rate, (4) fluid properties, and (5) method in which the individual phases are introduced into the channel. Since the present work is related to the cooldown of a vertical transfer line, and because of the importance and role of two-phase flow in this process, previous works related in this area will be reviewed.

1.3 Two-phase Flow in a Vertical Tube

Investigations concerning flow pattern, and thermo-fluid characteristics of two-phase flow in a vertical tube have been carried out by several researchers. The most fundamental and rigorous works were done by Laverty and Rhosenow [9], Forslund

and Rhosenow [10], and Kawaji and Banerjee [12]. In Kawaji and Banerjee's work, water was considered as a working fluid, while in the other researcher's work, liquid nitrogen was used. In the following, each of these works is briefly discussed.

Laverty and Rhosenow [9] studied film boiling of saturated nitrogen flowing upward through a uniformly heated tube. Analysis of experimentally determined tube wall temperature distributions showed that a significant amount of vapor superheat was present throughout the film-boiling process. The specific study configuration was a uniformly heated tube with vertical flow upward through the tube and with pure saturated liquid entering. The visual test section was a pyrex tube (0.512 in. od, 0.417 in. id) internally coated with a transparent electrical conducting coating. The quantitative test section was a 304 stainless tube (0.375-in-od, 0.319-in-id) which was 47.8 in. long. In both of these, liquid nitrogen was employed as the test liquid in tubes heated electrically by alternating current. The experimental program consisted of two phases. The objective of the first phase was to determine qualitatively the characteristics of the two-phase flow regimes which occurred as a result of the film-boiling process. The second phase of the experimental program was devoted to quantitative measurement of the film-boiling heat transfer coefficient. Analysis of the experimental data followed in order to determine the mechanisms through which heat was carried to the two-phase mixture and by which evaporation of the liquid takes place. From visual study it was determined that there were basically two flow regimes which occurred. At the beginning of the heated section, where the vapor fraction was small, the flow was annular with the liquid in the center and the vapor in the annulus. Because of the large velocity increase caused by the generation of low-density vapor, the drag force on the liquid core increased at greater tube lengths to the point that the core was torn apart into filaments and droplets of liquid. As the breakup continued,

the flow went through a somewhat gradual transition to a dispersed flow regime in which small droplets and filaments of liquid were carried along in a vapor matrix. In conclusion, the results obtained from the analysis and experimental data for nitrogen are summarized as follows:

1) For film boiling of saturated liquid flowing upward through a uniformly heated vertical tube, there were two basic regimes: Near the inlet the flow was annular with the liquid in the core and vapor in the annulus; at higher vapor fractions the core was broken up to give a dispersed flow regime in which droplets and filaments were carried along in a vapor matrix.

2) In most cases, the breakup of annular flow was gradual and tube wall temperature reached a maximum in the vicinity of the transition; but at mass flows greater than about 180,000 $lbm/hr - ft^2$, with high heat fluxes, there was a depression of wall temperature following the maximum which indicated that a critical Weber number might be involved at which the breakup began suddenly.

3) Once transition had proceeded to the degree that drops were relatively uniformly dispersed, the heat transfer might be considered to be a two-step process in which all of the heat from the wall was transferred to the vapor and heat was transferred from the vapor to the liquid.

(a) An equation was given for the heat-transfer coefficient between the wall and the vapor.

(b) Evaporation rate of the liquid was controlled by drop size, vapor velocity and acceleration, and vapor temperature.

(c) Because the evaporation heat-transfer coefficient was not large compared to the wall-to-vapor coefficient, a significant amount of vapor superheat was presented, making it difficult to obtain a simple expression for the overall heat-transfer coefficient.

Investigations by Forslund and Rohsenow [10], extended Laverty's work by including the effects of droplet breakup, "Leidenfrost" heat transfer from the wall to the droplets, and modified the drag coefficients for accelerating droplets. Measurements were also made to verify the existence of the substantial amount of vapor superheat in the presence of liquid droplets, as predicted by the analysis. Three, 8-ft long, stainless-steel test sections (0.228, 0.323, and 0.462 in. ID) and one 4 ft long (0.323 in. ID) were used for the experimental tests. To verify the single-phase correlation for heat transfer to super heat vapor, a series of tests were performed only in the 0.323 in–dia, 4-ft-long tube. The observations of photographs suggested that droplet size was primarily a function of heat flux. Since the acceleration of the vapor was a function of heat flux and relatively independent of the mass flux, the foregoing observation suggested that droplet size may be determined by the rate of vapor acceleration. During the course of the calculations, droplet size was obtained along the length. They concluded:

1) The large departure from thermal equilibrium in dispersed flow film boiling was confirmed in this study.

2) Heat transfer tests yielded film boiling and superheating heat transfer coefficients based on equilibrium conditions that were much lower than single-phase heat transfer coefficients based on an equivalent flow rate of pure vapor. When it was assumed that the liquid played no role in the heat transfer at the tube wall, an appropriate single-phase heat transfer correlation was applied to the measured heat transfer rate and tube wall temperature, and significant amounts of vapor superheat (hence a reduction in the amount of vapor generated) resulted.

3) An additional amount of heat transferred directly to the droplets at the wall was important at low qualities and high mass velocities.

4) The droplet breakup process along the tube was governed by a critical

Weber number criterion which allowed an average droplet size ($We_{critical} = 7.5$).

5) The departure from equilibrium was mainly dependent on the mass flux, and to a smaller degree on the heat flux.

An experimental and theoretical analysis was performed by Kawaji and Banerjee [11,12] in the study of bottom reflooding of a heated vertical tube. The test section was made of 3.66 m Inconel tube with 14.3-mm-id. and 0.8-mm wall thickness. It was resistance heated by a manually adjustable d-c source. To avoid any ambiguity regarding the calculation of the transient values of the heat flux to the fluid and to facilitate these calculations (as well as the installation of the thermocouples), the test section was left uninsulated. Simultaneous void fraction and wall temperature measurements were made during the bottom-reflooding of the vertical Inconel tube under constant injection rates at different heights of the tube under various initial and boundary conditions. To support interpretation of these data, flow regime visualization experiments were also conducted by reflooding a heated quartz tube.

In the flow visualization experiments, a vertical 1.5 m quartz tube externally heated with a gas burner over a length of 0.5 m was quenched by injecting subcooled water from the bottom. Flow patterns occurring under constant inlet flow conditions were recorded with a high speed movie camera.

In constant-injection reflood, two distinct flow regimes were possible near the quench front. If the coolant was injected rapidly and remained subcooled at the quench front, inverted annular flow occurred in which the liquid column extended above the quench front, separated from the wall surface by a thin vapor film. Heat transfer rates were expected to be quite high in this region, but would decrease significantly with height as the vapor film became thicker.

On the other hand, if the coolant was injected slowly and became saturated

below the quench front, the flow changed to an annular droplet flow regime. With a short annular flow region, periodic bursts of vapor occurred in the boiling zone followed by upward ejection of liquid. While bursts were observed in the flow visualization experiment, no quantitative measurements were made. The ejected liquid elongated into filaments that eventually broke up into fragments of various sizes and shapes. The filaments and fragments would collide against the wall or with one another and shatter into smaller droplets. Small droplets were entrained upstream and continued to flow upward, but large fragments tended to fall back and accumulated in the boiling zone until another burst of vapor occurred and the process was repeated.

Whenever the wave crests reached the quench front, sputtering occurred and the quench front advanced incrementally. The droplets formed during sputtering were either entrained by vapor or fell down. This appeared to be a different mechanism from what they observed for a shorter annular flow region. In either case, the unquenched region was entirely in the dispersed flow regime and the quench rate was much lower than in the inverted annular flow case. In summary, the flow regimes identified above the quench front in constant-injection, high reflooding-rate tests were inverted annular, transition, and dispersed flow. Chordal-average void fraction of 10-30 percent, 30-70 percent, and 70-90 percent were typical of the three flow regimes, respectively. In constant-injection, low reflooding-rate tests, annular droplet flow and dispersed flow regimes existed below and above the quench front, respectively. The void fractions were above 80 percent in both flow regimes.

Also, they formulated a transient, one-dimensional two-fluid model to simulate the heat transfer and fluid flow characteristics of the inverted annular film boiling regime. The mathematical model was derived from the general two-field conservation equations, and its structure was examined. Their model considered

an interphase momentum interaction due to the vapor thrust and surface tension as well as the interfacial friction. Kawaji also analyzed the linear stability of the two-fluid equation system that he used. His analysis indicated that the governing equations were stable to short-wavelength disturbances and that the growth of long-wavelength instabilities would result in transition to a dispersed flow regime. The length of the most unstable waves was also derived in the analysis and agreed well with the available data. For dispersed flow, the system was predicted to become unstable if the Weber number exceeded a critical value of 8.

An expression for the wavelength of the most unstable interfacial waves in inverted annular flow was also obtained from the dispersion relation. The expression was successful in predicting the interfacial wave data obtained by De Jarlais [21] for adiabatic, inverted annular flow in a glass tube.

1.4 Objective

In most of the cooldown studies discussed in the above sections, either enthalpy change of fluid alone or forced convection heat transfer coefficients based on vapor properties were considered to evaluate heat transfer from pipe to fluid. However, it should be noted that nearly 85-90 percent of the cooldown to cryogenic temperature is due to film boiling of liquid in the tube. Sirinvansan [7] and Chi [8] considered the importance of film boiling, but their analysis was for a short cryogenic transfer line and because of over simplification, their approach is not suitable for the present study.

Since the film boiling is the dominate mechanism during the cooldown process, and because of the important role of two-phase phenomena in this process, the objectives of the present work are:

i) mathematical formulation of the problem, based on the observed flow pat-

tern, and consideration of the possible heat transfer mechanisms for each flow regime; and analysis of the two-phase regions utilizing the two-fluid model.

ii) the development of a code to predict the thermo-fluid parameters of the cooldown process of an open-to-air vertical tube carrying cryogenic fluid.

CHAPTER II

THEORETICAL ANALYSIS

2.1 Model

Formulation of the cooldown process in the present work is based on the flow pattern observed in past visual experiments. The flow pattern inside a vertical tube, as illustrated in figure (2-1), consists of liquid, two-phase, and vapor regions. For liquid nitrogen, the flow pattern observed by Laverty and Rohsenow [9], is similar to the one shown in figure (2-1a) in which the two-phase regions are Inverted Annular Film Boiling (IAFB) and Dispersed Flow Film Boiling (DFFB). Therefore, a model containing a flow field with four distinct regions (fully liquid, inverted annular film boiling, dispersed flow film boiling, and fully vapor) is considered. The conservation equations are one-dimensional for fully liquid and fully vapor regions, while for the two-phase region, based on the two-fluid model, one-dimensional, volume-averaged conservation equations are considered. In addition, to calculate the tube wall temperature history, a one-dimensional energy equation is formulated. In the following sections, each subject related to the analysis of the model will be discussed.

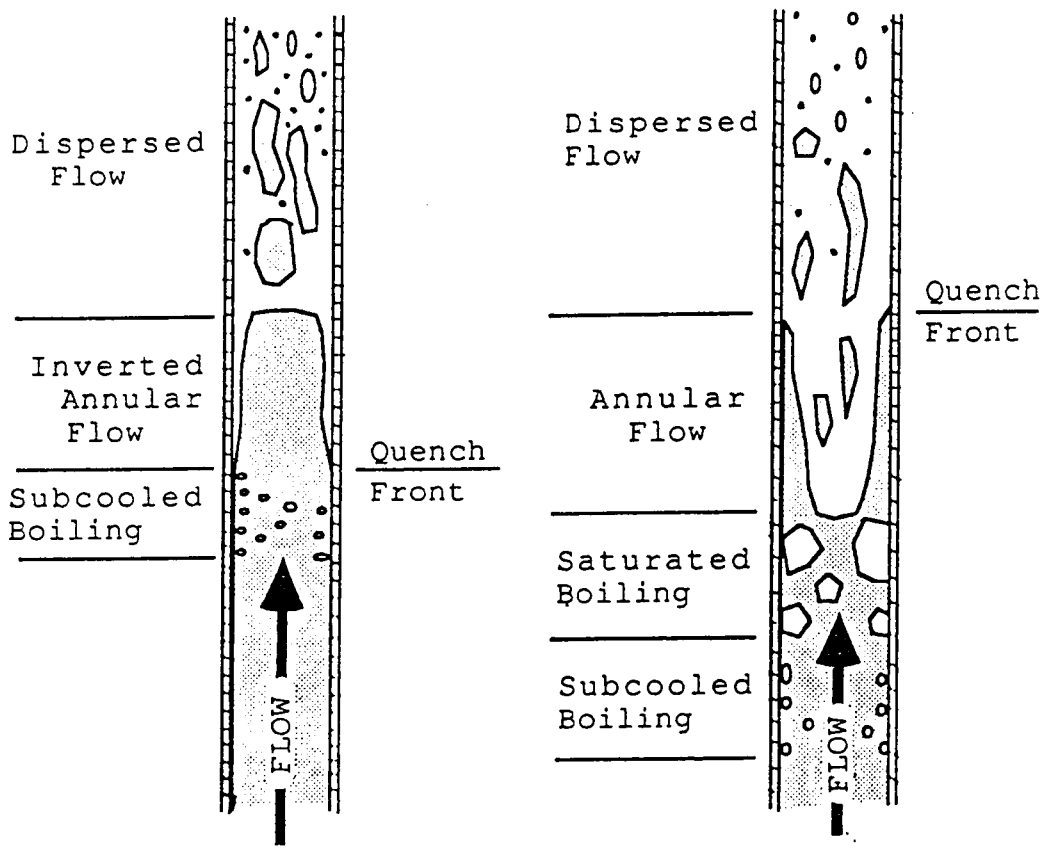

(a) Inverted annular flow
(typ. of high flooding rate)

(b) Annular flow
(typ. of low flooding rate)

Figure 2-1. Flow Pattern in the Vertical Tube, taken from reference [11].

2.2 Method of Analysis of Two-phase Flow

There are several possible approaches to the analysis of two-phase flow [13]. The first is descriptive-experimental which involves observing and recording measured parameters and trying to describe and explain the observable characteristics.

Correlation is the simplest form of analysis in which patterns in the data are presented quantitatively, using dimensionless relationships. Particularly when the phenomena are complicated, correlations for composite concepts such as friction factor, are the most useful products of research, and there may be little to be gained by further elaborate investigations of the details of the flow field.

Another approach to analyze two-phase flow involves Homogeneous Flow [14], in which the flow is divided into subregions with recognizably different properties. By definition, such a flow can never be homogenous, since in that case every element would have identical properties. The homogenous theory of two phase flow is an attempt to represent the flow as if it were a single phase flow, using "effective properties" and established techniques. It is the theory, not the reality that is homogenous. While this theory may provide a reasonable representaion of some variables of interest, e.g. pressure drop in annular-mist flow; it may be misleading in another context, such as the prediction of "dryout" that depends on the fraction of the liquid that flows as a film on the wall and is not typical of the average flow.

In the Two-fluid model (sometime called Separated Flow) each phase has different properties, e.g. temperature, density, and velocity, and is assumed to satisfy some form of the usual conservation laws for mass, momentum, and energy. Each parameter is some sort of average. Averaging introduces errors that are corrected by adding more terms or coefficients to the equations. Two-fluid models may be a good way of representing a spray, or annular flow. In setting up the conser-

vation equations one may arbitrarily choose, within limits, to designate certain terms as primary and others as empirical, particularly when dealing with interactions between phases. This is a subjective choice. As long as consistency and mathematical integrity are maintained, there is no more fundamental principle to which one can appeal to determine which version is correct. The only criterion is utility for the particular purpose for which one is performing the analysis. There is rarely a clear, basic constitutive equation except for highly idealized models that are geometrically simple and are at best an approximation to a much more complicated reality. Realizing that the two-fluid model has weaknesses, some researchers have sought greater precision by being more explicit about averaging. This usually means that terms in the equations appear as integrals over space and time of continuum parameters such as velocity.

In the present work, a two-fluid model is used to analyze the two-phase regions.

2.2.1 Two-fluid Model

The singular characteristic of two-phase or of two immiscible mixture is the presence of one or several interfaces separating the phases or components. In analyzing two-phase flows, the standard method of continuum mechanics can be applied. Thus a two-phase flow is considered as a field which is subdivided into single phase regions with moving boundaries between phases. The standard differential balance equations hold for each of the subregions with appropriate boundary conditions to match the solutions of these differential equations at the interfaces. Hence, in theory, it is possible to formulate a two-phase flow problem in terms of the local instant variable. It will be called a local instant formulation in order to distinguish it from formulations based on various methods of averaging.

Analysis of the local instantaneous form of the conservation equations is dis-

cussed by Delhaye & Achard [15], Vernier & Delhaye [16] and Ishii [17]. The general approach is to operate on the conservation equations to produce a new set in which the new dependent variables are time, area, or space averaged. The resulting set of equations is simpler, but information is lost in the averaging process and must now be supplied in the form of auxiliary relationships. For two-phase flows, these auxiliary relationships are for heat, mass and momentum transfer between each phase (i.e., across the phase interfaces) and between each phase and the boundaries. In two-phase flows the presence of interfacial surfaces introduces great difficulties in the mathematical and physical formulation of the problem.

From the mathematical point of view, a two-phase flow can be considered as a field which is subdivided into single phase regions with moving boundaries separating the constituent phases. The differential balance holds for each sub-region; however, it can not be applied to the set of these sub-regions in the normal sense without violating the above conditions of continuity.

From the point of view of physics, the difficulties which are encountered in deriving the field and constitutive equations appropriate to two-phase flow systems come from the presence of the interface, and the fact that both the steady and dynamic characteristics of two-phase flows depend upon the structure of the flow.

Although there is reasonable agreement between various formulations for the averaged two-phase flow models under identical physical situations and assumptions, as pointed out by Wallis [18] and Yadigaroglu & Lahey [19], there are still differences due to different ways of incorporating the various empiricisions required for the auxiliary relationships.

Averaging operators have been discussed by Delhaye & Achard [15] and Ishii [17] in detail. The commonly used averaging procedures are: (i) volume or area averaging, with no averaging in time; (ii) time averaging, with no averaging in

space; (iii) area averaging, with no averaging in space; (iv) area/space averaging or time/space averaging.

In the present study, a set of one-dimensional two-fluid equations for unequal phase velocities, unequal temperatures and unequal pressures is considered. More details about conservation equations for two-fluid model are disscussed in Appendix A. These equations have been developed for two-fluid flows, and have been volume and area averaged for the prediction of one-dimensional transient flow. These two-fluid representations of the two-phase flows are, in principle, extremely powerful, both because of the generality of the equations and the flexibility to adopt appropriate constitutive relations for distinct physical situations.

This two-fluid model is based on six field equations, i.e., two continuity, two momentum and two energy equations. The interfacial transfer conditions for mass, momentum and energy bind the transport processes of each phase. Since these equations basically express the conservation laws, they should be supplemented by various constitutive equations which specify molecular diffusions, turbulent transports, and interfacial transfer mechanisms as well as a relation between the thermodynamic state variables.

2.3 Inverted Annular Film Boiling

In this section, attention is focused on the flow pattern where a long liquid column is formed above the quench front, separated from the wall by a thin film of vapor. This regime is generally referred to as Inverted Annular Film Boiling (IAFB) regime and is characterized by the presence of waves on the vapor-liquid interface and by liquid subcooling at the quench front. With increasing vapor quality, the liquid core is broken and finally the flow pattern changes to dispersed flow. The term "vapor-liquid interface" refers to the interface between the vapor

phase and the liquid column in this regime.

Inverted annular flow occurs in confined boiling heat transfer systems, when low quality flow is coupled with wall surface temperature and heat flux values too high to allow direct liquid/wall contact. The resulting flow pattern is a liquid core surrounded by a blanket annulus of vapor. Inverted annular flow may occur in light water reactor accident situations in which, after a loss of core coolant, core reflood brings coolant into the confined regions between very hot fuel rods [21]; or it may occur in cryogenic heat transfer systems, such as those found in rocket propulsion applications [22].

It can be said that very limited studies have appeared on the fluid-dynamic mechanisms of the post CHF (Critical Heating Flux) two-phase flow. The main reason for this lack of information on the flow characteristics, is considerable experimental difficulties associated with flow measurements in this region. Due to the high temperature of the wall to sustain the film boiling, flow visualization requires special attention. Furthermore, local flow and temperature measurements of liquid and vapor in this adverse two-phase flow condition is extremely difficult and costly. Often the heat transfer and fluid-dynamics are so tightly coupled that is almost impossible to obtain accurate fluid-dynamic data.

Some understanding of the film boiling mechanisms has been obtained from visual observations such as those using high speed motion pictures and flash photography. Visualizations of the flow patterns have been made using a quartz tube for a sight glass in many studies. A visual experimental study of liquid nitrogen film boiling in a vertical tube by Laverty and Rhosenow [9] demonstrated that similar two-phase flow regimes also existed at very low quality and were broken up at higher qualities to form liquid slugs and dispersed droplets. They concluded "the drag force on the liquid core increases down stream due to higher gas flux,

and eventually the core is torn apart into filaments and droplets". Forslund and Rhosenow [10] extended the above experiments and measured the droplet size at the exit of the heated section. It was observed that the size of the droplets present appeared to be relatively insensitive to the liquid flow rate and quality, however, it was affected strongly by the heat flux. Smaller droplets were observed at higher heat fluxes.

Kalinin et al [23-24] performed similar experiments using liquid nitrogen in a vertical down flow system. They also confirmed the existence of inverted annular, slug, and dispersed droplet flows. However, they observed a different mechanism of liquid core disintegrations in this transient quenching experiment. They explained that the cyclic changes in the flow regime between the inverted annular and slug flows were caused by cyclic pressure changes at the leading edge of the liquid due to the rapid vaporization.

Cumo [25] studied the rewetting of a hot wall by falling water film. The formation of rivulet flow and subsequent droplet generations, by sputtering of a liquid film, were observed. Two different size groups of droplets were generated. A large number of smaller droplets having the mean diameter of about 0.2 mm were generated by escaping vapor bubbles near the tip of the rivulet. The larger drops were generated due to the detachment of the rivulet by the film boiling. The mean diameter of the larger droplets was in order of 3 mm.

De Jarlais and Ishii [26] experimented steady-state inverted annular flow of Freon 113 in an up flow configuration, which was established in a transparent test section. Using a special inlet configuration consisting of long aspect-ratio liquid nozzles coaxially centered within a heated quartz tube, idealized inverted annular flow initial geometry was established. In addition, inlet liquid and gas velocities were measured and varied systematically. Gas species and liquid inlet

subcooling were also varied. By utilizing both still photographs and high speed motion pictures, the fluid-dynamic behavior of the liquid core, and subsequent downstream break-up of this core into slugs, ligaments, and/or droplets of various sizes was observed. In general, for low inlet liquid velocities (roughly less than 15 cm/s) it was observed that after the initial formation of roll waves on the liquid core surface, a disturbed region of high surface area, with attendant high momentum and energy transfers, occurred. This disturbed region appeared to propagate downstream in a quasi-periodic pattern. Increased inlet liquid flow rates, and high gas annulus flow rates tended to diminish the significance of this disturbed region.

The mathematical models for Inverted Annular Flow heat transfer mechanisms have been reported by Chan and Yadigaroglu [27], Elias and Chambre [28]. A brief discussion of each model will be presented.

Chan [27] formulated a one-dimensional two-fluid model to analyze the heat transfer mechanism in the IAFB with a turbulent homogenous liquid-vapor mixture core above the quench front. The pressures in these regions were assumed equal. Heat was transferred from the wall to the interface by conduction and radiation through the vapor film, and from the interface to the mixture core at a rate given by Dittus-Boelter correlation with the assumption that the interface was not moving. The net vapor generation rate was then determined by the difference between the two heat transfer rates. A fraction of the vapor generated at the interface was allowed to mix with the liquid core. However, this fraction had not been determined and was left as a free parameter in the model.

Ellias and Chambre [28] obtained an analytical solution of the two-dimensional energy conservation equation in the vapor region of the IAFB regime. Their model

assumed a constant film thickness, vapor generation only at the quench front (no vapor generation along the interface) and a laminar vapor flow with a flat velocity profile. They showed that a linear temperature profile was gradually developed in the vapor film which caused the wall heat flux to vary as a function of distance from the quench front. The vapor film thickness was a free parameter in the model and by choosing some appropriate values of it, the heat flux calculations were made to fit experimental data. Based on the data, a simple correlation was then derived to determine the vapor film thickness as a function of the local equilibrium quality at the quench front.

The flow regimes observed to co-exist in the flow channel during cooldown are shown in figure (2-1a). Briefly, the dispersed droplets flow regime precedes the inverted annular film boiling (IAFB) regime which, in turn, precedes the nucleate and transition boiling regimes; single phase liquid prevails below the boiling region. The thermofluid behavior of each flow regime is described by a system of rate equations governing the mass, momentum and energy exchanges in the regime. The following sections discuss the governing equations and the heat transfer models.

2.3.1 Volume-Averaged Conservation Equations For the IAFB Regime

The experimental results [9,11] produced the following features in the IAFB:

1) waves developed along the liquid-vapor interface

2) volume of the liquid column changed with time

3) entrainment occurred near the top of the liquid column

To analyze transient behavior in boiling two-phase flow, non-equilibruim modeling is essential. Also the mathematical model should predict all of the above features. To achieve this, a two-fluid model with appropriate constitutive relations must be considered.

A generalized one-dimensional two-fluid model has been derived by Banerjee and Chan [29]. Starting from this generalized two-fluid model, we can simplify it by assuming that the average of the product of some dependent variables is equal to the product of averages of these variables. Then, the resulting simplified model has the volume-averaged conservation equations which are given as follows:
Liquid Mass:

$$\frac{\partial}{\partial t}(\alpha\rho)_l + \frac{\partial}{\partial z}(\alpha\rho u)_l = -m_l''' \qquad (2-1)$$

Vapor Mass:

$$\frac{\partial}{\partial t}(\alpha\rho)_v + \frac{\partial}{\partial z}(\alpha\rho u)_v = m_l''' \qquad (2-2)$$

Liquid Momentum:

$$\frac{\partial}{\partial t}(\alpha\rho u)_l + \frac{\partial}{\partial z}(\alpha\rho uu)_l + \alpha_l\frac{\partial p_l}{\partial z} - \Delta p_{li}\frac{\partial \alpha_l}{\partial z} = \tau_i''' - \rho_l\alpha_l g - m_l''' u_l \qquad (2-3)$$

Vapor Momentum:

$$\frac{\partial}{\partial t}(\alpha\rho u)_v + \frac{\partial}{\partial z}(\alpha\rho uu)_v + \alpha_v\frac{\partial p_v}{\partial z} - \Delta p_{vi}\frac{\partial \alpha_v}{\partial z} = -\tau_i''' + m_l''' u_i - \rho_v\alpha_v g - \tau_{wv}''' \qquad (2-4)$$

Liquid Energy:

$$\frac{\partial}{\partial t}(\alpha\rho h)_l + \frac{\partial}{\partial z}(\alpha\rho uh)_l = -m_l''' h_{l,sat} + q_{lH}''' \qquad (2-5)$$

Vapor Energy:

$$\frac{\partial}{\partial t}(\alpha\rho h)_v + \frac{\partial}{\partial z}(\alpha\rho uh)_v = m_l''' h_{v,sat} + q_v''' \qquad (2-6)$$

The energy equations have been further simplified by neglecting the kinetic energy and axial conduction terms. To reflect the transient behavior of the cooldown

and to predict the interfacial wave phenomena along the liquid-vapor interface, the time-derivative terms have been included in the model. Pressure difference between two phases has been taken into account.

The above conservation equations can be applied to any two-phase flow process. In order to apply them to a particular flow regime of interest, proper constitutive relations must be considered. These relations are expressing the interfacial area and the interfacial transfer terms (mass, momentum, energy) in accordance with the physics of that particular flow regime. The following sections will describe the derivation of the phasic pressure difference ΔP_{ki} and the constitutive relations.

2.3.2 Pressure Difference Between Phases

The interface-phase pressure difference terms Δp_{li} and Δp_{vi} in equations (2-3) and (2-5) can be evaluated as follows. The pressure in the vapor phase is assumed to be radially uniform and equal to the pressure at the interface; thus, the term $\Delta p_{vi} = 0$, and Δp_{li} equals Δp_{lv}, where Δp_{lv} is the pressure difference between the liquid phase and vapor phase. The pressure difference between the liquid and the vapor is as follows:

$$\Delta p_{lv} = p_v - p_l = \Delta p_{vt} + \Delta p_{st} \qquad (2-7)$$

where

Δp_{vt} = pressure difference due to vapor thrust

Δp_{st} = pressure difference due to surface tension

The pressure difference due to surface tension, Δp_{st}, is given by,

$$\Delta p_{st} = -\sigma(\frac{1}{R_r} + \frac{1}{R_z}) \qquad (2-8)$$

where R_r and R_z are the radii of the curvature in the transverse and axial section respectively. From Lamb [30], the sum of the inverses of the radii of principal

curvature for an axially symmetric liquid column shown in figure (2-2) is,

$$\frac{1}{R_r} + \frac{1}{R_z} = \frac{1}{R\sqrt{\alpha_l}} + \frac{\partial^2 \delta}{\partial z^2} \qquad (2-9)$$

where

δ = vapor film thickness

R = radius of the flow channel

α_l = liquid fraction

The film thickness and liquid fraction for a cylindrical geometry are related as follows:

$$\delta = R(1 - \sqrt{\alpha_l}) \qquad (2-9a)$$

Combining equations (2-8) and (2-9), equation (2-8) is expressed as follows,

$$\Delta p_{st} = -\sigma(\frac{1}{R\sqrt{\alpha}} + \frac{\partial^2 \delta}{\partial z^2}) \qquad (2-10)$$

The pressure exerted by the vapor on the liquid core, Δp_{st} is:

$$\Delta p_{vt} = m_l''(v_{vn} - v_{ln}) \qquad (2-11)$$

where

m_l'' = mass transfer across the interface

v_{vn} = normal velocity of vapor across the interface

v_{ln} = normal velocity of liquid across the interface

In the equation (2-11), the mass flux can be expressed as

$$\begin{aligned} m_l'' &= \rho_v v_{vn} \\ &= \rho_l v_{ln} \end{aligned} \qquad (2-12)$$

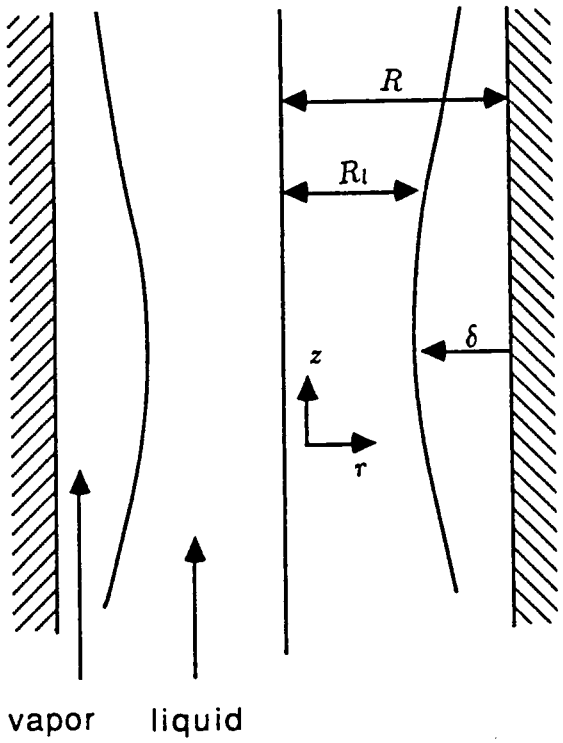

Figure 2-2. Inverted Annular Flow Geometry.

where ρ_k is the density of phase k. By substituting equation (2-12) into equation(2-11), we obtain

$$\begin{aligned}\Delta p_{vt} &= m_l''^2(\frac{1}{\rho_v} - \frac{1}{\rho_l}) \\ &\approx m_l''/\rho_v \\ &= q_{evap}''^2/\rho_v h_{fg}^2 \end{aligned} \qquad (2-13)$$

where q''_{evap} is the amount of heat used for vaporization and h_{fg} is the latent heat of vaporization. Note that Δp_{vt} is now expressed in terms of the heat used for vaporization.

Physically, the vapor thrust pressure given by equation (2-13) has a stabilizing effect on the growth in amplitude of liquid-vapor interface. As the interface gets closer to the wall, a larger amount of heat is transferred to the liquid column; and as a result, a larger amount of vapor is generated. The resulting vapor thrust will push the interface away from the wall, preventing the wave from growing in amplitude. Incorporation of this thrust pressure term into the two-fluid equations can increase the stability of the numerical solution. As surface tension attempts to minimize the surface area of the interface, it has the effect of limiting the wave growth by exerting a surface on the interface. The effect of the surface tension term on the numerical solution of the momentum equation has been investigated by Ramshaw et al [31]. They found that the addition of this term in the two-fluid model is able to improve the stability of the numerical solution.

Finally, we can relate the vapor pressure to the liquid pressure by the following expression:

$$\Delta p_l - \Delta p_v = \Delta p_{st} + \Delta p_{vt} \qquad (2-14)$$

where Δp_{vt} and Δp_{st} are given by equation (2-8) and (2-13), respectively

2.3.3 Constitutive Relations

The conservation equation set contains the following unknown terms in addition to the major dependent variables:

$$m_l''', \tau_i''', \tau_{wv}''', q_{lH}''', q_v'''$$

These terms are evaluated by means of constitutive models and incorporated into the six conservation equations to solve for the six variables $\alpha_l, u_v, u_l, h_v, h_l, p_v$. The liquid fraction α_l is equal to the difference between unity and the void fraction α_v; p_l is related to p_v by equation (2-14). The constitutive relations are generally expressed in terms of analytical expression or empirical correlations. The following subsections describe the methods to construct these relations for the present regime.

2.3.4 Heat Transfer

Before discussing the details of constructing the constitutive relations for the IAFB regime, the overall picture of the heat transfer model for the regime will be introduced. The geometry of the regime is similar to a concentric annular duct with a hot outer wall and cold inner wall (liquid surface). The two walls are separated by a thin vapor film. Since the spacing between the walls is usually very small, the annular geometry of the regime can be approximated by a parallel plate geometry. The assumed heat transfer mechanism in the IAFB regime is shown in figure (2-3). The vapor-liquid interface, where vaporization occurs, is assumed to be at saturation temperature. In this regime the following heat transfer mechanisms exist:

1) wall-to-vapor convection

2) wall-to-liquid radiation

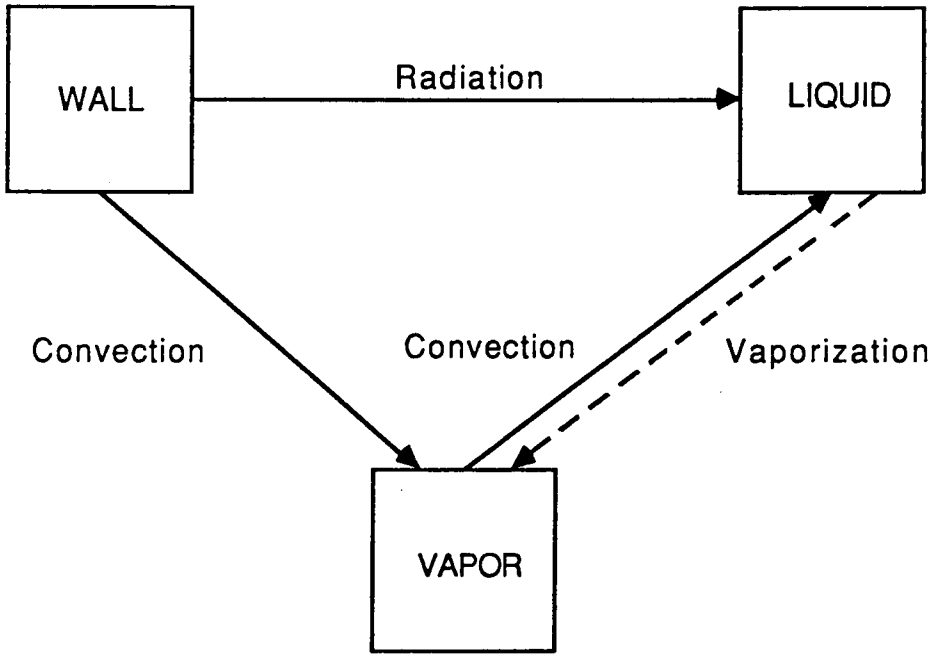

Figure 2-3. Inverted Annular Flow Heat transfer Mechanism.

3) vapor-to-liquid convection

therefore, the heat transfer from the hot wall into the fluid is by convection to the vapor and radiation to the liquid column:

$$q''_w = q''_{rad} + q''_{wv} \qquad (2-15)$$

The heat flux received by the liquid column is due to radiation from the wall and convection from the vapor phase:

$$q''_l = q''_{vl} + q''_{rad} \qquad (2-16)$$

This heat flux (q''_l) is then used for removing the subcooling of the liquid column and for vapor generation:

$$q''_l = q''_{lH} + q''_{evap} \qquad (2-17)$$

Where q''_{lH} is the liquid heating flux, and q''_{evap} is the heat for vaporization. Substituting equation (2-16) into equation (2-17) and rearranging the terms, q''_{lH} can be expressed as:

$$q''_{lH} = q''_{vl} + q''_{rad} - q''_{evap} \qquad (2-18)$$

At the same time, the increase in sensible heat of the vapor flow (the heat used to heat up the vapor stream) is given by the total amount of heat transmitted to vapor from the hot wall minus the amount of heat conducted to the liquid, i.e.,

$$q''_v = q''_{wv} - q''_{vl} \qquad (2-19)$$

Note that the quantities q''_{lH}, q''_v and q''_{lv} (which is used to evaluate the vaporization rate) are explicit parameters in the two-fluid conservation-equations set (equation

(2-1) through (2-6)). They are determined by the constitutive models discussed next.

In summary, the wall heat flux transmitted to the fluid in the IAFB regime is distributed in three ways:

1) for vaporization (q''_{evap})
2) for increasing vapor superheat (q''_v)
3) for removal of subcooling from the liquid (q''_{lH})

The following subsections will describe methods of estimating these individual heat fluxes.

2.3.4.1 Heat Transfer Model of the Vapor Film

The convection heat transfer rates from the wall to vapor and from vapor to liquid are given by the inner and outer-surface Nusselt number formulation by Kays [32] for convective heat transfer between parallel plates.

$$q''_{wv} = \frac{k_v Nu_1}{2\delta}(T_w - T_v) \qquad (2-20)$$

$$q''_{vl} = \frac{k_v Nu_2}{2\delta}(T_v - T_l) \qquad (2-21)$$

The Nusselt numbers are specified in terms of Nusselt number for the case of only one side heated or cooled and the influence coefficient Ω.

$$Nu_1 = \frac{Nu^*}{1 + \Omega(q''_{wv}/q''_{vl})} \qquad (2-22)$$

$$Nu_2 = \frac{Nu^*}{1 + \Omega(q''_{vl}/q''_{wv})} \qquad (2-23)$$

The vapor film is considered to be laminar just above the quench front, but turbulence may be initiated in the vapor flow by transverse flow of vapor generated at

the interface. If the flow in the vapor film is laminar, heat transfer from the wall is by molecular conduction only and the Nusselt, Nu^*, and influence coefficient, Ω, in equation (2-22) and (2-23) are 5.385 and 0.346 respectively for the case of constant wall heat flux.

The effect of turbulence is considered to be significant, since laminar film boiling models underpredict the experimental data. Kays and Leung [33] computed values of Nu^* and Ω for vapor Reynolds number greater than 10^4 and various Prandtl numbers.

2.3.4.2 Radiation Heat Transfer

For radiation from the wall to the liquid column, by assuming that the vapor film is transparent and that the wall is gray, Siegel [34] suggested the following :

$$q''_{rad} = \frac{\sigma^r(T_w^4 - {T_{sat}}^4)}{\frac{1}{\epsilon_w} + \frac{1}{\epsilon_l\sqrt{\alpha_l}} - 1} \qquad (2-24)$$

The view factor was calculated assuming infinitely long, concentric cylinders.

2.3.4.3 Total Heat Fluxes for Wall, Vapor and Liquid

The wall heat flux is the summation of transmitted radiation flux to the liquid column and transferred convection flux to the vapor:

$$q''_w = q''_{wv} + q''_{rad} \qquad (2-25)$$

The vapor heating flux is given by:

$$q''_v = q''_{wv} - q''_{vl} \qquad (2-26)$$

The total heat flux received by the liquid column is given by:

$$q''_l = q''_{vl} + q''_{rad} \qquad (2-27)$$

2.3.4.4 Liquid Heating Flux

The total heat flux received by the subcooled liquid column, is utilized for:

i) some fraction for the conduction heating of the subcooled liquid column

ii) the rest is used for the evaporation at the surface

$$q''_l = q''_{lH} + q''_{\text{evap}} \qquad (2-28)$$

The liquid heating flux is clearly dependent on the local subcooling of the bulk liquid and the thickness of the thermal boundary layer near the surface. In order to estimate its value, a laminar plug flow was assumed in the liquid column and the following thermal entry problem was considered:

$$\rho_l c_{p_l} u_l \frac{\partial T_l}{\partial z} = k_l \left(\frac{\partial^2 T_l}{\partial r^2} + \frac{1}{r} \frac{\partial T_l}{\partial r} \right) \qquad (2-29)$$

with boundary conditions:

$$T_l(r,z) = T_0 \quad \text{at } z = 0, \quad 0 \le r \le R_l \qquad (2-29a)$$

$$T_l(r,z) = T_{\text{sat}} \quad \text{at } r = R_l, \quad z > 0 \qquad (2-29b)$$

$$\frac{\partial T_l}{\partial r} = 0 \quad \text{at } r = 0, \quad z > 0 \qquad (2-29c)$$

The assumption of a radially uniform temperature profile at entry is based on the possible mixing of liquid near the quench front due to turbulence created by rapid and frequent growth and collapse of bubbles on the wetted surface below the quench front.

The radial velocity profile, u_l, is expected to change with the axial distance above the quench front, in a manner difficult to estimate because of the free surface of the liquid core. Qualitatively, however; the radial velocity profile showed change from a parabolic profile below the quench front with the center velocity at

maximum to an inverted parabola near the top of the liquid core. By assuming a flat velocity profile and replacing z with $u_l t$, equation (2–29) was transferred into a transient conduction equation. An analytical solution for this case is readily available in a series form as given by Carslaw and Jaegar [35].

$$\Theta = 2\sum_{n=1}^{\infty} \frac{J_0(\beta_n r/R_l)}{\beta_n J_1(\beta_n)}\, e^{-\beta_n z^+} \qquad (2-30)$$

where

$$\Theta = (T_{\rm sat} - T_l(r, z^+))/(T_{\rm sat} - T_0) \qquad (2-31)$$

$$\beta_n = \text{ roots of } J_0(\beta) \qquad (2-32)$$

$$z^+ = k_l z/(R_l c_{p_l} \rho_l u_l) \qquad (2-33)$$

The average liquid temperature and liquid heating flux can be calculated from equation (2–29) as follows:

$$\Theta_{av}(z^+) = 4\sum_{n=1}^{\infty} \frac{1}{\beta_n} \exp(-\beta_n z^+) \qquad (2-34)$$

or

$$\frac{q''_{lH}}{k_l(T_{\rm sat} - T_0)/R_l} = -2\sum_{n=1}^{\infty} \frac{1}{\beta_n} \exp(-\beta_n z^+) \qquad (2-35)$$

2.3.5 Interface Mass Transfer Term

Vaporization rate of the liquid per unit area at the interface is given by:

$$m''_l = q''_{evap}/h_{fg} \qquad (2-37)$$

and the interfacial area concentration, A'''_i:

$$A'''_i = \frac{4\alpha_l^{\frac{1}{2}}}{D} \qquad (2-38)$$

therefore, the rate of mass transfer per unit volume is:

$$m_l''' = 4\frac{\sqrt{\alpha_l}}{Dh_{fg}}(q''_{evap}) \qquad (2-39)$$

2.3.6 Interface Heat Transfer

At the interface the rate of liquid heating flux per unit volume is:

$$q'''_{lH} = A_i''' q''_{lH} \qquad (2-40)$$

or

$$q'''_{lH} = 4\alpha^{0.5}\frac{q''_{lH}}{D} \qquad (2-41)$$

2.3.7 Momentum Transfer Term

The shear stress terms are in units of force per unit volume, and either empirical correlations or approximate analytical expressions may be used. They should account for the effect of fluid acceleration; however, only the steady-state stress can be provided with reasonable accuracy at present. The shear stresses are generally expressed in the form:

$$\tau''' = \frac{p_w}{A} f \frac{\rho}{2}|u|u \qquad (2-42)$$

where

p_w/A = wetted perimeter per unit flow area

f = friction factor

u = field velocity

The friction factor applicable to the inverted annular flow regime is not readily available in the literature. Since the liquid velocity is expected to be an order of

magnitude less than the vapor velocity, it is reasonable to model the situation as a steady vapor flow in a narrow annular gap. The friction factor correlation for fully developed turbulent flow in an annulus is given by:

$$f = \frac{0.085}{Re^{0.25}} \qquad (2-43)$$

where

$$Re = \rho_v u_v (2\delta)/\mu_v$$

For this type of flow in an annulus, inner and outer friction factors generally vary from each other, depending on the diameter ratio. However, for sufficiently thin vapor film, the two friction factors can be assumed equal. Thus, the value given by equation (2-43) is used for both the wall and interfacial friction factors.

The wetted perimeter to the flow p_w/A, for wall and interfacial friction shear stresses are given by:

wall:

$$\frac{p_w}{A} = \frac{4}{D} \qquad (2-44)$$

interfacial:

$$\frac{p_w}{A} = \frac{4\sqrt{\alpha_l}}{D} \qquad (2-45)$$

The fluid density is that of vapor and the relevant velocities for the two stresses are as follows:

wall:

$$u = u_v \qquad (2-46)$$

interfacial:

$$u = (u_v - u_i) \tag{2-47}$$

For steady laminar flow in the vapor film, the velocity distribution was solved analytically, assuming that the liquid-vapor interface moves at a constant velocity u_i. The momentum equation and boundary conditions are as follows.

$$\frac{1}{r}\frac{\partial}{\partial r}\left(r\frac{\partial}{\partial r}u_r(r)\right) = \frac{1}{\mu_v}\frac{\partial p}{\partial z} \tag{2-48}$$

$$\text{at } r = R, \qquad u_v(R) = 0 \tag{2-48a}$$

$$\text{at } r = R_l, \qquad u_v(R_l) = u_i \tag{2-48b}$$

The solution for the velocity profile is,

$$u_v(r) = \frac{1}{4\mu}\frac{\partial p}{\partial z}\left[r^2 + R^2 + (R^2 - R_l^2)\frac{ln(r/R)}{ln(R_l/R)}\right] + \frac{u_i ln(r/R)}{ln(R_l/R)} \tag{2-49}$$

The velocity profile given by equation (7-49) is averaged over the cross sectional area to obtain the average vapor velocity,

$$u_v = \frac{1}{8\mu}\left(\frac{\partial p}{\partial z}\right)\left[\frac{R_l^2 - R^2}{ln(R_l/R)} - R^2 - R_l^2\right] - u_i\left(\frac{1}{2ln(R_l/R)} - \frac{R_l^2}{R^2 - R_l^2}\right) \tag{2-50}$$

The above equation is solved for $\dfrac{\partial p}{\partial z}$ in terms of the average vapor and interfacial velocities.

$$u_v(r) = \frac{1}{4\mu_v}\left(\frac{\partial p}{\partial z}\right)\left[r^2 - R^2 + (R^2 - R_l^2)\frac{ln(r/R)}{ln(R_l/R)}\right] + \frac{u_i ln(r/R)}{ln(R_l/R)} \tag{2-51}$$

$$\tau_i''' = -8\mu\left(\frac{u_v u_i}{2ln(R_l/R)} - \frac{R_l^2 u_i}{R^2 - R_l^2}\right) / \left(R^2 + R_l^2 + \frac{R^2 - R_l^2}{ln(R_l/R)}\right) \tag{2-52}$$

The shear stresses at the inner and outer surfaces are evaluated from the first derivative of the velocity profile with respect to r.

$$\begin{aligned}\tau_i''' &= \mu\frac{\partial u_r}{\partial r}\Big|_{r=R_l} \\ &= \frac{1}{4}\left(\frac{\partial p}{\partial z}\right)\left[2R_l + \frac{R^2 - R_l^2}{R_l ln(R_l/R)}\right] + \frac{\mu u_i}{R_l ln(R_l/R)}\end{aligned} \tag{2-53}$$

$$\tau'''_{wv} = -\mu \frac{\partial u_r}{\partial r}\Big|_{r=R_l}$$
$$= -\frac{1}{4}\left(\frac{\partial p}{\partial z}\right)\left[2R + \frac{R^2 - R_l^2}{Rln(R_l/R)}\right] - \frac{\mu u_i}{Rln(R_l/R)} \qquad (2-54)$$

Shear forces per unit volume in terms of the average and interfacial velocities, outer diameter and liquid volume fraction are obtained by substituting equation (2–51) for the $\frac{\partial p}{\partial z}$ term in equations (3–53) and (3–54) and multiplying the result by the perimeter to area ratio, equations (2–44) and (2–41) respectively.

$$\tau'''_{wv} = \frac{16\mu_v}{D^2}\left[\frac{-u_l/2\xi + u_v(2\xi + \alpha_v)}{\alpha_v + (1+\alpha_l)\xi} + \frac{u_l(1 + 2\alpha_l\xi/\alpha_v + \alpha_l + \alpha_v/(2\xi))}{\alpha_v + (1+\alpha_l)\xi}\right] \qquad (2-55)$$

$$\tau'''_i = \frac{16\mu_v}{D^2}\left[\frac{u_l/2\xi - u_v(2\xi\alpha_l + \alpha_v)}{\alpha_v + (1+\alpha_l)\xi} + \frac{u_l(2\alpha_l + 2\alpha_l\xi/\alpha_v + \alpha_v/(2\xi))}{\alpha_v + (1+\alpha_l\xi)}\right] \qquad (2-56)$$

where $\xi = ln\sqrt{\alpha_l}$.

The interfacial velocity, u_i, is expected to decrease with distance from zero to the quench front upward due to vapor drag and viscous forces in the liquid. When u_i exceeds the average liquid velocity, however, further increase in u_i is limited because vapor drag and viscous forces counteract each other. If the liquid column does not extend too high, it is reasonable to set u_i equal to the average velocity in the liquid column over the entire portion of the inverted annular flow.

The effect of vaporization on interfacial friction is considered by including a reduction factor derived from the experimental data discussed by Jeromin [36]. The data on the reduction of turbulent skin friction coefficient due to air injection along a flat plate was used to develop a simple correlation for the reduction factor, F_{red}, in terms of the vaporization rate.

$$F_{\text{red}} = \exp\left[-0.5189x - 0.0974x^2\right] \qquad (2-57)$$

where

$$x = \frac{1}{2f_i}\left(\frac{m_l'''}{\rho_v}\frac{D}{u_v}\right) \qquad (2-58)$$

2.3.8 Transition to Dispersed Flow

The transition from the inverted annular flow regime to dispersed droplet flow regime under the constant-injection cooldown was found to be related to the instabilities of the long interfacial waves which were developed at the vapor-liquid interface in the former regime [11–12].

As shown by Kawaji and Banerjee [11–12], the set of conservation equations used in the present two-fluid model (for the inverted annular flow regime) is able to predict long interfacial waves, which can render the mathematical model subject to the low frequency numerical instabilities. Therefore, as was seen in Kawaji's model, the transition criterion comes directly from the predicted long-wave length instabilities in the inverted annular flow, which consequently bring about the necking of the liquid during the computation process.

In the present model, if the wave amplitude, which is expressed in terms of variations of the local fraction, at any location is found to satisfy the following criterion, necking of the liquid is assumed to occur at that location:

$$\alpha_{l_j} < 0.5 \quad \text{or} \quad \frac{\alpha_{l_{j-1}} - \alpha_{l_j}}{\Delta z} > 0.15 \quad \text{and} \quad \alpha_{l_{j+1}} > 0.6 \qquad (2-59)$$

where α_l is the liquid fraction, and the subscript j is referred to the local node j.

Once necking has been detected, the liquid portion above the necking point is treated as an isolated liquid plug. Then, the plug is assumed to shatter and transform into a population of droplets before entering into the dispersed flow regime.

2.4 Dispersed Flow

Observations from the past experimental studies [9,11] indicate that the liquid column near the top of the IAFB regime becomes unstable and breaks up into liquid plugs. These liquid plugs again break down into small droplets of various sizes, which are then carried downstream by vapor flow.

Dispersed flow is characterized by the presence of a large quantity of fine liquid droplets in a continuous vapor flow. Momentum and heat transfer in this particular type of flow is largely affected by the droplet deposition on the duct wall, the vaporization of the droplets and the latent heat transport associated with it. The study of heat transfer in dispersed droplet flows is motivated by its importance in various applications, ranging from the operations of steam generators and cryogenic machinery, and the safety of nuclear reactors during the loss-of-flow accidents, to the spray combustion processes. Due to the complexities of the transport processes occurring in the flows, experimental approaches have failed to measure the detailed characteristics of the flows; and a rigorous computational physical model including all the major transport mechanisms has not yet been presented.

Models used to treat dispersed flow can be classified as empirical or phenomenological. Empirical models fit the experimental data to a proposed relationship, while phenomenological models take into account the physical processes involved. Phenomenological models can be further subdivided into models which utilize the existing heat transfer correlations and those that solve the conservation equations.

Correlations are normally developed using data from a limited number of sources and, as such, are typically limited to a range of flow conditions and one fluid. Many correlations begin with an accepted equation for single-phase heat

transfer, such as Dittus-Boelter correlation, which is then modified to account for such effects as thermal nonequilibrium, droplet size, ratio of vapor to liquid velocities, void fraction, etc. Some correlations have been developed by Dougall and Rohsenow [37], Groeneveld [38], and Groeneveld and Delomore [39]. The inherent assumption in expressing the heat transfer coefficient in the above form is that heat is transferred to the liquid-vapor mixture by a forced convection mechanism and that the two-phases are at thermal and mechanical equilibrium. Although simple in the form and to use, the domain of applicability of each empirical correlation is limited to the range of test conditions from which the correlation was developed. Furthermore, there is experimental evidence of significant vapor superheat, and the thermal non-equilibrium in dispersed flow as reported by Laverty and Rohsenow [9], Forslund and Rohsenow [10].

Most phenomenological approaches start with an assumed heat transfer model which encompasses the major transfer processes occurring in the flow. Using correlations to characterize individual mechanisms, the model predicts the flow as it moves along the pipe. This requires a step-by-step solution scheme and must be implemented on a computer. The advantage in this approach is that it accounts for specific heat transfer mechanisms within the flow.

Various workers have attempted to explain the dispersed flow heat transfer through the identification of individual mechanisms. Liquid entrainment plays an important role in the heat transfer aspect in the cooldown process. As a result, research on the thermal behavior of the droplet flow has been widely performed. Tong et al. [40] conducted experiments to measure the entrained droplet size distribution and velocities in a large bundle (161 rods) under dispersed flow condition in reflood. They observed that the measured droplet velocities, in some runs, were insensitive to droplet sizes, while in other runs, droplet velocities tended to de-

crease as droplet size increased. This occurred randomly and seemed insensitive to the boundary conditions of the runs. No plausible theory was offered to explain the discrepancies. Tong also used the measured droplet size distribution and velocity data to calculate the radiation and convection heat transfer rates of the wall. He then repeated the calculation process using the Sauter Mean Diameter (SMD) as the average of the distribution. The results using SMD to calculate the heat transfer rate were virtually identical to those performed with the exact size distribution. This finding allows us to use the simpler SMD over the droplet size spectrum in the modeling procedures.

Ardon and Hall [41] performed single tube reflood experiments using a silica glass test section to study the breakup and motion of the droplets under atmospheric pressure. Droplet sizes were obtained by analysis of a sequence of flash photographs of the liquid-vapor mixture flow. Droplet velocities were measured using high speed photography. The droplets were seen to be generated just above the quench front by disintegration of waves formed in the wetted part of the flow channel (where annular flow prevailed). The mean droplet diameter was observed to attain an equilibrium value after a distance of about 40 cm from the quench front, as a result of the breakup of large droplets under aerodynamic forces. A simple relaxation model was also developed to describe the spatial evolution of the droplet Sauter Mean Diameter. The predictions were reasonably agreeable with the measurements.

Kawaji [11] developed a two-fluid dispersed flow model to account for the variation of droplet velocity with size. The entrainable droplets were divided into eleven groups based on their sizes. The droplet size spectrum was represented by ULLND (upper-limit log-normal distribution function) and based on which, the Sauter Mean Diameter of each group was calculated. The field equations were

then solved for each group with the assumption that the intra-group transfer of mass, momentum and energy due to droplet collision, breakup and coalescence were negligible.

Thermodynamic nonequilibrium in dispersed two-phase flow first was suggested by Parker and Grosh [42]. Laverty and Rhosenow [9], attempting to analyze the nonequilibrium effect in dispersed flow, proposed a model whereby heat transfer in the flow was considered to be a two-step process in which all the heat input from the wall is transferred to the vapor and then from the vapor to the liquid droplets. Forslund and Rhosenow [10] improved this model by accounting for droplet breakup and by modifying the drag coefficient of the accelerating drops. In addition, a "Leidenfrost" heat transfer from the wall to the droplets at low vapor qualities was included.

Ganic and Rhosenow [43] studied the structure of fully-developed dispersed flow, paying special attention to droplet deposition on the duct wall, the possible successive states of drop-wall interactions and the heat transfer to a single drop deposited on the heated wall. Bhatti [44] assumed that the axial motion of droplets was with the local gas velocity without slip and investigated the transverse motion of droplets under the influence of Stokes's drag, buoyancy, gravity and inertia forces. Later Ganic and Rhosenow [45] examined the deposition of liquid drops in dispersed flow in greater detail. Chen et al. [46] developed a phenomenological model and proposed a correlation of the convective vapor heat transfer in post-CHF region by using a momentum-transfer analogy, allowing for thermodynamic nonequilibrium. Yao [47] proposed a model to calculate the forced convection heat transfer in laminar droplet flow in the thermal entrance region of a circular tube with constant wall temperature, without considering the slip between the phases. The saturated droplets moving in the superheated vapor stream were treated as

distributed heat sinks. The variations in the droplet size and population density of the droplets were not considered. Later, the reduction in droplet size, the increase in the vapor velocity and the dilution of the droplet density along the tube were all included by Rane and Yao [48] and Yao and Rane [49]. Calculations were performed from the inlet of the thermal entrance region to the final fully-developed single-phase flow of vapor far downstream.

The phenomenological approach to the prediction of dispersed flow heat transfer is more mechanistic and the method has greater flexibility in application to a wider variety of situations. The overall heat transfer process is divided into several separate mechanisms. This way, non-eqilibrium effects can be taken into account. In general, the heat transfer mechanisms commonly considered in dispersed flow include the following:

1) Convection from channel wall to vapor

2) Convection from vapor to drops

3) Radiation among wall surface, liquid drops and vapor

Although drops are known to enhance overall heat transfer, the exact mechanism is still unclear and the following views have been proposed.

i) Heat Sink Effect

Sun, Gonzales and Tien [50] developed a model to calculate the radial vapor temperature profile for a steady laminar mist flow, assuming that the drops are distributed uniformly in the flow channel and act as heat sinks. In their model, however, axial variation of the vapor was neglected. Later, Yao [48], Rane and Yao [49], and Yao and Rane [48] considered the axial temperature variation and solved a two-dimensional vapor energy equation.

ii) Wall-Drop Interaction

In the models proposed by a number of workers (Ganic and Rohsenow [44,46]

and Koizumi et al [51]), drops are assumed to be impinging on the wall surface as they travel along the flow channel. The transverse motion of drops necessary for impingement on the wall surface may be included by turbulent diffusion in the vapor stream and has been studied in this context by Ganic and Rohsenow. Drops may also acquire lateral velocity during generation or from disturbances in flow patterns.

iii) Turbulent Diffusivity Effect

Yong and Spencer [52] attributed the enhancement of heat transfer (due to drops) to the increase in turbulent intensity of the vapor stream caused primarily by droplet drag. The effect of drops was introduced into the convective heat transfer model by modifying the local friction appearing in the analytical expression for the turbulent Nusselt number which can be derived based on Reynolds analogy for heat and momentum transfer (Kays [32]).

In the present work, because of significant volume fractions of liquid in the flow transition and dispersed flow regimes, the wall-drop interaction was considered to be primarily important.

Fluid-dynamic calculations are particularly important in prediction of dispersed flow heat transfer, because the local liquid volume fraction depends on the rate of drop entrainment and transport; and heat transfer rate depends strongly on the local void fraction, as evident in the experimental data. Thus, a detailed model was considered to calculate the drop transport in the dispersed flow regime as described in the next section.

2.4.1 Two-Fluid Model of the Dispersed Flow

A portion of liquid core at the upper part of the inverted annular flow breaks up into a liquid slug due to interface instability, and detaches from the rest of the

core. In this case, a mass of liquid is introduced to the vapor stream, and then shatters into a spectrum of drops. In the present model, it is assumed that once liquid detachment has been detected to occur, the detached liquid chunk immediately shatters and transforms into a population of droplets with its size spectrum represented by a distribution function, and with its maximum possible droplet diameter (or maximum stable droplet diameter) specified by a critical Weber number.

The dispersed flow analysis is composed of a one-dimensional, two-fluid model with five conservation equations chosen to describe the motion and energy of vapor and liquid phases. Because of the significant thermal and mechanical non-equilibrium observed in past experiments, separate equations for the two-phases were considered. The liquid energy equation was included because of the possible subcooling of drops in the process. The time and volume averaged equations are given below. In these equations, averages of products are once again assumed to be equal to products of averages. In addition, the drops are assumed to be perfect spheres as shown in figure (2-4), with a population distribution function.

Drop Continuity:

$$\frac{\partial}{\partial t}(\alpha_l \rho_l) + \frac{\partial}{\partial z}(\eta_l \alpha_l \rho_l u_d) = -m_l''' \qquad (2-60)$$

Vapor Continuity:

$$\frac{\partial}{\partial t}(\alpha_v \rho_v) + \frac{\partial}{\partial z}(\alpha_v \rho_v u_v) = m_l''' \qquad (2-61)$$

Drop Momentum:

$$\frac{\partial}{\partial t}(\eta_l \alpha_l \rho u_d) + \frac{\partial}{\partial z}(\eta_l \alpha_l \rho_l u_d u_d) = \tau_d''' - \eta_l \alpha_l \rho_l g - \eta_l m_l''' u_d \qquad (2-62)$$

Drop Energy:

$$\frac{\partial}{\partial t}(\alpha_l \rho_l h_l) + \frac{\partial}{\partial z}(\eta_l \alpha_l \rho_l u_d h_l) = -m_l''' h_{l,sat} + q_{dH}''' \qquad (2-63)$$

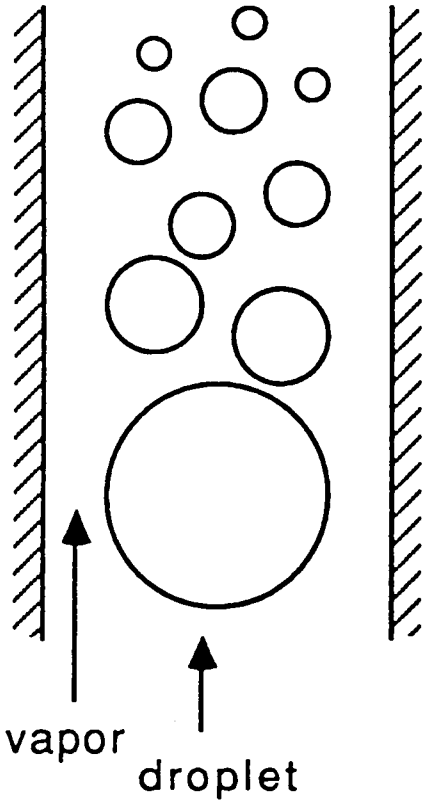

Figure 2-4. Dispersed Flow Geometry.

Vapor Energy:

$$\frac{\partial}{\partial t}(\alpha_v \rho_v h_v) + \frac{\partial}{\partial z}(\alpha_v \rho_v u_v h_v) = m_l''' h_{v,sat} + q_v''' \qquad (2-64)$$

In the drop conservation equations η_l, which is the volume fraction of the entrainable drops, has been incorporated into the equation system because of the importance of the drop size in accurate calculation of the drop transport. In this model, it is assumed that vapor pressure is constant and equal to atmospheric pressure; therefore, the vapor momentum equation is not solved. Solution of two-fluid equations (2-60) through (2-64) requires constitutive relations for interfacial mass, momentum and energy transfer terms and these constitutive relations have been developed from standard correlations.

2.4.2 Drop Size Distribution

Various workers have studied the size distribution for a population of drops in dispersed flow. Ardon and Hall [41] measured drop size at various elevations above the quench front during quenching of a quartz tube. In their experiment, the coolant injection rates were low and the flow regime near the quench front was of an annular type. They observed that the drops were initially generated at the quench front due to the break-up of surface waves on the liquid film upon arrival at the quench front. Drops broke up into smaller drops as they were entrained and transported upward by vapor. To correlate the drop size data, they used an upper-limit, log-normal (ULLN) distribution function first proposed by Mugele and Evans [53]. The volume fraction of drops in size ranging from D_d to $(D_d + dD_d)$ is given by the following expression:

$$\frac{dV}{dy} = \frac{\beta}{\sqrt{\pi}} e^{-\beta^2 y^2} \qquad (2-65)$$

where

$$y = ln(aw); w = \frac{D_d}{D_{max} - D_d} \qquad (2-66)$$

The maximum diameter, D_{max}, in the above equation is the limiting size of drops which can exist at a given elevation. Ardon and Hall used the diameter of the quartz tube for D_{max} and found that the same equation correlated the drop sizes quite well at different elevations above the quench. They noted, however, that the limiting drop size appears to be determined by interactions beween drops and vapor stream. This observation implies that if the relative velocity varies along the flow path with increasing vapor velocity due to vaporization of drops, the limiting size should change along the flow channel. They also found that the Sauter mean diameter of the sample decreased downstream of the quench front due to a fragmentation process, then reached an equilibrium value at about 40 cm above the quench front, and remained relatively constant downstream.

Using the tube diameter for D_{max}, values of the distribution parameters a and β in the equilibrium size distribution were found to be 1.1212 and 0.6474 respectively. The same values are adopted here.

In the present model, the shape of the size distribution at all elevations in the dispersed flow regime is assumed to be given by equation (2-65) with the tube diameter replacing D_{max}. The true maxim drop diameter, however, depends on whether or not drops of maximum diameter can be entrained upstream and carried upward, and also if they are stable with regards to drop-vapor interaction. Therefore, the size distribution is cut off at the maximum diameter which is determined by the methods discussed in the later sections. Also the cumulative volume fraction is given by,

$$V = \frac{1}{\sqrt{\pi}} \int_{-\infty}^{\beta y} e^{-v^2} dV \qquad (2-67)$$

For the above volume distribution, the number distribution is given by the following equation (Mugele and Evans):

$$\frac{dn}{dy} = \frac{\beta}{\sqrt{\pi}} e^{-(\beta y + \frac{3}{2\beta})^2} \qquad (2-68)$$

With the adopted values of distribution parameters, the drop size distribution is highly skewed towards small diameters.

2.4.3 Maximun Stable Drop Diameter

Drop break-up mechanisms determine the stable maximum size of a drop that can exist stably at any elevation. The most possible mechanism of break-up which has been observed in different experiments, is areodynamic break-up. In general, aerodynamic break-up occurs due to the vapor inertial forces overcoming the surface tension forces and can be characterized by a critical Weber number based on the relative velocity and vapor density.

$$We_c = \frac{\rho_v (u_v - u_d) D_d}{\sigma} \qquad (2-69)$$

For the critical Weber number, values ranging from 6 to 22 have been reported by Hinze [54], Lane [55], and Forslund and Rohsenow [10]. Using the critical Weber number criterion, the maximum stable diameter is determined from the following equation:

$$D^s_{max} = \frac{\sigma We_c}{\rho_v u_v^2} \qquad (2-70)$$

In the present model, a critical Weber number of 15 is adopted.

The critical Weber number criterion may specify a maximum stable diameter greater than the tube diameter; or just above the inverted annular flow regime, slugs of liquid may exist with equivalent spherical diameters larger than the tube

diameter due to the elongated shape. In any case, it is assumed that the maximum stable diameter is less than or equal to the tube diameter under all conditions.

2.4.4 Entrainable Drop Diameter

For given local vapor velocity, the maximum size of drops that can be carried upward is determined from the balance of gravity and drag forces. By equating gravity and the drag forces acting on a drop, the maximum entrainable diameter, D^e_{max}, is obtained.

$$D^e_{max} = \frac{0.75 C_D \rho_v u_v^2}{g(\rho_l - \rho_v)} \qquad (2-71)$$

All of the drops in the population with diameters less than D^e_{max}, are considered to be carried upward. Thus, at a given elevation, the maximum diameter of the drop population should be related to the maximum entrainable diameter in the upstream region. In addition, it can exceed the maximum stable diameter. Therefore, in the present model, the maximum diameter at a given elevation is set equal to the smaller of the maximum stable diameter calculated at that elevation and the lowest maximum entrainable diameter calculated in regions upstream.

2.4.5 Entrainable Volume Fraction

The unnormalized volume fraction of drops carried upward is obtained by integrating the volume distribution function with respect to diameter from zero to D^e_{max}.

$$\eta^e_l = \frac{1}{\sqrt{\pi}} \int_{-\infty}^{\beta y^e_{max}} e^{-u^2} du \qquad (2-72)$$

$$y^e_{max} = ln(\frac{a D^e_{max}}{D - D_{max^e}}) \qquad (2-73)$$

$$\eta_l^* = \frac{1}{\sqrt{\pi}} \int_{-\infty}^{\beta y_{max}^e} e^{-u^2} du \qquad (2-74)$$

$$y_{max} = ln(\frac{aD_{max}}{D - D_{max}}) \qquad (2-75)$$

$$D_{max}^e = \frac{0.75 C_D \rho_v u_v^2}{g(\rho_l - \rho_v)} \qquad (2-76)$$

The entrainable volume fraction can be defined as the fraction of total volume of drops which can be entrained and carried upward and is given by the ratio of the above integrals.

$$\eta_l = \eta_l^e / \eta_l^* \qquad (2-77)$$

2.4.6 Various Mean Diameters

The liquid momentum equation describes the motion of the entrained drops. Since the entrained drops have a size distribution, appropriate mean diameters may be used to represent the entire group of the entrained drops in calculating, interfacial mass, momentum and energy transfer terms.

There are various mean diameters obtainable from a given drop size distribution, each appropriate for a specific purpose. The mean diameters are defined and calculated using either the number or volume distribution function as follows (Mugele and Evans [53]).

$$D_{qp}^{q-p} = \frac{\int_0^{D_{max}} D^q \frac{dn}{dD} dD}{\int_0^{D_{max}} D^p \frac{dn}{dD} dD} = \frac{\int_0^{D_{max}} D^{q-3} \frac{dv}{dD} dD}{\int_0^{D_{max}} D^{p-3} \frac{dv}{dD} dD} \qquad (2-78)$$

A general relationship also exists between different mean diameters.

$$D_{qp}^{q-p} = \frac{D_{q0}^q}{D_{p0}^q} \qquad (2-79)$$

As will be shown later, the required mean diameters for drag force and heat transfer calculations are the area-weighted, volume-weighted and Sauter-mean diameters. Using the size distribution function adopted for the present study, various mean diameters have been calculated.

2.4.7 Interfacial Drag

The drag force acting on a single particle in a continous vapor phase under steady flow conditions can be given by,

$$F_D = \frac{C_D}{2}|\rho_v - \rho_l|(\rho_v - \rho_l)\frac{\pi}{4}D_{20}^2 \qquad (2-80)$$

where A_d = projected area of the particle.

The drag force is related to the interfacial shear force through the following relation:

$$\tau_d''' = \frac{6\alpha_l F_D}{\pi D_{30}^3} \qquad (2-81)$$

To describe the interfacial shear for a population of drops with diameters less than the maximum entrainable diameter, one approach is to use the population mean values of the projected area and volume in equation (2-80). This approach is referred to as the single-group approach. Inherent in this approach is the assumption that a single equation of motion with an appropriately formulated interfacial drag term can correctly represent the motion of a whole population of drops.

Equation (2-61) is directly used together with the mean diameter in drag force calculation. The drag coefficient in equation (2-80) is commonly expressed as a function of the drop Reynolds number Re_d; the area-weighted mean diameter,D_{20} is used to calculate the drop Reynolds number, because the drag correlation is derived from the drag force using the projected area of particles.

For a particle, the drag coefficient varies with Reynolds number in several ways. In the viscous regime, the drag coefficient is strongly dependent on the Reynolds number. For the viscous regime, Rowe [56] gives:

$$C_D = \frac{24}{Re_d}(1 + 0.15Re_d^{0.687}) \qquad (2-82)$$

A similar equation has been used by Forslund and Rohsenow[10], and Ishii and Zuber [57]. For $Re > 10^3$, the drag coefficient becomes essentially constant at about 0.45 and this value holds for Re_d up to 2.10^5 (Ishii and Zuber). The drag correlation is valid under steady flow conditions.

For strongly accelerating drops, Ingebo [58] obtained the following empirical correlation.

$$C_D = 27/Re_d^{0.84} \qquad (2-83)$$

However, the particle diameters used by Ingebo to derive his correlation were very small size, therefore, they experienced strong acceleration and equation (2-82) is adopted, with a minimum value of 0.45.

In order to calculate the average drag force for a population of drops, the drag coefficient, projected area and volume appearing in equations (2-80) and (2-81) are calculated using the mean diameter discussed in the previous section. The main uncertainty remains, however, in the dominant term of equation (2-80), which is the square of the relative velocity between the two-phases. For a given vapor velocity, smaller drops are expected to move faster than large drops and thus the relative velocity should be less. Assuming that equation (2-62) truly represents the motion of the whole population, the relative velocity in equation (2-80) is calculated based on the drop velocity obtained from equation (2-62).

2.4.8 Heat Transfer

As it is illustrated in figure (2-5) the heat transfer mechanisms incorporated into the present model include the following:

1) Convection from the wall surface to vapor, and from vapor to drops

2) Radiation among wall, vapor and drops

3) Wall-drop interaction

Constitutive relations for each of these mechanisms are described below.

2.4.8.1 Convection Heat Transfer

a) Wall-to-Vapor Convection

The wall-to-vapor convection heat transfer rate is calculated using a Dittus-Boelter heat transfer coefficient.

$$q'''_{wv} = 0.023\frac{k_l}{D_t}(\rho_v u_v D_t)^{0.8} Pr^{0.33}(T_w - T_v) \qquad (2-84)$$

The vapor properties are evaluated at the film temperature.

b-) Convection from Vapor to Drops

If drops and superheated vapor flow at different velocities, then the convective heat transfer rate can be specified in terms of a Nusselt number for a sphere;

$$Nu = \frac{h_{vd} D_{20}}{k_f} = 2 + C_2 Re_d^{0.5} Pr_f^{0.33} \qquad (2-85)$$

where

$$Re_d = \frac{D_{20}(u_v - u_d)\rho_v}{\mu}$$

The value of C_2 has been experimentally found by Lee and Ryley [59] to be equal to 0.74 for water drops evaporating in superheated steam at low pressures.

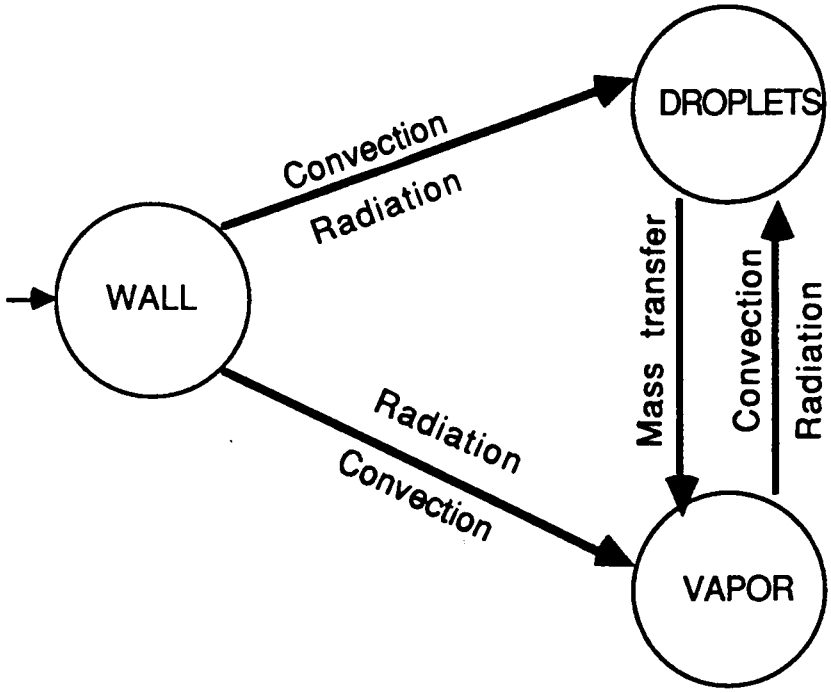

Figure 2-5. Dispersed Flow Heat Transfer Mechanism.

Their experiments covered the range of drop Reynolds numbers between 64 and 250, vapor superheats of up to 35 deg C, and initial drop diameters from 0.23 mm to 1.13 mm. The degree of superheat found in reflood may be much higher, but the value of C_2 has been found by various workers to be relatively constant under different experimental conditions. Thus, C_2 is set equal to 0.74 in the present model.

In Lee and Ryley's experiments, the relative velocity was equal to the vapor velocity, since the drops were suspended stationary on a fixed wire. In actual dispersed flow, drops may have both axial and transverse velocity components. In addition, the effect of adjacent drops evaporating simultaneously and producing saturated vapor nearby may be of some significance to the rate of vapor-to-drop convection heat transfer. Lee and Ryley's correlation includes the effect of simultaneous mass transfer on heat transfer but not the multi-particle effect. Both the transverse drop velocity and the proximity effects are neglected here.

The appropriate mean diameter to use in the above heat transfer correlation is the surface area-weighted mean diameter, D_{20}. Also, the drop's interfacial area concentration per unit liquid-vapor mixture volume, A_i''', is given by:

$$A_i''' = \frac{6\alpha_l}{D_{32}} \qquad (2-86)$$

The volumetric heat transfer rate is then obtained by combining equations (2-85) and (2-86).

$$q_{vd}''' = \frac{6\alpha_l}{D_{32}} \frac{k_f}{D_{20}} (2 + 0.74 Re_d^{0.5} Pr_f^{0.33})(T_v - T_d) \qquad (2-87)$$

2.4.8.2 Radiative Heat Transfer

For radiative heat transfer calculations, the following network model developed by

Sun, Gonzales and Tien [50] is used:

$$q''_{wv}{}^{r} = F_{wv}\sigma^{r}(T_w^4 - T_v^4) \qquad (2-88)$$

$$q''_{wd}{}^{r} = F_{wd}\sigma^{r}(T_w^4 - T_d^4) \qquad (2-89)$$

$$q''_{vd}{}^{r} = F_{vd}\sigma^{r}(T_v^4 - T_d^4) \qquad (2-90)$$

where

$$F_{ij} = (R_i + R_j + R_i R_j / R_k)^{-1} \qquad (2-91)$$

and

$$R_v = \frac{(1-\epsilon_v)}{\epsilon_v(1-\epsilon_v\epsilon_l)} \qquad (2-92a)$$

$$R_d = \frac{(1-\epsilon_l)}{\epsilon_l(1-\epsilon_v\epsilon_w)} \qquad (2-92b)$$

$$R_w = \frac{(1-\epsilon_w)}{\epsilon_w} + (1-\epsilon_v\epsilon_l)^{-1} \qquad (2-92c)$$

For situations encountered in the cooldown, both vapor and drops are considered to be optically thin and the Planck mean absorption coefficient is used to evaluate the vapor emissivity.

$$\epsilon_v = 1 - e^{-a_v D_H} \qquad (2-93)$$

$$a_l = 0.74\pi D_d^2 N_d/4 \qquad (2-94)$$

where

N_d = number density of drops

For a population of drops with the upper-limit, log-normal size distribution described previously, an appropriate mean diameter should be used for D_d in equation (2-94). Since,

$$\alpha_l = \frac{\pi}{6} D_{30}^3 N_d \qquad (2-95)$$

$$D_{20}^2 = D_{30}^3 / D_{32} \qquad (2-96)$$

the expression for the absorption coefficient becomes,

$$a_l = 1.11 \alpha_l / D_{32} \qquad (2-97)$$

Thus,

$$\epsilon_l = 1 - e^{-(1.11 \alpha_l D_t / D_{32})} \qquad (2-98)$$

2.4.8.3 Wall-Drop Interaction

Forslund and Rohsenow[10] conducted experiments on dispersed flow film boiling using nitrogen in a heated vertical tube. They developed the following correlation for film boiling of drops near the tube wall surface.

$$q'''_{wd} = C_1 h_{wd} (\pi D_{20}^3 / 4) N d^{2/3} (T_w - T_{sat}) \qquad (2-99)$$

The heat transfer coefficient used was that of film boiling of small drops on a horizontal plate developed by Baumeister, Hamill and Schoessow [60].

$$h_{wd} = [\frac{k_f^3 h_{fg}^* g \rho_v \rho_l}{(T_w - T_{sat}) \mu_v (\pi D_{30}^3 / 6)^{1/3}}]^{1/4} \qquad (2-100)$$

where

$$h^*_{fg} = h_{fg}(1 + \frac{7}{20}c_p(T_w - T_{sat})/h_{fg})^{-3} \qquad (2-101)$$

The constant C_1, is a parameter accounting for the differences in geometry between flat plate and vertical tube, and the type of packing of drops near the wall surface. Forslund and Rohsenow [10] chose a value of 0.2 for C_1 to best match the predictions of the above model with their data.

The number density of drops per unit volume, N_d, can be expressed in terms of the liquid volume fraction and volume mean diameter, D_{30}, as follows:

$$N_d = \frac{6\alpha_l}{\pi D^3_{30}} \qquad (2-102)$$

Combining equation (2-100) and (2-102), the heat flux due to the wall-drop interaction is given by following equation.

$$q''_{wd} = 0.2552[\frac{k^3_f h^*_{fg} g \rho_v \rho_l}{\mu_v D_{30}}]^{0.25} \alpha_l^{\frac{2}{3}} (T_w - T_{sat})^{0.75} (\frac{D_{30}}{D_{32}})$$

Here, the ratio (D^2_{20}/D^2_{30}), has been replaced by (D_{30}/D_{32}) using equation (2-78). The volumetric heat flux is given by:

$$q'''_{wd} = \frac{4}{D_t} q''_{wd} \qquad (2-104)$$

2.4.9 Overall Heat Transfer Model

The total heat flux from the wall to drops and vapor is given by:

$$q''_w = q''_{wv} + q'''^r_{wv} + q'''^r_{wd} + q''_{wd} \qquad (2-109)$$

The net rate of heat transfer to vapor per unit volume is given by:

$$q_v''' = q_{wv}''' + q_{wv}^{'''r} - q_{vd}^{'''r} - q_{vd}''' \qquad (2-110)$$

where

$$q''' = \frac{4}{D_t} q'' \qquad (2-111)$$

The total heat transfer to the drops per unit volume is given by:

$$q_d''' = q_{vd}''' + q_{vd}^{'''r} + q_{wd}^{'''r} + q_{wd}''' \qquad (2-112)$$

If the drops are subcooled, heat received is used partially for vaporization and partially to raise the sensible heat. The proportion is dependent on the degree of liquid subcooling. For saturated drops, the heat received is used entirely for vaporization. In the energy partition model to be described next, the drop heating flux is first calculated and then subtracted from the total heat received by the drop to obtain the vaporization heat flux.

2.4.10 Droplet Energy Partition

Drops are possibly carried by superheated vapor. Thus, the drop surface is assumed to be at saturation and generating vapor even when the drop's bulk temperature has not yet reached saturation. Furthermore, internal circulation is neglected and the drops are assumed to behave thermally as solid particles.

The transient temperature profile for a sphere of radius R_d, initially at T_0 and the surface raised to T_{sat} for $t > 0$, is given by Carslaw and Jaegar [35].

$$\frac{T(r,t) - T_0}{T_{\text{sat}} - T_0} = 1 + \frac{2R_d}{\pi r} \sum_{n=1}^{\infty} \frac{(-1)^n}{n} \sin\left(\frac{n\pi r}{R_d}\right) e^{-\left(\frac{k_l}{\rho_l c_{p_l}} n^2 \pi^2 t / R_d^2\right)} \qquad (2-113)$$

Heat flux at the surface is calculated from the derivative of the temperature profile with respect to radius, r.

$$\frac{q''_{dH}}{2k_l(T_{\text{sat}} - T_0)/R_d} = -\sum_{n=1}^{\infty} e^{-\left(\frac{k_l}{\rho_l c_{p_l}} n^2 \pi^2 t/R_d^2\right)} \qquad (2-114)$$

The average drop temperature is calculated from $T(r,t)$.

$$\Theta_{av}(t) = \frac{T_{av} - T_0}{T_{\text{sat}} - T_0} = 1\frac{6}{\pi^2} \sum_{n=1}^{\infty} \frac{1}{n^2} e^{-\left(\frac{k_l}{\rho_l c_{p_l}} n^2 \pi^2 t/R_d^2\right)} \qquad (2-115)$$

equations (2–114) and (2–115) are evaluated for various values of t/R_d^2, and correlated with each other.

$$q''_{dH} = \frac{k_l}{D_d}(T_{\text{sat}} - T_0)F_2(\Theta_{av}) \qquad (2-116)$$

where

$$F_2 = 3.81173/\Theta_{av} - 2.92034 - 0.48955\Theta_{av} \quad \text{for} \quad \Theta_{av} < 0.6$$

$$= 2.55871/\Theta_{av} + 0.88880 - 3.44700\Theta_{av} \quad \text{for} \quad \Theta_{av} > 0.6$$

The initial temperature, T_0, is taken to be the temperature of the most recently formed drops, which broke off the liquid column in the inverted annular flow regime.

The volumetric drop heating flux is obtained by multiplying equation (2–116) by the interfacial area concentration, given by equation (2–106).

$$q'''_{dH} = \frac{6\alpha_l}{D_{32}} q''_{dH} \qquad (2-117)$$

If the drop heating flux is calculated to be larger than the total heat flux received, then the former is set equal to the latter value. The vaporization heat flux is the difference between the total heat flux received and the drop heating.

$$q'''_{\text{evap}} = q'''_d - q'''_{dH} \qquad (2-118)$$

Finally, the interfacial mass transfer rate appearing in the two-fluid equations is calculated from the vaporization heat flux as follows.

$$m_l''' = \frac{q_{evap}'''}{h_{fg}} \qquad (2-119)$$

2.5 Fully Liquid Region

In this region, it is assumed that only fully developed, steady flow of single-phase liquid exists and the region starts with channel inlet and ends in quench front. Conservation equations then are as follows:

Continuity:

$$\frac{\partial u_l}{\partial z} = 0 \qquad (2-120)$$

Energy:

$$\rho_l \frac{\partial h_l}{\partial t} + \rho_l u_l \frac{\partial h_l}{\partial z} = \frac{4}{D} q_w'' \qquad (2-121)$$

Equation (2-120) implies that below the quench front, the liquid has a constant velocity which is equal to the inlet velocity. To calculate liquid temperature, the wall heat flux should be incorporated into equation (2-121). The heat transfer mechanism is convection from the wall to the liquid. Therefore, the local wall heat flux is given by:

$$q_w'' = h_c(T_w - T_l) \qquad (2-122)$$

where

h_c = heat transfer coefficient

T_w = local wall temperature

T_l = local liquid temperature

To calculate h_c, in the present model, it is assumed that flow is laminar and the heat transfer coefficient is determined by Dittus-Boelter equation:

$$h_c = 0.023 Re_l^{0.8} Pr_l^{0.4} \frac{k_l}{D} \qquad (2-123)$$

As liquid propagates along the tube, it absorbs more heat and its temperature increases. Close to the quench front, if the channel wall temperature is sufficiently higher than liquid saturation temperature, incipient nucleat boiling takes place and heat transfer is increased due to nucleate boiling.

In spite of the voluminous literature on boiling heat transfer, the predictability of boiling incipience and convective boiling in flowing heat transfer systems is still quite limited. Available empirical and semiempirical techniques are mostly derived from water data and extended to liquid cryogen. For liquid nitrogen and liquid neon, Papell and Hendricks [59] suggested a correlation equation for boiling incipience, and solved it iteratively. This correlation was used to calculate the position of boiling incipience in a flow channel subject to uniform heat flux. Bergles and Rohsenow [60] developed a criterion for the onset of nucleate boiling of water which is valid over the pressure range of 15-2000 psia. Their criterion is as follows:

$$T_w - T_{sat} = [q''_w/(15.6p^{1.156})]^{(p^{0.0234}/2.4)} \qquad (2-124)$$

where

p = local pressure in psia

T_{sat} = saturation temperature corresponding to p

For cryogenic liquid, Frost and Dackowic [61] modified Bergles and Rhosenow's analysis as shown in the following:

$$T_w - T_{sat} = (\frac{4B}{k_l} q''_w)^{0.5} Pr \qquad (2-125)$$

where

$B = (2\sigma T_{sat} v_{fg})/h_{fg}$

σ = surface tension

v_{fg} = specific volume

h_{fg} = latent heat

Therefore, the total wall heat flux in the subcooled nucleate boiling regime is due to convection and nucleate of bubbles on the wall surface. A number of correlations have been proposed in which heat flux during forced convection boiling is calculated by combining heat transfer coefficients for pool boiling and forced convection. Correlations for prediction of heat transfer during boiling of cryogenic liquid are suggested by Shah [62], Klimenko [63], Barron [64], and Girratano [65]. However, using Girrantano's correlation leads to more accurate results.

The correlation of Shah [62] has been verified with a very wide range of data for many non-cryogenic fluids; however, it has been reported to give poor results for heat transfer to nitrogen in copper tubes. Klimenko's correlation [63] also shows poor agreement with nitrogen data. It predicts the wrong trend for the effect of vapor quality at higher pressures and heat fluxes. Barron [64] studied the development of an analytical correlation for the film boiling heat transfer coefficient around a spherical heating surface enclosed in an unheated vertical tube. Experimental runs were conducted with liquid nitrogen to verify the analytical correlation. The heating surface was an aluminum sphere having a diameter of 2.54 cm. The sphere was polished with an emery cloth to produce a smooth surface finish. The heat transfer coefficient data were obtained by a transient technique. The aluminum sphere, initially at room temperature, was suddenly plunged into the liquid nitrogen-filled pipe and the temperature-time plot was recorded. The analytical correlation was in good agreement with experimental data taken with a 2.54-cm-diameter aluminum sphere enclosed within various tubes, having diameters between 2.8 and 8.1 cm, with liquid nitrogen in film boiling. For the cryogenic liquid, Girratano et al [65] suggested the following correlation:

$$h_{total} = h_{nb} + h_c \qquad (2-126)$$

$$h_{nb} = 0.487(10)^{-10}[\frac{k_l \rho_l^{1.282} p^{1.75} c_{pl}^{1.5}}{(h_{fg}\rho_v)^{1.5}\sigma^{0.906}\mu_l^{0.626}}]\Delta T^{1.5} \qquad (2-127)$$

$$h_c = 0.023 Re_l^{0.8} Pr_l^{0.4} \frac{k_l}{D} \qquad (2-128)$$

$$Re_l = \frac{\rho_l u_l D}{\mu_l}, Pr_l = \frac{c_{pl}\mu_l}{k_l} \qquad (2-129)$$

In the present work, to calculate the total heat transfer flux, Girratano's correlation is considered.

2.5.1 Surface Quenching Phenomena

Quenching is the term used to describe the cooling of very hot metal by a cold liquid, for example the water spray used to cool steel in a rolling mill or the water used to cool an overheated nuclear reactor core. A nuclear reactor may be cooled by liquid (water) sprays, or by pumping large quantities of water into the core from the top (top flooding) or from the bottom (bottom reflooding), or by both.

When a hot surface whose temperature is above quench temperature is immersed in the liquid, stable film boiling occurs on the surface. The heat removed from the surface at this stage is through convection and radiation. As time increases, the vapor film becomes unstable; and local intermittent wetting of the surface takes place and the cooling rate increases. At a point when the surface wall temperature suddenly and rapidly drops to about the saturation temperature, the surface is considered to be completely quenched or wetted.

A similar succession of heat transfer processes as described above also occurs when a hot metal tube is quenched by coolant injected from the bottom of tube. A quench front is observed to propagate along the flow channel at various speeds. Upstream of the quench front (cold side of the tube), heat is removed from the wall

by means of nucleate boiling and convection to single-phase liquid. Downstream of the quench front (dry side of the tube), heat is transferred from the wall to the vapor flow, droplet flow, and inverted annular flow or annular flow. Furthermore, heat can also be conducted axially from the dry side to the wetted side, where the heat transfer coefficient can be many orders of magnitude larger than that on the dry side.

Although all of the above heat transfer phenomena were observed experimentally, the real physical mechanism of quenching a hot metal surface is still not well understood. In developing codes involved with quenching phenomena, one common approach to determine the quench speed is to use a quenching criterion based on the quench temperature. When the wall temperature drops to the quench temperature, the surface is assumed to be quenched by the coolant. Then, a much higher heat transfer coefficient is employed to calculate the heat transfer rate in order to have a rapid drop in wall temperature. There are several reference temperatures existing in literature to determine the quench temperature; for example, the Leidenfrost temperature, the minimum film boiling, and the saturation temperature.

In order to proceed with the modeling of the cooldown process in the present work, the quench front propagation is determined by the quench speed data obtained from the present experiments. Therefore, the quench speed is an input parameter to the model. Hence, the heat transfer and fluid-dynamic aspects of the process are decoupled from the rewetting aspects, and can be analyzed separately. This approach helps in examining the accuracy of the constitutive relations employed for the two-fluid model.

2.6 Heat Conduction in Flow Channel Wall

A thin-walled tube is considered to represent the flow channel in the present

model in order to analyze the experimental data. Chi [66] studied the response of the outside wall temperature to the inside wall temperature variations. He found that under the cooldown conditions, the difference between the two temperatures was small. This implies that the radial temperature gradient across the two surfaces can be ignored, and the one-dimensional approach will suffice for analyzing heat conduction in the wall. Thus, to determine the wall temperature history of the flow channel during the cooldown, a one-dimensional transient heat conduction equation is formulated as follows:

$$\rho_w c_{pw} \frac{\partial T_w}{\partial t} = \frac{\partial}{\partial z}(k_w \frac{\partial T_w}{\partial z}) - \frac{P_i}{A_w} q''_w \qquad (2-130)$$

where

z = axial coordinate

T_w = wall temperature of the flow channel

q''_w = heat flux to fluid flowing inside the tube

P_i = inside perimeter

A_w = cross sectional area of the tube wall

CHAPTER III

NUMERICAL ANALYSIS

3.1 Inverted Annular Film Boiling Regime

In general, the conservation equations described in section (2.3.1) must be solved together with the equations of state, which specify the fluid densities in terms of fluid temperature and pressure. Therefore, there are ten equations and ten dependent variables. The variables are:

$$\alpha_l, \alpha_v, u_l, u_v, p_l, p_v, h_l, h_v, \rho_l, \rho_v \qquad (3-1)$$

The equations include:

1) six conservation equations

2) relations for the volume fractions, using the following equation:

$$\alpha_l + \alpha_v = 1 \qquad (3-2)$$

3) equation (2-14) for the phasic pressure difference

4) two equations of state.

$$\rho_l = \rho_l(p_l, h_l) \qquad (3-3)$$

$$\rho_v = \rho_v(p_v, h_v) \qquad (3-4)$$

To solve the above set of equations, using implicit technique, requires an implicit numerical scheme in which either a large matrix has to be inverted or iterations are carried out until the convergence of all the dependent variables is achieved

at every time step. Usually, the computational effort and cost of such a numerical scheme is enormous.

The numerical solution method described in this section is a semi-implicit, finite-difference scheme which needs few iterations per time step. At atmospheric pressure, liquid density can be reasonably assumed to remain constant with respect to temperature. On the other hand, vapor density is a strong function of temperature at low pressure. It decreases significantly with temperature at atmospheric pressure. Other vapor properties such as viscosity, specific heat and thermal conductivity are assumed to be dependent only on temperature.

In the following equations, M_k, G_k, and H_k denote the phasic mass, $\alpha_k\rho_k$, momentum, $\alpha_k\rho_k u_k$, and energy, $\alpha_k\rho_k h_k$, respectively for phase k, which are the quantities to be conserved. Also let j,n and N represent the node, the iteration step and time step. The steps for solution are as follows:

1) the liquid continuity equation is finite-differenced, as

$$M_{l_j}^{n+1} = M_{l_j}^{N} + \frac{\Delta t}{\Delta z}(G_{l_{j-1}}^{n+1} - G_{l_j}^{n}) - \Delta t m_{l_j}^{'''n+1} \qquad (3-5)$$

Since the calculations are carried out from the bottom node upward, values of variables below the current node and at the current iteration step can be considered to be known. After solving equation (3-5), the liquid and void fractions at node j are given by,

$$\alpha_{l_j}^{n+1} = M_{l_j}^{n+1}/\rho_l \qquad (3-6)$$

$$\alpha_{v_j}^{n+1} = 1 - \alpha_{l_j}^{n+1} \qquad (3-7)$$

2) the vapor continuity and energy equations are solved together to obtain the vapor temperature and density. In solving the energy equation, the source terms

(vapor heating flux and energy transfer due to the mass transfer) are recognized to be highly dependent on the vapor temperature. For this reason, the heat transfer rates are first expressed as functions of the vapor temperature. From equations (2-20) and (2-17),

$$q''_{wv} = \frac{Nu^*}{(1-\Omega^2)}\frac{k_v}{2\delta}(T_w + \Omega T_l - (1+\Omega)T_v) \qquad (3-8)$$

$$q''_{wv} = \frac{Nu^*}{(1-\Omega^2)}\frac{k_v}{2\delta}(-\Omega T_w - T_l + (1+\Omega)T_v) \qquad (3-9)$$

The net volumetric heat flux received by the vapor is given by,

$$q'''_v = \frac{4}{D}(q''_{wv} - q''_{vl}) = A_1 + A_2 T_v \qquad (3-10)$$

where

$$A_1 = \frac{2Nu^* k_v}{D\delta(1-\Omega)}(T_w + T_l) \qquad (3-11)$$

$$A_2 = -\frac{k_v Nu^*}{D\delta(1-\Omega)} \qquad (3-12)$$

The interfacial mass transfer rate is also dependent on the vapor temperature, because vapor-to-liquid convection contributes to the evaporation heat flux.

$$q'''_{evap} = \frac{4}{D}(q''_{vl} + q''_{rad} - q''_{lH}) \qquad (3-13)$$

$$\begin{aligned} m'''_l &= \frac{q'''_{evap}}{h_{fg}} \\ &= A_3 + A_4 T_v \end{aligned} \qquad (3-14)$$

where

$$A_3 = \frac{4}{Dh_{fg}}(q''_{rad} - q''_{lH} + \frac{k_v Nu^*}{(1-\Omega^2)2\delta}(-\Omega T_w - T_l)) \qquad (3-15)$$

$$A_4 = \frac{2}{Dh_{fg}} \frac{k_v Nu^*}{\delta(1-\Omega)} \qquad (3-16)$$

The vapor energy equation is then implicity finite differenced as follows:

$$H_{v_j}^{n+1} = H_{v_j}^N + \frac{\Delta t}{\Delta z}\left(H_{v_{j-1}}^{n+1} u_{v_{j-1}}^{n+1} - H_{v_j}^{n+1} u_{v_j}^{n+1}\right) + \Delta t\left(q'''^{n+1}_{v_j} + m'''^{n+1}_{l_j} h_{v,\,\mathrm{sat}}\right) \qquad (3-17)$$

Since, $H_{v_j}^{n+1} = \rho_{v_j}^{n+1} \alpha_{v_j}^{n+1} h_{v_j}^{n+1}$, we can rearrange equation (3-17) and solve for $h_{v_j}^{n+1}$.

$$h_{v_j}^{n+1} = \frac{H_{v_j}^N + \frac{\Delta t}{\Delta z} H_{v_{j-1}}^{n+1} u_{v_{j-1}}^{n+1} + \Delta t(q'''^{n+1}_{v_j} + m'''^{n+1}_{l_j} h_{v,sat})}{M_{v_j}^{n+1} + \frac{\Delta t}{\Delta z} G_{v_j}^{n+1}} \qquad (3-18)$$

The vapor continuity equation is also implicitly finite differenced as follows:

$$M_{v_j}^{n+1} = M_{v_j}^N + \frac{\Delta t}{\Delta z}(G_{v_{j-1}}^{n+1} - G_{v_j}^{n+1}) + \Delta t m'''^{n+1}_{l_j} \qquad (3-19)$$

The terms in the denominator of equation (3-18) are not known, but can be replaced with an expression which comes from equation (3-19). Also, by using equations (3-10) and (3-13), the following equation is obtained:

$$h_{v_j}^{n+1} = \frac{H_{v_j}^N + \frac{\Delta t}{\Delta z} H_{v_{j-1}}^{n+1} u_{v_{j-1}}^{n+1} + \Delta t\left(q'''^{n+1}_{v_j} + m'''^{n+1}_{l_j} h_{v,\,\mathrm{sat}}\right)}{M_{v_j}^{n+1} + \frac{\Delta t}{\Delta z} G_{v_j}^{n+1}} \qquad (3-20)$$

Since,

$$h_v = c_{p_v}(T_v - T_{sat}) + h_{v,sat} \qquad (3-21)$$

the left hand side of equation (3-8) is an explicit function of $T_{v_j}^{n+1}$ and rearrangement of the equation leads to a quadratic equation in $T_{v_j}^{n+1}$.

$$a(T_{v_j}^{n+1})^2 + bT_{v_j}^{n+1} + c = 0 \qquad (3-22)$$

where

$$a = c_{p_v} A_4 \Delta t \tag{3-23}$$

$$b = c_{p_v} M_{v_j}^N + \frac{\Delta t}{\Delta z} G_{v_{j-1}}^{n+1} c_{p_v} + A_3 \Delta t c_{p_v}$$

$$-A_2 \Delta t - h_{v,sat} A_4 \Delta t \tag{3-24}$$

$$c = (h_{v,sat} - c_{p_v} T_{sat})(\frac{\Delta t}{\Delta z} G_{v_{j-1}}^{n+1} + M_{v_j} + A_3 \Delta t) - H_{v_j}^N$$

$$-\frac{\Delta t}{\Delta z} H_{v_{j-1}}^{n+1} u_{v_{j-1}}^{n+1} - \Delta t A_1 - \Delta t A_3 h_{v,sat} \tag{3-25}$$

The desired value is the positive root of the quadratic equation (3-22).

$$T_{v_j}^{n+1} = \frac{-b + \sqrt{b^2 - 4ac}}{2a} \tag{3-26}$$

With the vapor temperature determined, various heat transfer rates can be calculated from equations (3-8), (3-9), (3-10), and (3-12). Interfacial mass transfer can be calculated from equation (3-14). Various vapor properties are also calculated with the new temperature. Vapor density is given by,

$$\rho_{v_j}^{n+1} = \rho_v(T_{v_j}^{n+1}) \tag{3-27}$$

$$M_{v_j}^{n+1} = \rho_{v_j}^{n+1} \alpha_{v_j}^{n+1} \tag{3-28}$$

3) the vapor continuity equation is finite differenced as follows to find the vapor mass flux and velocity.

$$G_{v_j}^{n+1} = G_{v_{j-1}}^{n+1} - \frac{\Delta z}{\Delta t}(M_{v_j}^{n+1} - M_{v_j}^{n+1}) + \Delta z m_{l_j}^{'''n+1} \tag{3-29}$$

$$u_{v_j}^{n+1} = G_{v_j}^{n+1} / M_{v_j}^{n+1} \tag{3-30}$$

Equations (3-18) and (3-29) are solved together from the quench front node upward. Thus, the values of the dependent variables H_v, G_v, M_v, and u_v at the $(j-1)$th node are all known, when their values at the j th node are to be calculated.

4) the momentum equations are solved as follows. First, the shear stress terms are evaluated from equations (2-42), or equations(2-55) and (2-56) with the most recent estimates of vapor velocity.

$$\tau_{i_j}^{'''n+1} = \tau_i'''(\alpha_{v_j}^{n+1}, \alpha_{l_j}^{n+1}, u_{v_j}^{n+1}, u_{l_j}^{n+1}, \rho_{v_j}^{n+1}) \qquad (3-31)$$

$$\tau_{wv_j}^{''' n+1} = \tau_{wv}'''(\alpha_{v_j}^{n+1}, \alpha_{l_j}^{n+1}, u_{v_j}^{n+1}, u_{l_j}^{n+1}, \rho_{v_j}^{n+1}) \qquad (3-32)$$

The vapor momentum equation is then finite-differenced to yield the vapor pressure.

$$\begin{aligned} p_{v_j}^{n+1} = p_{v_{j+1}}^{n+1} + \frac{\Delta z}{\alpha_{v_j}^{n+1}}[&(G_{v_j}^{n+1} - G_{v_j}^{N})/\Delta t + \\ &F(G_{v_j}^{n+1}u_{v_j}^{n+1} - G_{v_{j-1}}^{n+1}u_{v_{j-1}}^{n+1} -)/\Delta z + \\ &(1-F)(G_{v_{j+1}}^{n+1}u_{v_{j+1}}^{n+1} - G_{v_j}^{n+1}u_{v_j}^{n+1})/\Delta z + \\ &\tau_{i_j}^{'''n+1} + \tau_{wv_j}^{''' n+1} + M_{v_j}^{n+1}g - m_{l_j}'''] \end{aligned} \qquad (3-33)$$

where $F = 1$ when $G_{v_j}^{n} \geq 0$, otherwise $F = 0$

It is assumed that the pressure of the vapor in the dispersed flow regime is equal to the exit pressure, which is equal to the atmospheric pressure; therefore, the pressure at the top of the inverted annular flow regime is considered to be equal to the exit, and equation (3-33) is solved from the top node downward.

5) the liquid momentum equation is finite-differenced as follows:

$$\begin{aligned} G_{l_j}^{n+1} = G_{l_j}^{N} + \Delta t[&F(G_{l_{j-1}}^{n+1}u_{l_{j-1}}^{n+1} - G_{l_j}^{n+1}u_{l_j}^{n+1} -)/\Delta z + \\ &(1-F)(G_{l_j}^{n+1}u_{l_j}^{n+1} - G_{l_{j+1}}^{n}u_{l_{j+1}}^{n})/\Delta z + \end{aligned}$$

$$\alpha_{l_j}^{n+1}(p_{l_j}^{n+1} - p_{l_{j+1}}^{n+1})/\Delta z + \Delta p_{lv_j}^{n+1}(\alpha_{l_{j+1}}^{n+1} - \alpha_{l_j}^{n+1})/\Delta z$$

$$+\tau_{i_j}''' - M_{l_j}^{n+1} g - m_{l_j}''' u_{l_j}^n] \qquad (3-34)$$

The term $G_{l_j}^{n+1} u_{l_j}^{n+1}$ can be written as $(G_{l_j}^{n+1})^2/M_{l_j}^{n+1}$ and brought to the left hand side. The result is a quadratic equation and solving that, $G_{l_j}^{n+1}$ can be found. The result is as follows:

$$a_1(G_{l_j}^{n+1})^2 + b_1 G_{l_j}^{n+1} + c_1 = 0 \qquad (3-35)$$

and

$$G_{l_j}^{n+1} = \frac{-b_1 + \sqrt{b_1^2 - 4a_1c_1}}{2a_1} \qquad (3-35a)$$

where

$$a_1 = \Delta t/\Delta z M_{l_j}^{n+1} \qquad (3-36)$$

$$b_1 = 1 \qquad (3-37)$$

$$c_1 = -G_{l_j} + \Delta t[[-FG_{l_{j_1}}^{n+1} u_{l_{j_1}}^{n+1} + (1-F)G_{l_{j+1}}^{n+1} u_{l_{j+1}}^{n+1}]/\Delta z -$$

$$\alpha_{l_j}^{n+1}(p_{l_j}^{n+1} - p_{l_{j+1}}^{n+1})/\Delta z - \Delta p_{lv_j}^{n+1}(\alpha_{l_{j+1}}^{n+1} - \alpha_{l_j}^{n+1})/\Delta z -$$

$$\tau_{i_j}'''^{n+1} + M_{l_j}^{n+1} g + m_{l_j}''' u_{l_j}^n] \qquad (3-38)$$

The equations described in the steps 1-5 are solved iteratively at each time step until the solution converges.

6) the liquid energy equation is solved explicitly outside the iteration loop for the above five equations. It is finite-differenced as follows, with a superscript, N, indicating the time step.

$$H_{l_j}^{N+1} = H_{l_j}^N + \Delta t[F(u_{l_{j-1}}^N H_{l_{j-1}}^N - u_{l_j}^N H_{l_j}^N)/\Delta z +$$

$$(1-F)(u_{l_j}^N H_{l_j}^N - u_{l_{j+1}}^N H_{l_{j+1}}^N)/\Delta z]-$$

$$\Delta t m_{l_j}^{'''N} h_{l,sat} + \Delta t q_{lH_j}^{'''N} \qquad (3-39)$$

The above overall solution scheme for the inverted annular flow regime is shown by a flowchart in figure (3-1).

3.2 Dispersed Flow Film Boiling

The steps for the numerical solution of this region are:

1) the drop continuity equation is explicitly finite differenced as follows:

$$(\rho_l \alpha_l)_j^{N+1} = (\rho_l \alpha_l)_j^N + \frac{\Delta t}{\Delta z}[(\rho_l \alpha_l u_d)_{j-1}^N - (\rho_l \alpha_l u_d)_j^N] - m_{l_j}^{'''N} \Delta t \qquad (3-40)$$

Assuming the liquid density to be constant, solution of the above equation yields liquid and void fractions at the new time step.

$$\alpha_{l_j}^{N+1} = (\rho_l \alpha_l)_j^{N+1}/\rho_l \qquad (3-41)$$

$$\alpha_{l_j}{}^{N+1} = 1 - \alpha_{l_j}^{N+1} \qquad (3-42)$$

2) the vapor continuity and energy equations are both implicitly finite differenced as follows:

$$(\rho_v \alpha_v)_j^{N+1} = (\rho_v \alpha_v)_j^N + \frac{\Delta t}{\Delta z}[(\rho_v \alpha_v u_v)_{j-1}^N - (\rho_v \alpha_v u_v)_j^N] + m_l^{'''N} \Delta t (3-43)$$

$$(\rho_v \alpha_v h_v)_j^{N+1} = (\rho_v \alpha_v h_v)_j^N \frac{\Delta t}{t}[(\rho_v \alpha_v u_v u_v h_{v_{j-1}})_{j-1}^N - (\rho_v \alpha_l u_v h_{v_j})_j^N] +$$

$$(q_{v_j}^{'''N+1} + m_l^{'''N+1} h_{v,sat})\Delta_t \qquad (3-44)$$

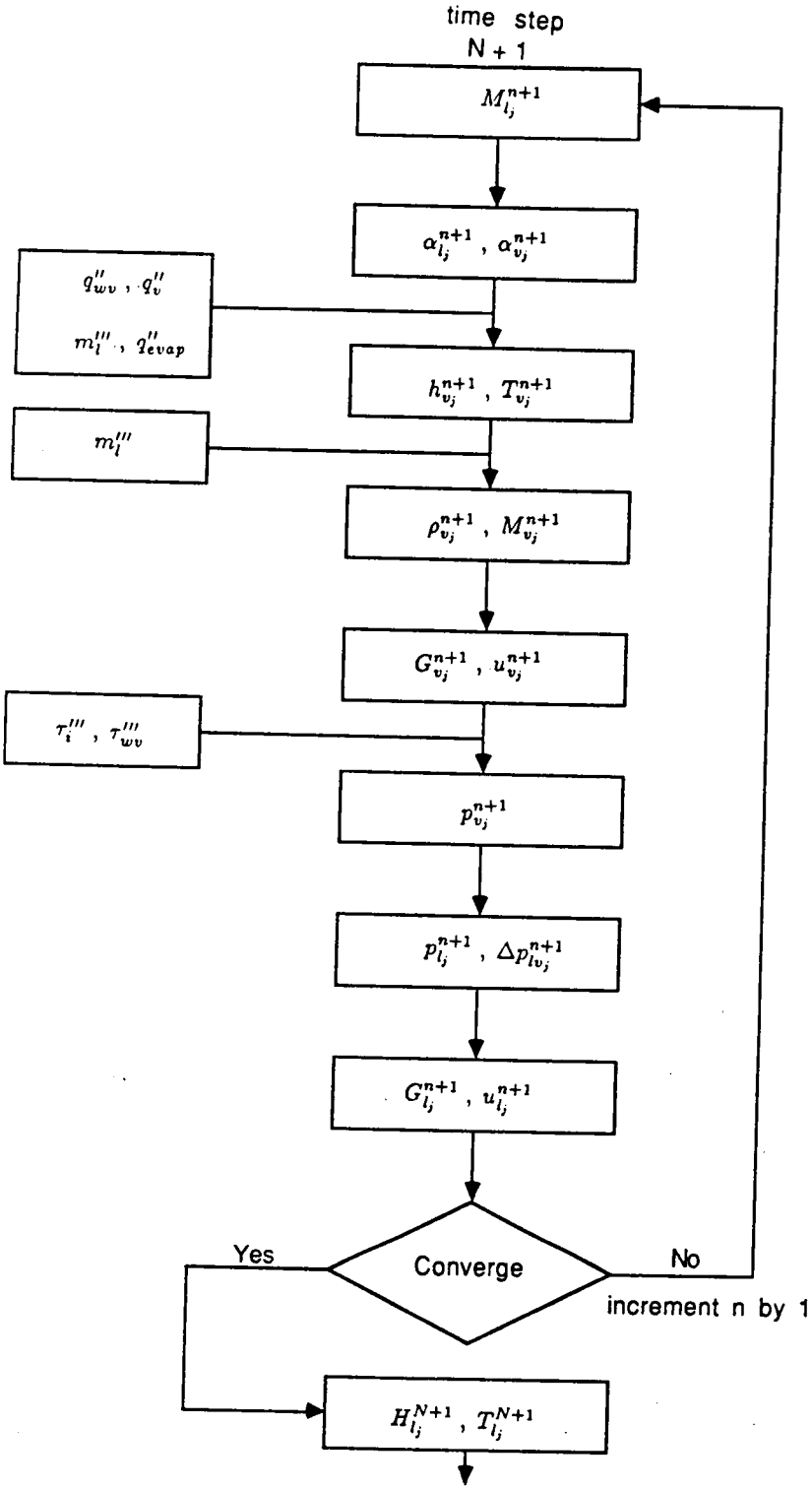

Figure 3-1. Inverted Annular Flow Solution Scheme.

The above equations are then combined to give the specific enthalpy of vapor.

$$h_{v_j}^{N+1} = \frac{(\rho_v \alpha_v h_v)_j^N + \frac{\Delta t}{\Delta z}(\rho_v \alpha_v u_v)_{j-1}^{N+1} h_{v_{j-1}}^{N+1} + \Delta t \left(q_{v_j}^{'''N+1} + m_{j_j}^{'''N+1} h_{v,\,\mathrm{sat}} \right)}{(\rho_v \alpha_v)_j^N + \frac{\Delta t}{\Delta z}(\rho_v \alpha_v u_v)_{j-1}^{N+1} + m_{l_j}^{'''N+1} \Delta t} \tag{3-45}$$

In this equation, $h_{v_j}^{N+1}$, $m_{l_j}^{'''N+1}$, and $q_{v_j}^{'''N+1}$ are all dependent on the vapor temperature at the new time step, $T_{v_j}^{N+1}$.

Assuming that the most dominant effect of the vapor temperature on the vaporization rate is through vapor-to-drop convection, the mass transfer term is written as follows:

$$m_{l_j}^{'''N+1} = \frac{1}{h_{fg}}[(q_{wd}^{'''} + q_{wd}^{'''r} + q_{vd}^{'''r} - q_{dH}^{'''})_j^N + A_{i_j}^{N+1} h_{vd_j}^{N+1}(T_{v_j}^{N+1} - T_{d_j}^N)] \tag{3-46}$$

For vapor heating flux, the dominant effect of the vapor temperature is assumed to be on the convection rate from wall to vapor and from vapor to drops.

$$q_{v_j}^{'''N+1} = (q_{wv}^{'''r} - q_{vd}^{'''r})_j^N + \frac{4}{D_t} h_{wvj}{}^{N+1}(T_{w_j}^N - T_{v_j}^{N+1})$$

$$- A_{i_j}^{'''N+1} h_{vd_j}^{N+1}(T_{v_j}^{N+1} - (T_{v_j}^{N+1} - T_{d_j}^N) \tag{3-47}$$

By substituting equations (3-46) and (3-47) into equation (3-45), and using the following relation,

$$h_v = h_{v,sat} + c_{p_v}(T_v - T_{sat}) \tag{3-48}$$

equation (3-45) can be reduced to a quadratic equation in $T_{v_j}^{N+1}$.

$$a_2(T_{v_j}^{N+1})^2 + b_2 T_{v_j}^{N+1} + c_2 = 0 \tag{3-49}$$

where

$$a_2 = c_{p_{v_j}}^{N+1} \frac{\Delta t}{h_{f_g}} A_{i_j}^{'''N+1} h_{g_{d_j}}^{N+1} \tag{3-50}$$

$$b_2 = c_{p_{v_j}}^{N+1}\left[(\rho_v\alpha_v)_j^N + \frac{\Delta t}{\Delta z}(\rho_v\alpha_v u_v)_{j-1}^{N+1}\right.$$
$$\left. + \frac{\Delta t}{h_{f_g}}\left(q'''_{w_d} + q'''^{r}_{v_d} + q'''^{r}_{w_d} - q'''_{d_H}\right)_j^N - \frac{\Delta t}{h_{f_g}} A'''^{N+1}_{i_j} h^{N+1}_{v_{d_j}} T^N_{d_j}\right]$$
$$+ h_{v,\mathrm{sat}} A'''^{N+1}_{i_j} h^{N+1}_{v_{d_j}} \frac{\Delta t}{h_{f_g}} - c^{N+1}_{p_{v_j}} T_{\mathrm{sat}} A'''^{N+1}_{i_j} h^{N+1}_{v_{d_j}} \frac{\Delta t}{h_{f_g}}$$
$$- \frac{4\Delta t}{D\Delta z} h^{N+1}_{w_{v_j}} + A'''^{N+1}_{i_j} h^{N+1}_{v_{d_j}} \frac{\Delta t}{\Delta z} + \frac{\Delta t}{\Delta z h_{f_g}} A'''^{N+1}_{i} h^{N+1}_{v_{d_j}} \qquad (3-51)$$

$$c_2 = \left(h_{v,\mathrm{sat}} c^{N+1}_{p_{v_j}} T_{\mathrm{sat}}\right)\left[(\rho_v\alpha_v)_j^N + \frac{\Delta t}{\Delta z}(\rho_v\alpha_v u_v)_{j-1}^{N+1}\right.$$
$$\left. + \frac{\Delta t}{h_{f_g}}\left(q'''_{w_d} + q'''^{r}_{v_d} + q'''^{r}_{v_d} - q'''_{d_H}\right)_j^N - \frac{\Delta t}{h_{f_g}} A'''^{N+1}_{i_j} h^{N+1}_{v_{d_j}} T^N_{v_j}\right]$$
$$- (\rho_v\alpha_v h_v)_j^N - \frac{\Delta t}{\Delta z}(\rho_v\alpha_v u_v)^{N+1}_{j-1} h^{N+1}_{v_{j-1}}$$
$$- \frac{\Delta t}{\Delta z}\left\{\left(q'''^{r}_{w_v} - q'''^{r}_{v_d}\right)_j^N + \frac{4}{D} h^N_{w_{v_j}} T^N_{w_{v_j}} - A'''^{N+1}_{i_j} h^{N+1}_{v_{d_j}} T^N_{d_j}\right.$$
$$\left. + \frac{1}{h_{f_g}}\left[\left(q'''_{w_d} + q'''^{r}_{w_d} + q'''^{r}_{v_d} - q'''_{d_H}\right)_J^N - \frac{A'''^{N+1}_{i_j}}{h_{f_g}} h^{N+1}_{v_{d_j}} T^N_{d_j}\right]\right\} \qquad (3-52)$$

Once the vapor temperature at the new time step is calculated, the vapor density is determined and the vapor velocity is calculated from (3-43).

3) to find drop velocity and drop temperature, the drop momentum and energy equations are both explicitly finite differenced as follows: .

$$(\eta_l\rho_l\alpha_l u_d)_j^{N+1} = (\eta_l\rho_l\alpha_l u_d)_j^N - \frac{\Delta t}{\Delta z}[(\eta_l\rho_l\alpha_l u_d)_j^N u_{d_j}{}^N - (\eta_l\rho_l\alpha_l u_d)^N_{j-1} u^N_{d_{j-1}}]$$

$$+\Delta t[\tau'''^N_{d_j} - (\eta_l\rho_l\alpha_l)_j^N g - (\eta_l m'''_l u_d)_j^N] \qquad (3-53)$$

$$(\rho_l\alpha_l h_l)_j^{N+1} = (\rho_l\alpha_l h_l)_j^N - \frac{\Delta t}{\Delta z}[(\eta_l\rho_l\alpha_l u_d)_j^N h^N_{l_j} - (\eta_l\rho_l\alpha_l u_d)^N_{j-1} h^N_{l_{j-1}}]$$

$$+\Delta t(q'''^N_{dH_j} - m'''^N_{l_j} h_{l,sat}) \qquad (3-54)$$

The solution scheme described in this section is illustrated in Figure (3-2).

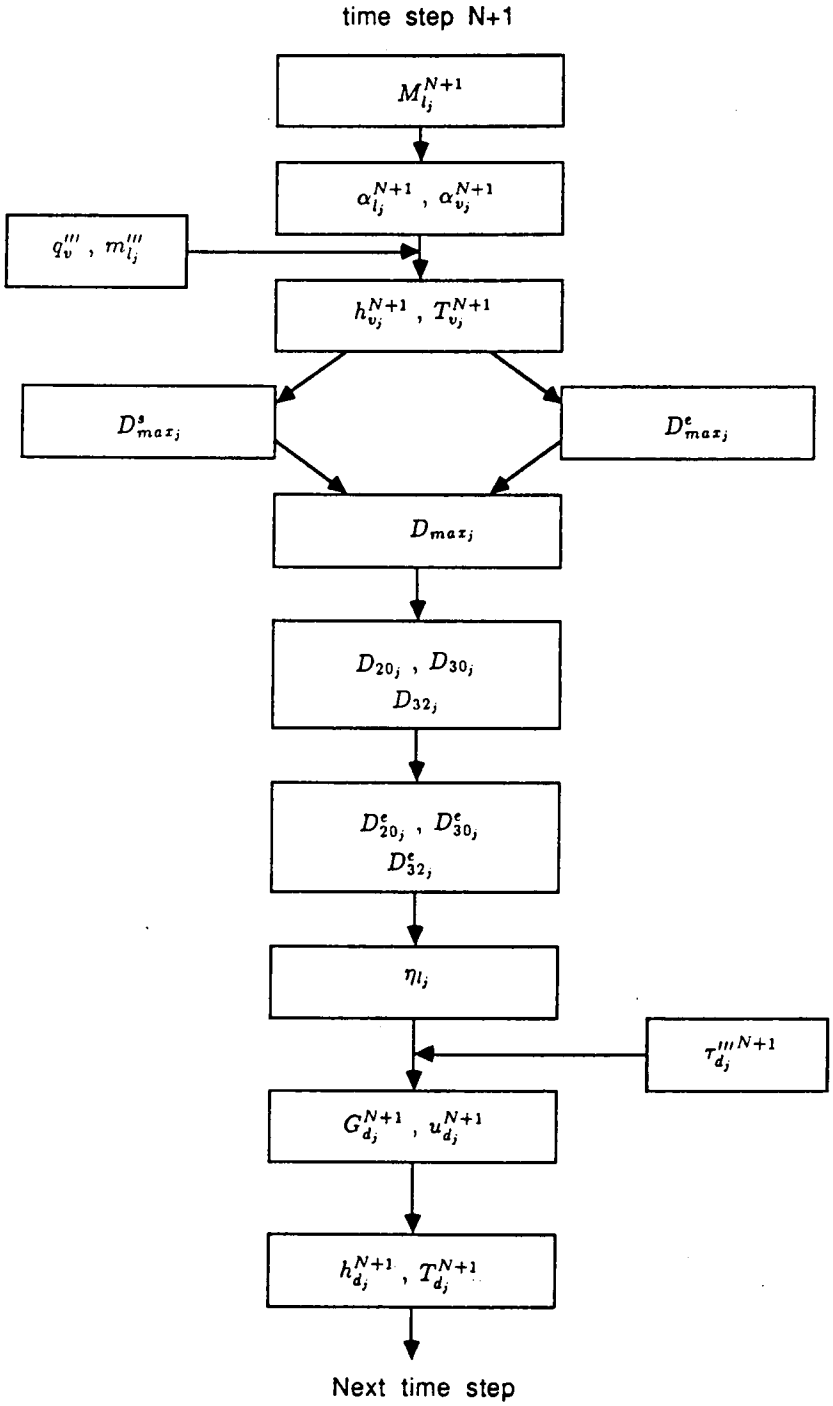

Figure 3-2. Dispersed Flow Solution Scheme.

3.3 Fully Liquid Region

In the liquid region, the velocity is assumed to be constant and equal to the inlet velocity. In order to find the liquid temperature, liquid energy equation (equation (2-121)) is finite differenced explicitly as follows:

$$h_{l_j}^{N+1} = h_{l_j}^{N} + \Delta t \left[\frac{4 q_w''^{N}}{D} - \frac{u_{l_{j+1}}^{N} h_{l_{j+1}}^{N} - u_{l_j}^{N} h_{l_j}^{N}}{\Delta z} \right] \qquad (3-55)$$

3.4 Heat Conduction in Flow Channel Wall

Equation (2-130) is solved numerically using an explicit finite difference method. The thermophysical properties are considered to be temperature dependent. The finite difference formulation of the equation is given by:

$$T_{w_j}^{N+1} = T_{w_j}^{N} + \frac{\Delta t}{(\rho_w c_{p_w})_j^{N}} \left[k_{w_j}^{N} \left(\frac{T_{w_{j+1}}^{N} - 2T_{w_j}^{N} + T_{w_{j-1}}^{N}}{(\Delta z)^2} \right) + \left(\frac{T_{w_{j+1}}^{N} - T_{w_j}^{N}}{\Delta z} \; \frac{k_{w_{j+1}}^{N} - k_{w_j}^{N}}{\Delta z} \right) - \frac{P_i}{A_w} \, q_{w_j}''^{N} \right] \qquad (3-56)$$

3.5 Overall Solution scheme

The objective of the present work is to investigate the flow channel wall temperature history and thermo-fluid parameters during the cooldown process. This section will describe the solution procedure, the nodalization, and the numerical stability criteria.

3.5.1 Solution Procedure

The flow channel is subdivided axially into a number of nodal points. The flow and heat transfer calculations are performed at every time step in order to

obtain the local wall heat transfer coefficient, which is required to determine the flow channel's wall temperature. The overall computational scheme is illustrated in figure (3-3), and the calculation procedures are as follows:

1) the input data is read and the variables are initialized.

2) the inverted annular flow regime calculations are performed. The solution scheme for the inverted annular flow regime was described in section (3-1), and a flow chart was shown in Figure (3-1). At each time step, volume fractions, phase velocities and pressures, vapor temperature and heat transfer rates are calculated at each fluid-dynamic node iteratively.

3) calculations continue for the single-phase liquid. In this step, liquid temperature from the inlet to the quench front is computed.

4) the dispersed flow model is solved as described in section (3-2) and shown by a flow chart (Figure 3-2). Volume fractions, phase velocities and temperatures, and heat transfer rates are calculated.

5) the wall temperature at the new time step is calculated.

6) in the model, quench front propagates forward during the cooldown with a velocity obtained from experimental data. At the end of each time step, the quench front location, and the dependent variables are updated for the next computation step.

3.5.2 Nodalization

For fluid-dynamic and heat-transfer calculations, two different grid sizes are used. A schematic of the flow channel and nodalization used in the computer code is shown in Figure (3-4). The nodalization is designed to save some computing time without sacrificing accuracy. The nodes are listed as follows:

1) each grid in the single-phase region, inverted annular flow and the axial

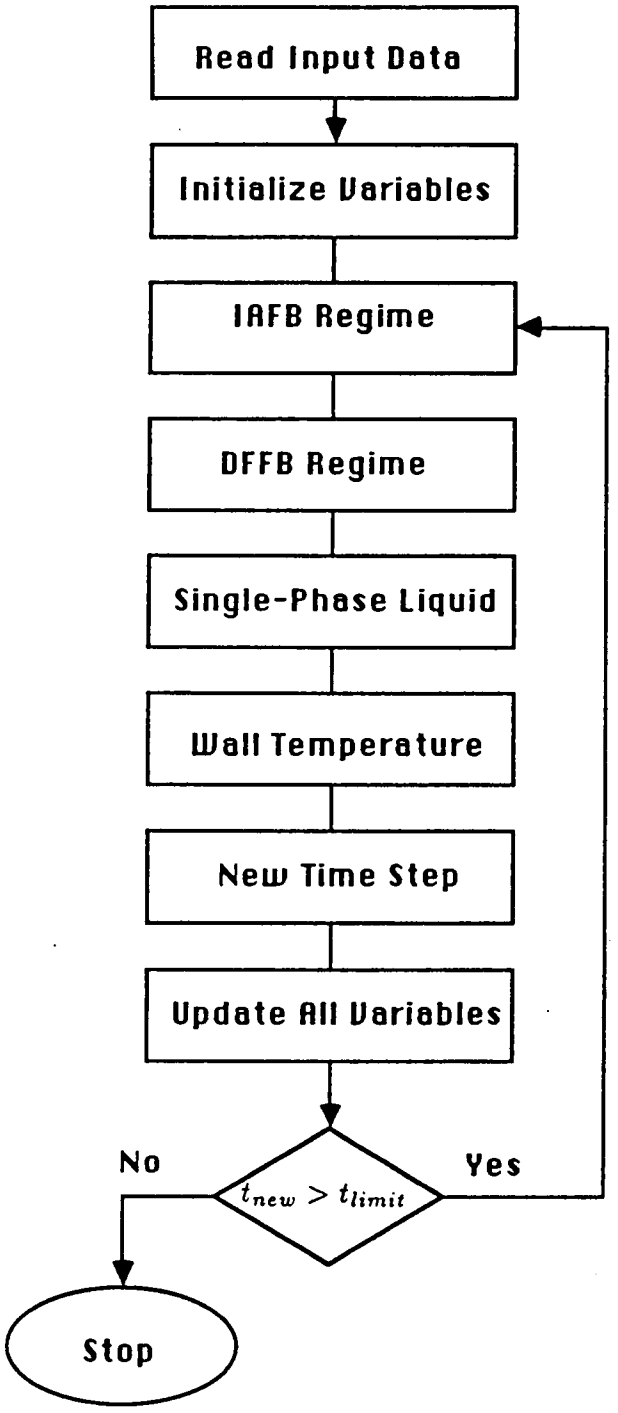

Figure 3-3. Overall Solution Scheme.

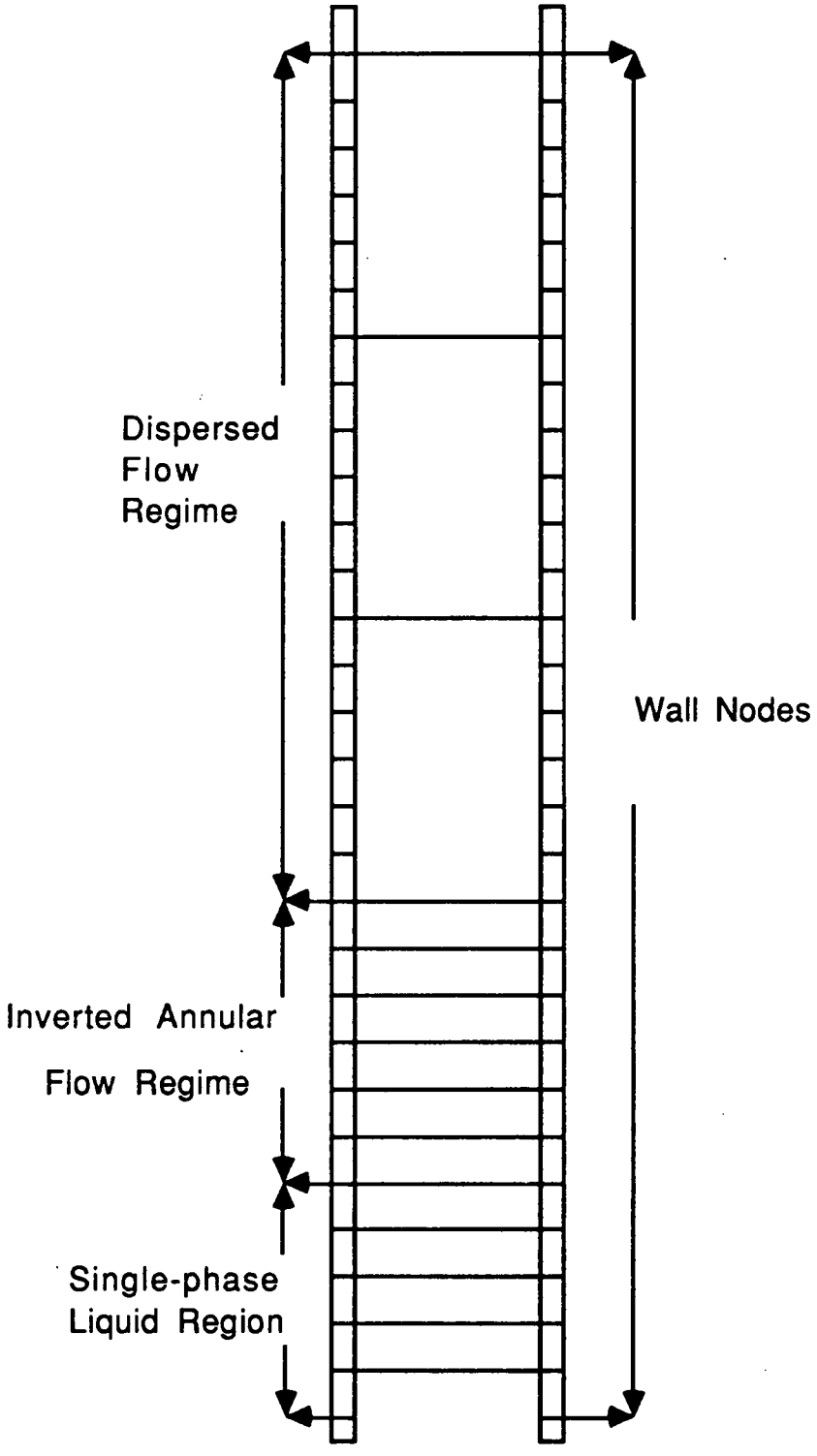

Figure 3-4. Noding Scheme.

grid spacing is equal to 1 inch.

2) each grid in the dispersed flow region is 13 inches.

3.5.3 Numerical Stability - Time Step Size

The time increment for the next time step is computed from the fluid-dynamic node size and maximum fluid velocity calculated in the previous time step, so that the Courant condition given below is not violated:

$$\frac{u_{max}\Delta t}{\Delta z} < 1 \qquad (3-57)$$

In the following chapter, the calculated results from the code will be analyzed and compared with experimental data.

CHAPTER IV

DISCUSSION AND RESULTS

In order to calculate the thermo-fluid parameters during the cooldown process, based on the model described in CHAPTER II and the numerical solutions discussed in CHAPTER III, a code was developed and validated for both water and liquid nitrogen as working fluids. The computed results are compared with the experimental data for water and liquid nitrogen. References [67], [68], [69], and [70] are used in order to calculate the thermodynamic and transport properties needed for the calculations. In the following sections, the comparison of calculations with experimental data in each case will be presented.

4.1.1 Description of Experiment for Water

In this case, the calculations were compared with Kawaji's data [71] for the bottom reflood of a heated vertical tube. The test section was 12 ft Inconel tube with 14.3-mm-id and 0.8-mm wall thickness and was resistance heated. The wall was not insulated and a convection heat transfer model from the wall to the surrounding was considered. The inlet flow rate was kept at a constant rate. Initial wall and inlet water temperatures were $1050^{o}\ F$ and $80^{o}\ F$, respectively. In addition, the quench front and its speed were determined from experimental data. The quench front equations for each test are as follows:

$$z_{qf} = At + Bt^2 + Ct^3 \qquad (4-1)$$

where

z_{qf} = Quench Front Location

t = Time

a) coolant inlet velocity 3 in/sec

$A = 1.10481360$, $B = 0.00271739$, $C = -0.00004313$; below 74 $in.$

$A = 1.25916755$, $B = -0.00197486$, $C = -0.00000755$; above 74 $in.$

b) coolant inlet velocity 5 in/sec

$A = 1.66089070$, $B = 0.01846154$, $C = -0.00032389$; below 74 $in.$

$A = 1.69043159$, $B = 0.00996912$, $C = -0.00012086$; above 74 $in.$

4.1.2 Results for Water

Simulation of two different reflood experiments (inlet velocities of 3 and 5 in/sec), indicated reasonably good agreement between the calculated values and the data as shown in Figure (4-1).

For both tests, the calculated values of the wall temperatures for lower elevations are in good agreement with the experimental values, while values for the higher elevations are underpredicted.

4.2.1 Description of Experiment for Liquid Nitrogen

For liquid nitrogen, the predicted values are compared with McGee's experimental data [72]. The purpose of his experimental investigation was to study the effect of quench front cooling, using cryogen cooling in a vertical copper tube. Liquid nitrogen was used as the working fluid and derived from a dewar into a test section from a pressurized GN2 tank. The experimental set up consisted of; 1) supply system; 2) test section; 3) data acquisition system. The experimental set up is shown in Figure (4-2). The tests were performed with tank pressures of 2-10 psi. The liquid inside the dewar was assumed to be at the saturation temperature.

The supply system, as shown in Figure 4-2, consisted of a pressurized dry

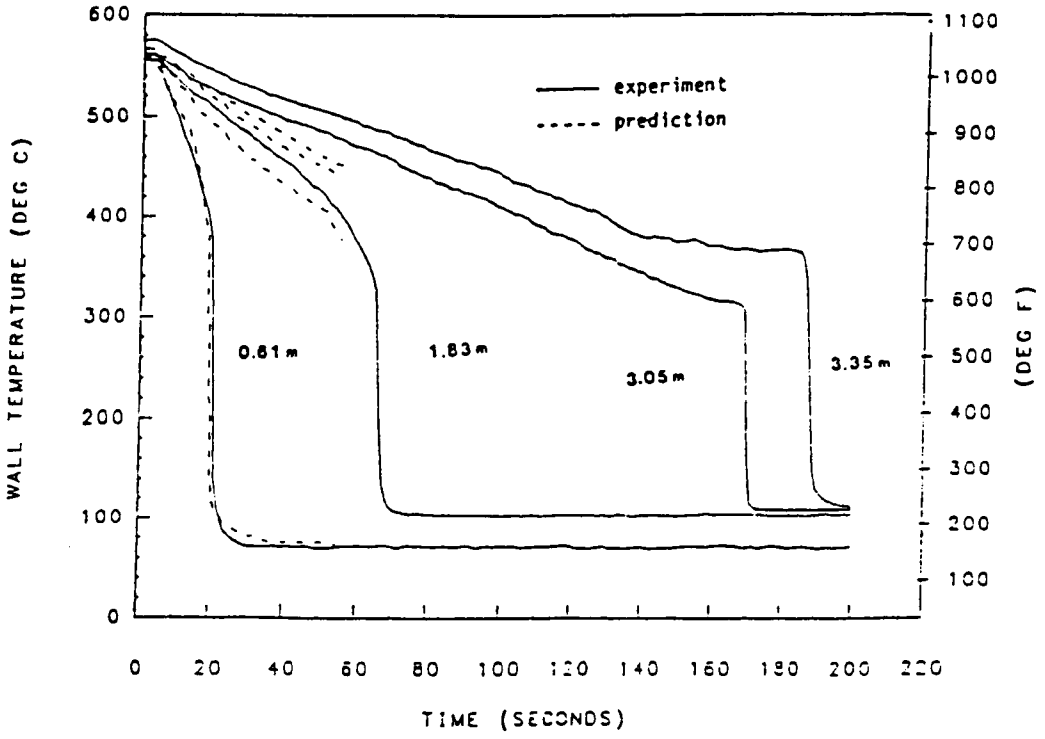

(inlet velocity = 3 in/sec)

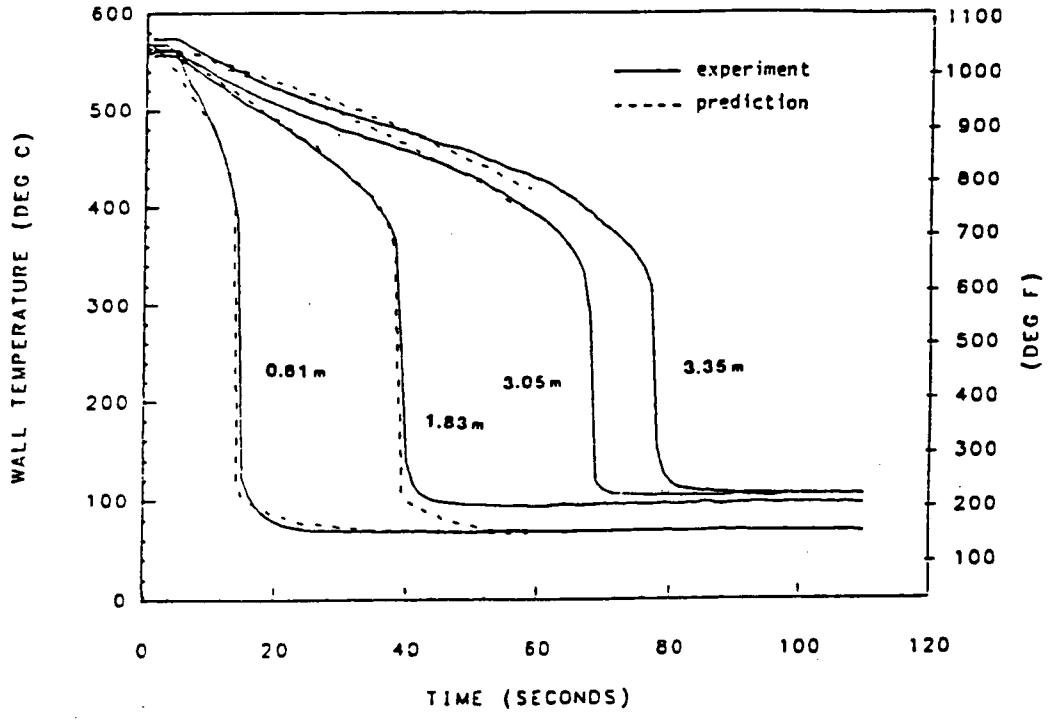

(inlet velocity = 5 in/sec)

Figure 4-1. Comparison of calculated results with experimental data (water).

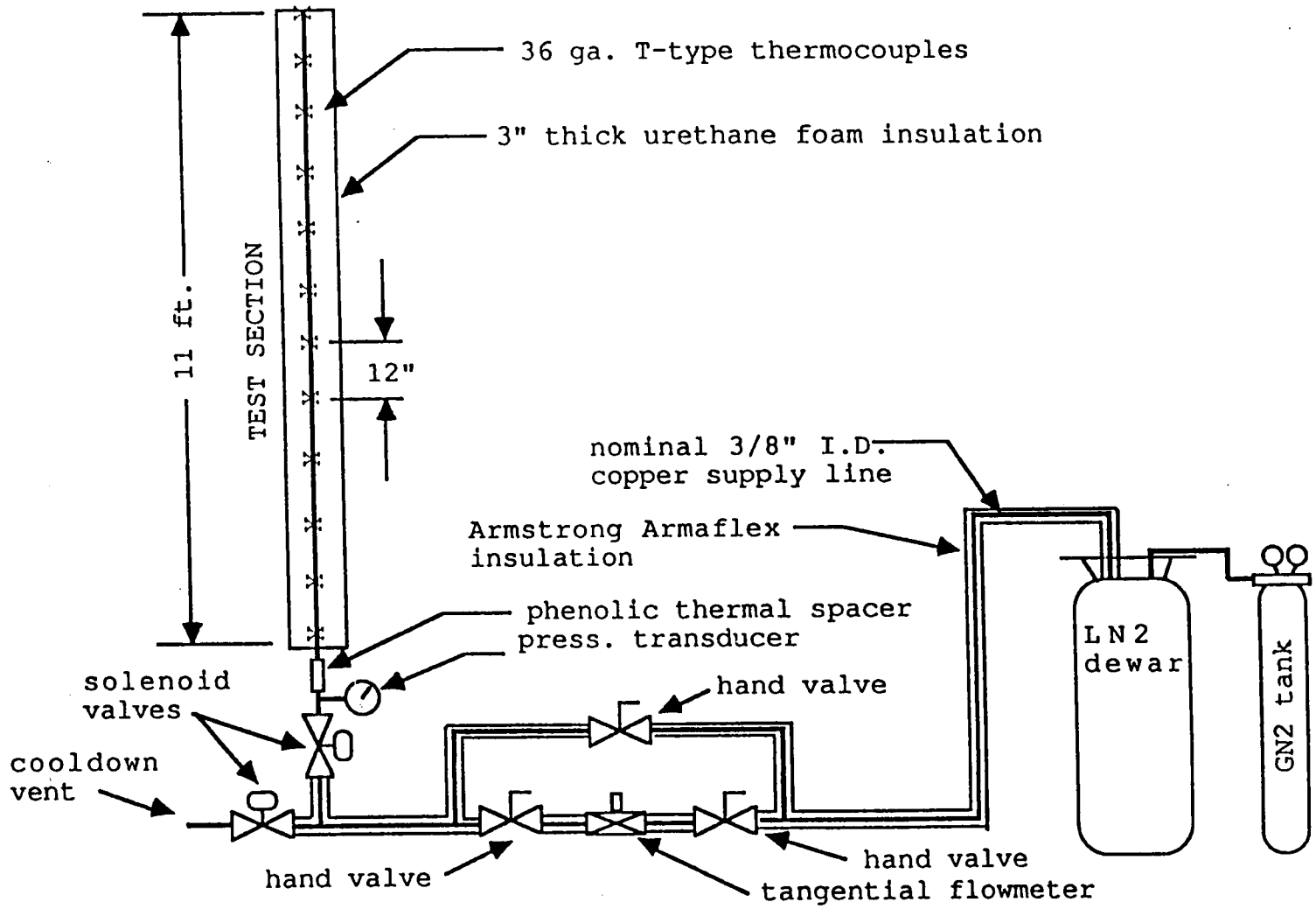

Figure4-2. Diagram of Set up for Cooldown Experiment, taken from McGee [72].

nitrogen gas tank, a 160 Liter dewar, a turbine flow meter, and a nominal 3/8 inch I.D. copper supply line. In order to minimize the heat flux to the supply line, the line was insulated. The turbine flow meter was used to monitor the liquid flow rate during the experiment. The supply line was cooled down to a stable operating temperature (near saturation temperature) before allowing the liquid to flow through the test section. The test section used to simulate a cryogenic transfer line was comprised of a 12 foot vertical section of nominal 3/8 in. I. D. copper tube. The test section was well insulated using a 3 inch thick urethane foam insulation. Thermocouples were placed every 12 inches along the test section. The LN2 and GN2 in the test section were allowed to vent to the atmosphere through the top of the test section during each run. Each test run was continued until quenching was achieved throughout the test section, and a stable operating temperature was maintained. The test matrix consisted of making runs at 2, 2.5, 3, 4, 5, 10 psig pressures supplied by the GN2 tank. In order to implement the computational procedure, quench front velocity (which is a necessary input parameter) can be found from the experimental results. The quench front information for different experimental conditions is shown in Figure 4-3.

4.2.2 Results for Liquid Nitrogen

The calculations to be presented for the liquid nitrogen were generated using two different versions. The model used in Version 1 is exactly as described in CHAPTER II. To improve the calculated results and to formulate the cooldown process as closely as possible to the experimental data, Version 2 was developed. Quench front velocity computed from the experimental data is used as an input parameter. The initial and boundary conditions are as follows:

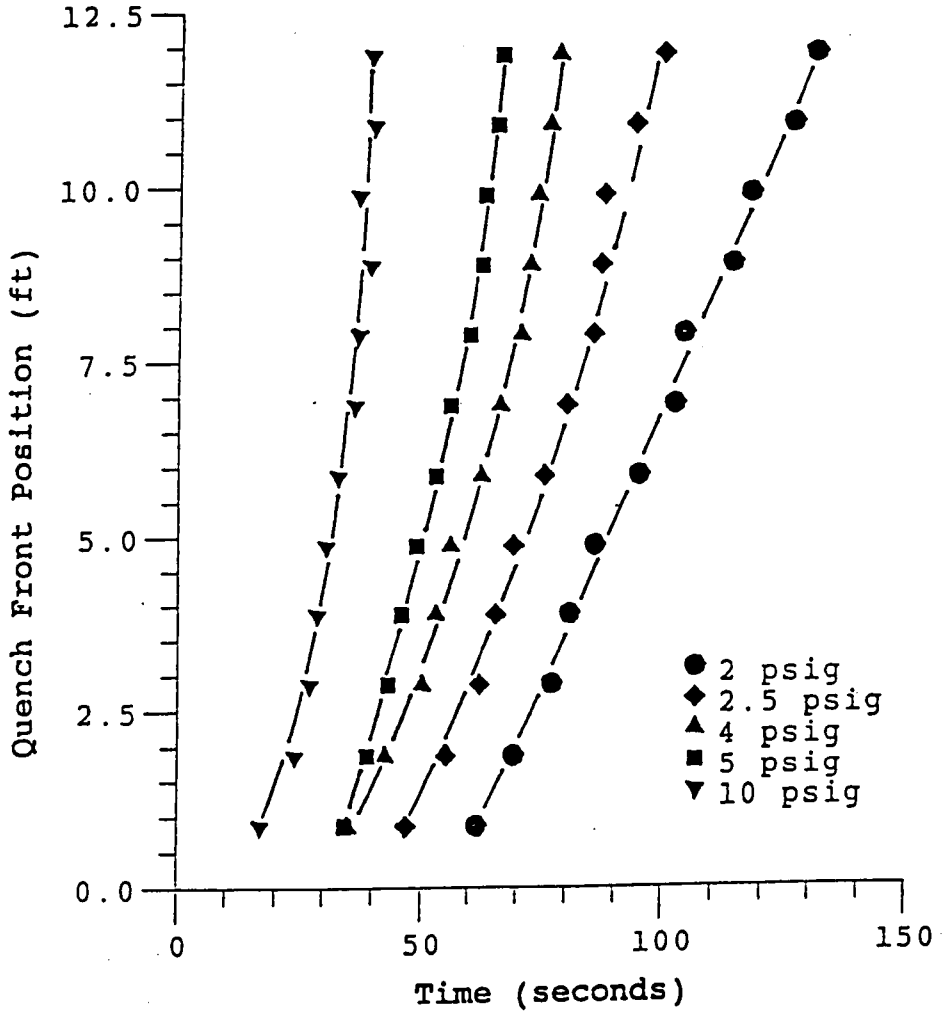

Figure 4-3. Quench Front Location Vs. Time, ref.[72].

Initial Conditions

1) tube wall has an initial temperature T_0, or for any location for the tube wall:

$$T_w = T_0$$

2) it is assumed that initially the tube is filled with the vapor at a film temperature (average of the wall and saturation temperatures),

$$T_v = T_{film}$$

where

$$T_{film} = 0.5(T_w + T_{sat})$$

Boundary Conditions

1) the initial vapor pressure in the tube is the same everywhere in the tube, and equal to the exit pressure which is at atmospheric pressure:

$$p_v = p_{atm}$$

2) the inlet liquid velocity is at a constant rate.

Table 4.1 shows the quench front gradient and inlet velocity for each test. The initial and boundary conditions are the same for both versions. A description of each version and comparison with the experimental results will be presented in the next subsections.

4.2.2.1 Version 1

In this case, it was considered that as soon as the inlet valve is opened the liquid enters into the inlet, and the flow field achieves a pattern as described in CHAPTER II, consisting of fully liquid, inverted annular flow, dispersed flow,

Table 4.1. Quench Front Gradient and Inlet Velocity

Test Run (psi)	Inlet Velocity (liquid) in/sec	Slope of $QF\frac{dz}{dt}$ in/sec
3	7.0	2.47218
5	11.5	4.12500
10	24.0	5.73493

and fully vapor. Calculations proceeded for the test run of 5 *psi* and comparison between the calculated and experimental results are shown in Figures 4-4 through 4-9 for this case. In this version, the calculated wall temperature for the lower elevations were overpredicted, while for the mid elevations, calculations were in a reasonable agreement with the experimental data. The results for the higher elevations (close to the top) were underpredicted. By careful reviewing of the quench front data (Figure 4-3), one can notice that quench time for the first location (1 ft) is almost half that of the last location (12 ft). Since the quench speed and movement are almost at a constant rate, the overprediction of the lower elevations could be due to the following hypothesis. Initially, the valve temperature is near room temperature, which is relatively much higher than the liquid temperature. When the inlet valve is opened and liquid passes through, it absorbs the heat and cools the valve down until its temperature drops to a value which allows the nitrogen to pass as a liquid. Therefore, in the initial period of the cooldown process, the tube wall could be cooled by the vapor generated at the inlet valve and not by the two-phase flow mechanism as described before. After the inlet valve is cooled to the temperature that allows the fluid to enter into the inlet as a single-phase liquid, the quench front starts moving and two-phase regions and flow field, which was described in CHAPTER II, will proceed. By adding a vapor cooling mechanism for the early portion of the cooldown time, Version 1 can be modified. This modification led to the development of Version 2, which will be discussed in the next subsection.

4.2.2.2 Version 2

In the second version, it is considered that when the inlet valve is opened and liquid enters into the line, the flow model is slightly different than Version 1.

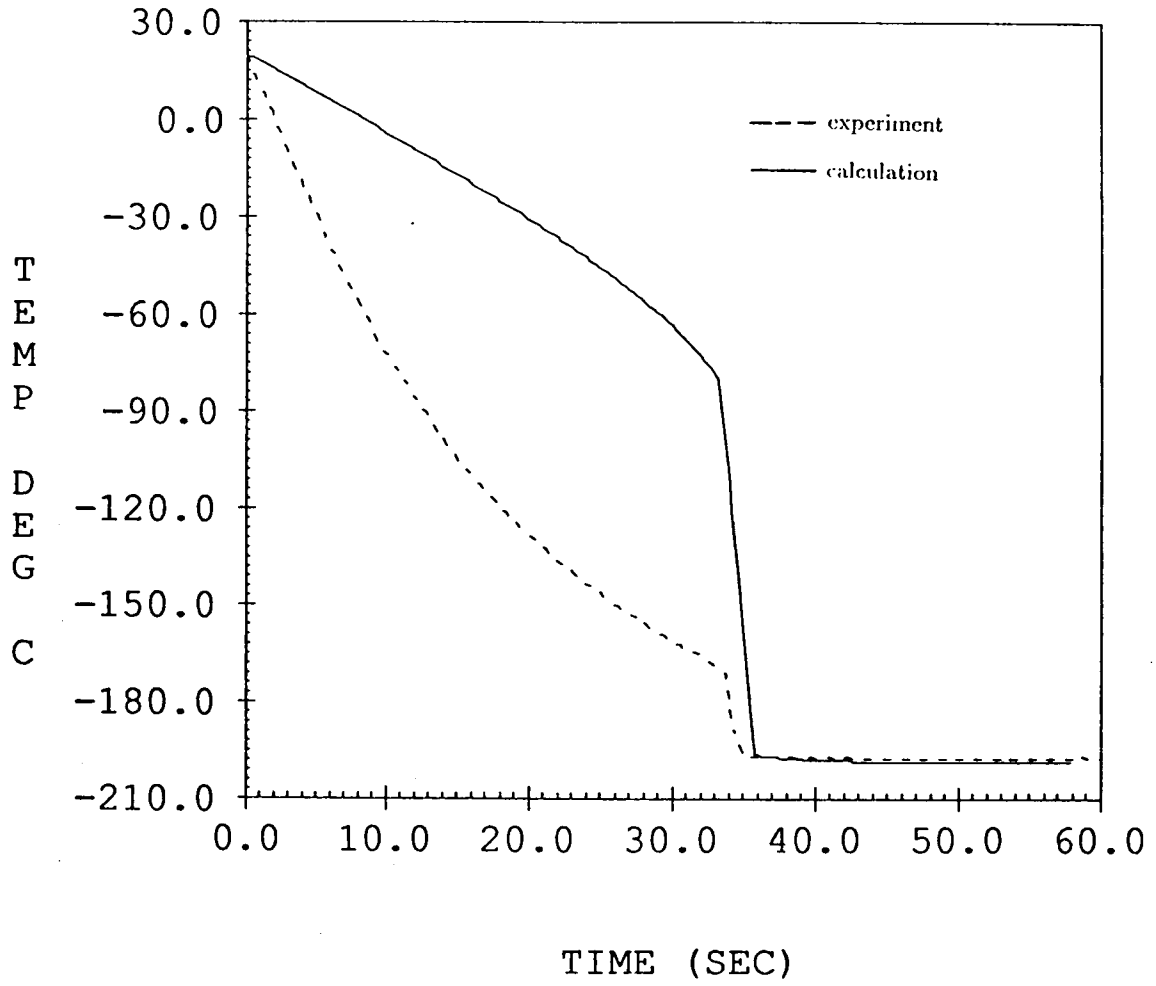

Figure 4-4. Version 1 Wall Temperature History at 1 *Ft* (Run 5 *psi*).

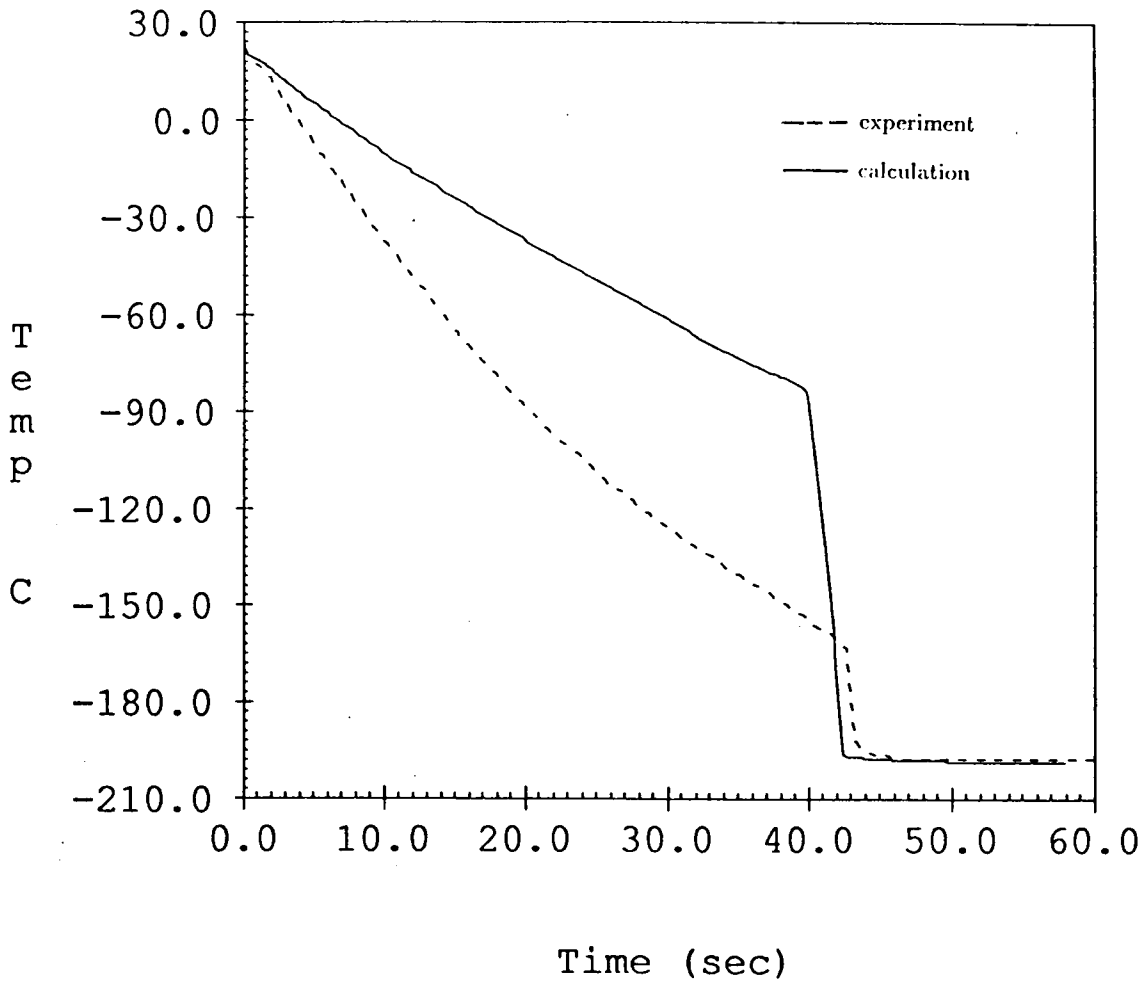

Figure 4-5. Version 1 Wall Temperature History at 3 *Ft* (Run 5 *psi*).

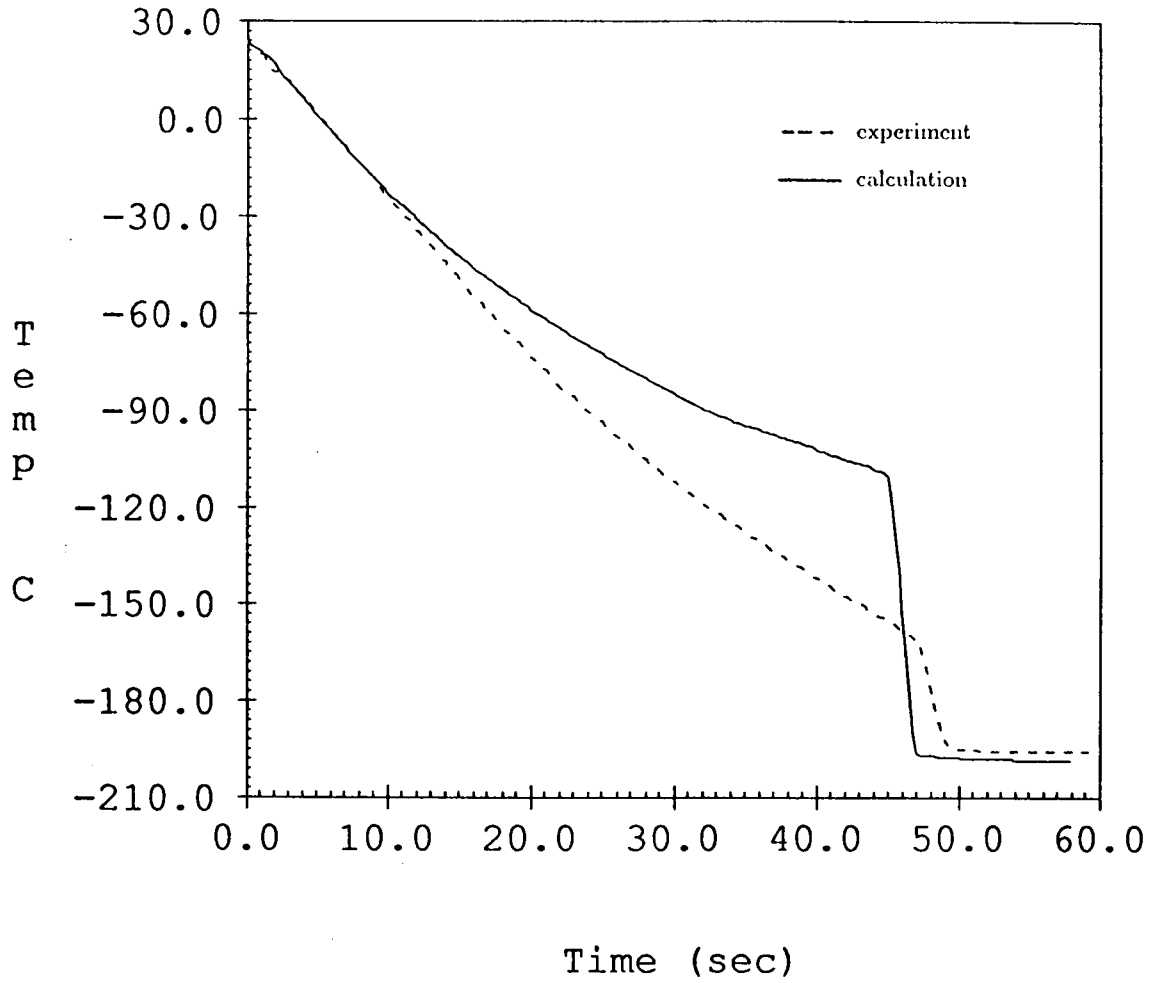

Figure 4-6. Version 1 Wall Temperature History at 5 *Ft* (Run 5 *psi*).

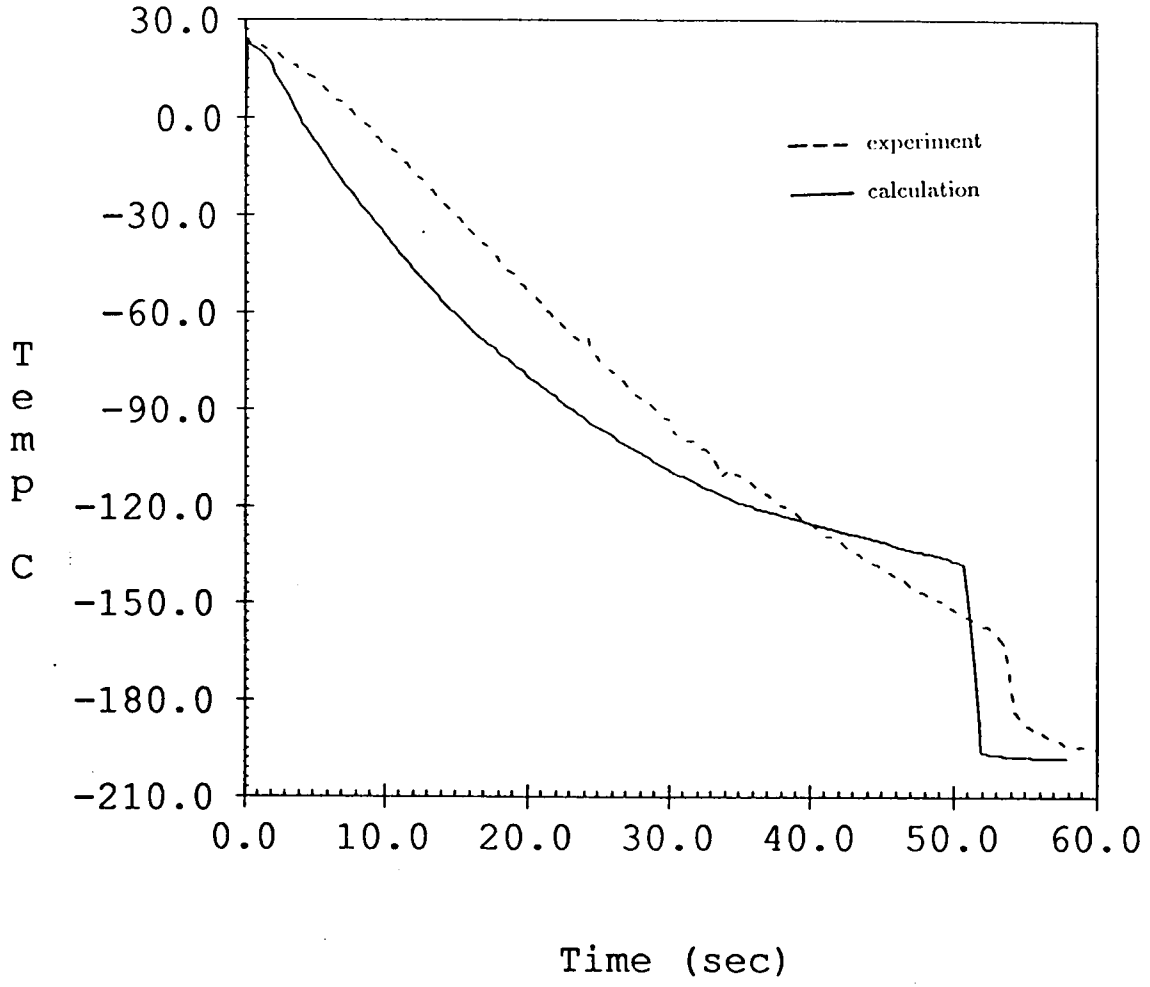

Figure 4-7. Version 1 Wall Temperature History at 7 *Ft* (Run 5 *psi*).

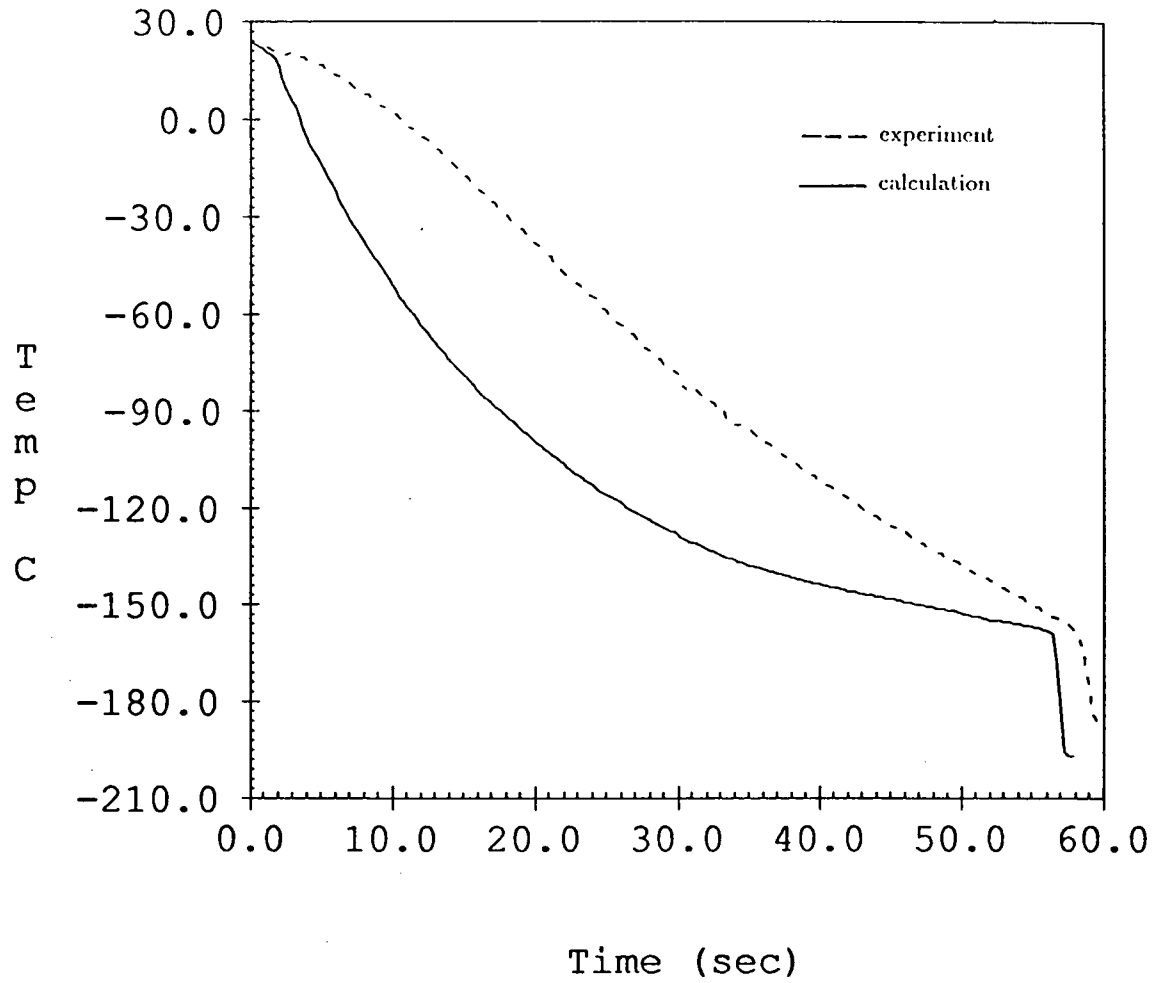

Figure 4-8. Version 1 Wall Temperature History at 9 *Ft* (Run 5 *psi*).

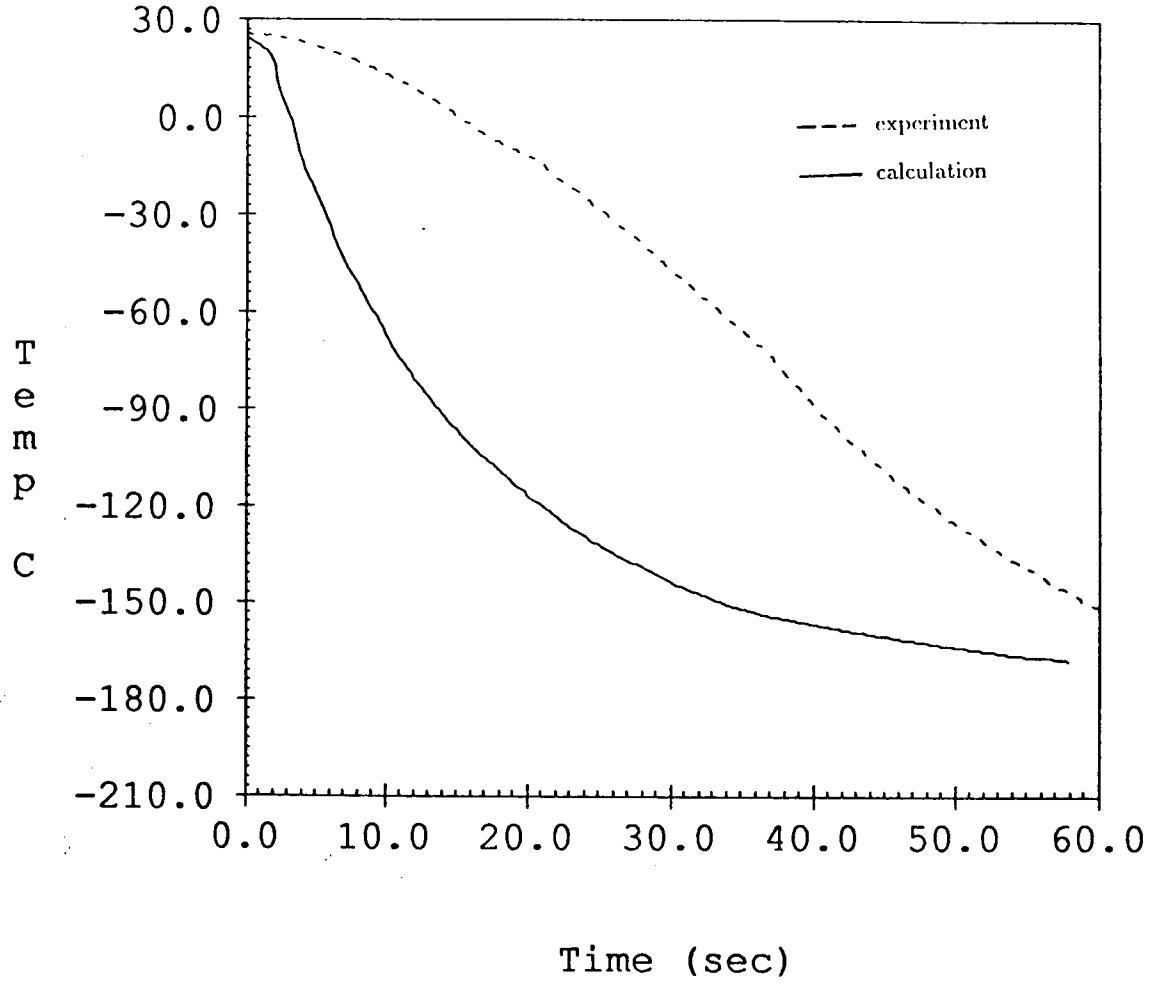

Figure 4-9. Version 1 Wall Temperature History at 11 *Ft* (Run 5 *psi*).

Initially the valve temperature is close to room temperature, which is much higher than the liquid temperature. It is assumed that, when liquid passes through the valve, liquid absorbs more heat and the valve temperature is reduced until it drops near saturation temperature which allows nitrogen to pass through as a liquid. Therefore, based on this assumption, it is considered that as the valve is opened, for some time the liquid absorbs the heat, vaporizes and this vapor enters into the line. Calculations in this version start with the vapor region, due to generation in the valve, and later the flow pattern follows with fully liquid, inverted annular flow, dispersed flow, and fully vapor. The following conditions are considered:

1) T_w (at the end of vapor cooling) = T_w (initial wall temperature for the two-phase cooling)

2) p_v (initial vapor pressure for the two-phase cooling) = p_{atm}

3) all conservation equations for each regime are one-dimensional

The calculations were performed for three different test runs (3, 5, and 10 *psi*) and comparison with the experimental results are illustrated in Figures 4-10 through 4-26 for each test. Indeed, this change has increased the accuracy of the predicted results. The predicted results are in good agreement with experimental results in the case of 5 and 10 *psi*. The values in the two-phase regions are over-predicted, which mean the heat fluxes are underpredicted. Several possible reasons could lead to underprediction of the heat flux.

In the inverted annular flow regime, the interfacial shear was modeled based on a laminar flow of vapor in a straight annulus. Lowering the interfacial factor would decrease the interfacial friction, which would decrease interfacial drag and lead to a thinner vapor film and, therefore, increased heat transfer rates. Another possible factor is the energy partition function, which determines the vaporization rate for a subcooled liquid column. The present model for the energy partition

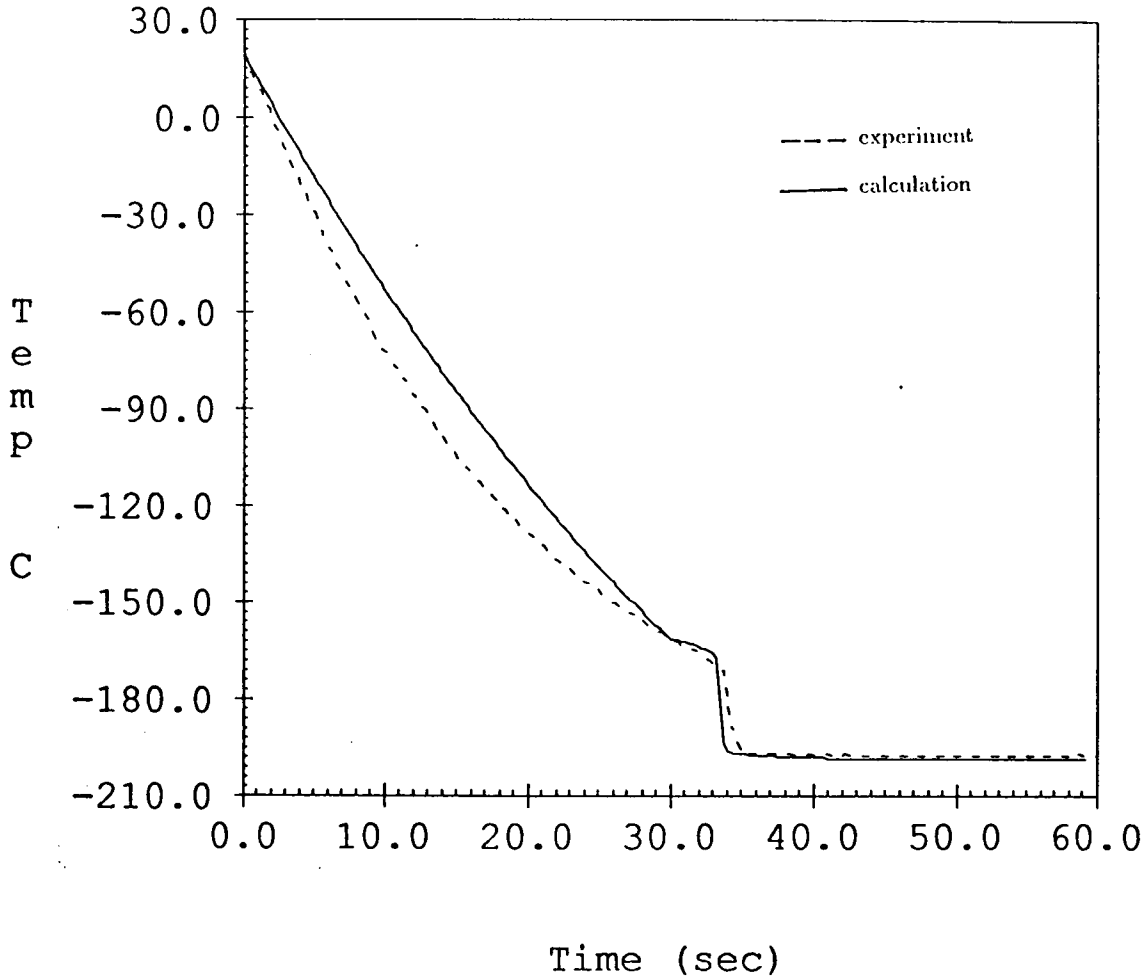

Figure 4-10. Version 2 Wall Temperature History at 1 Ft (Run 5 psi).

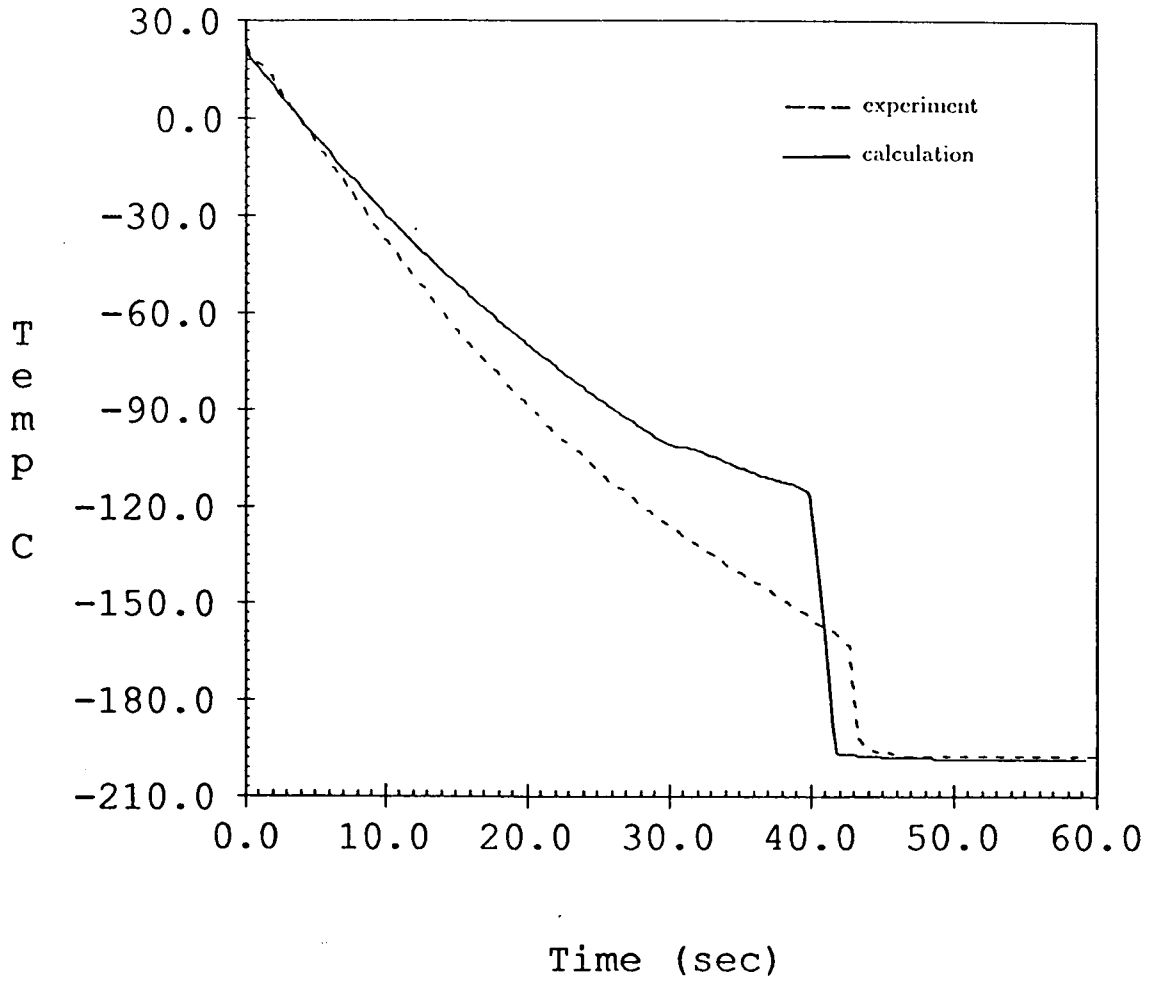

Figure 4-11. Version 2 Wall Temperature History at 3 *Ft* (Run 5 *psi*).

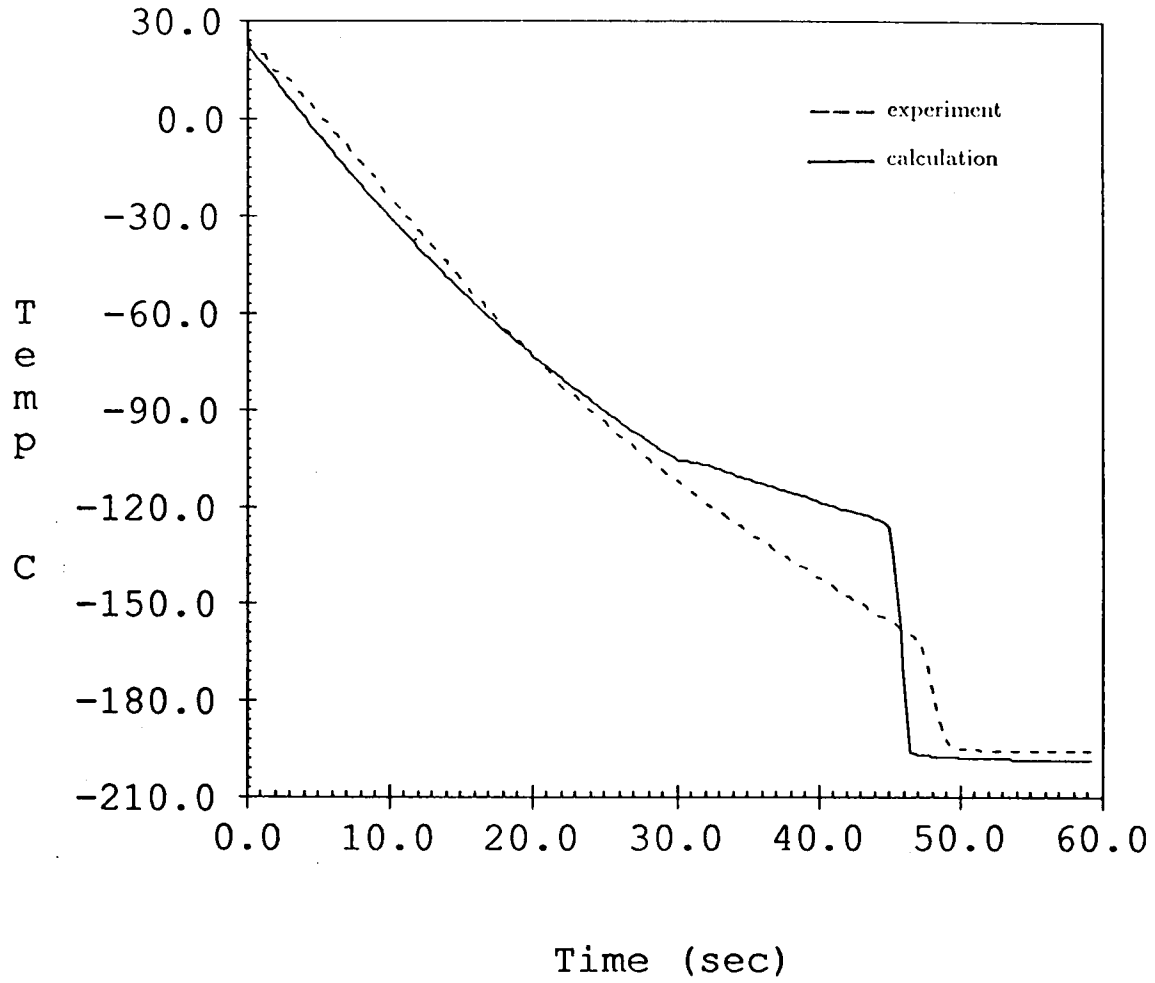

Figure 4-12. Version 2 Wall Temperature History at 5 Ft (Run 5 psi).

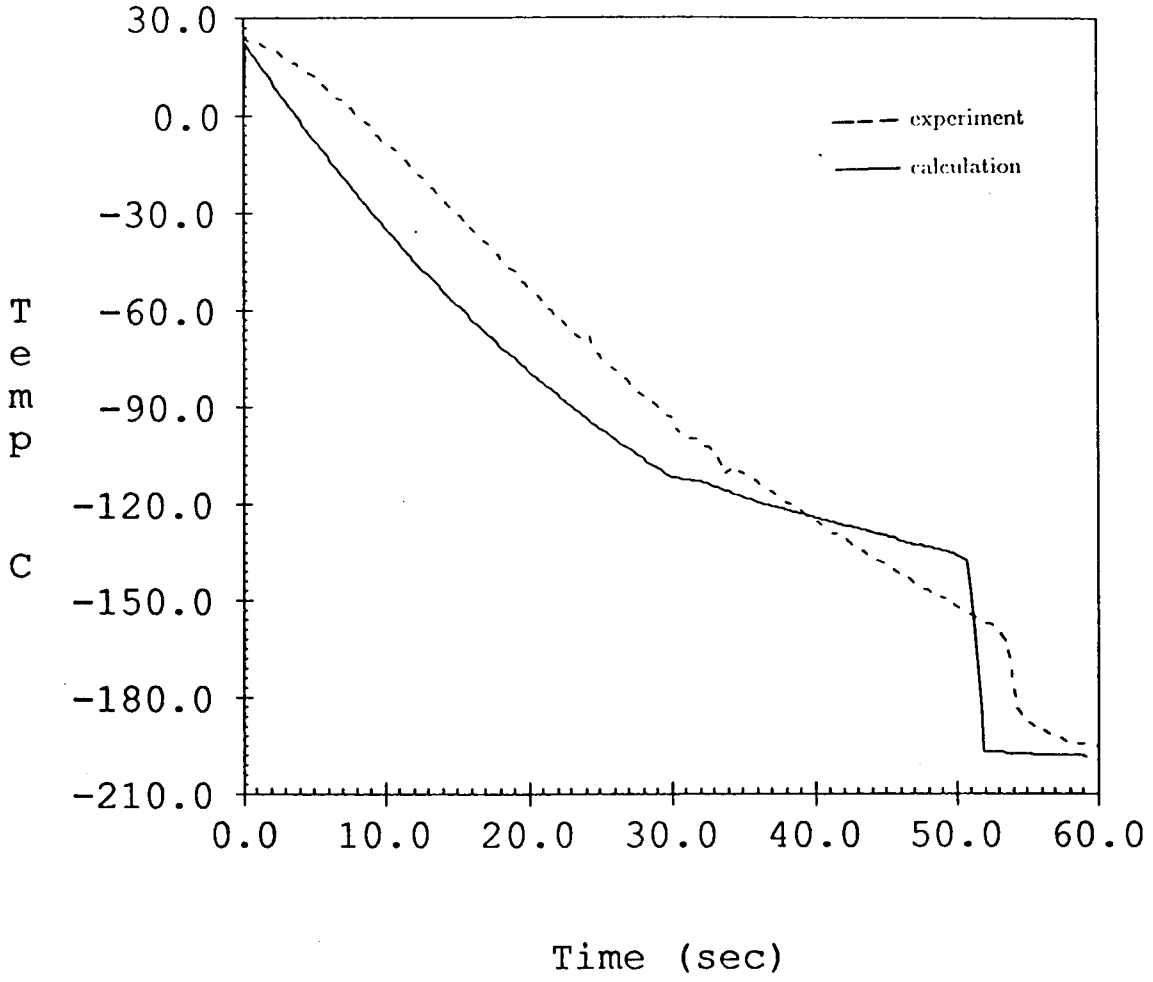

Figure 4-13. Version 2 Wall Temperature History at 7 *Ft* (Run 5 *psi*).

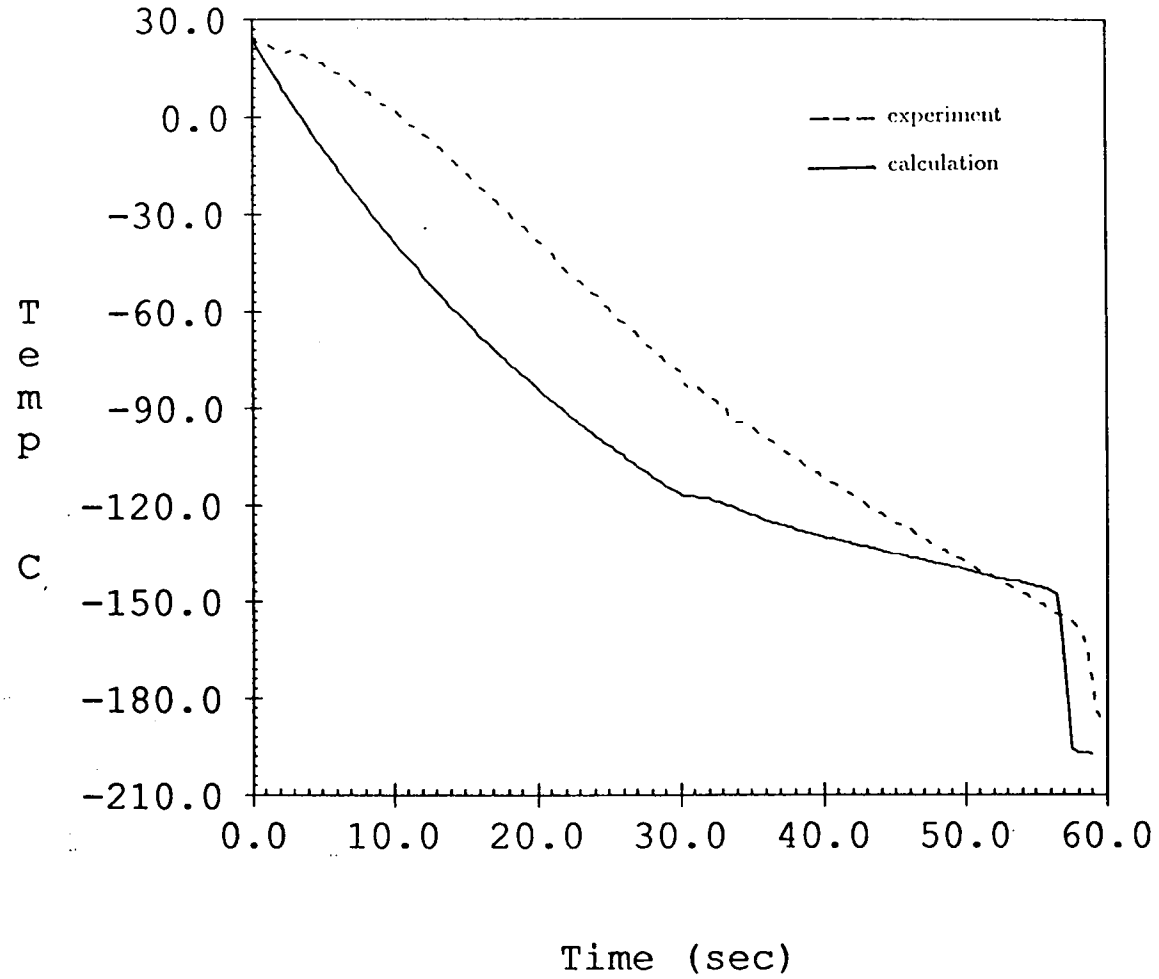

Figure 4-14. Version 2 Wall Temperature History at 9 *Ft* (Run 5 *psi*).

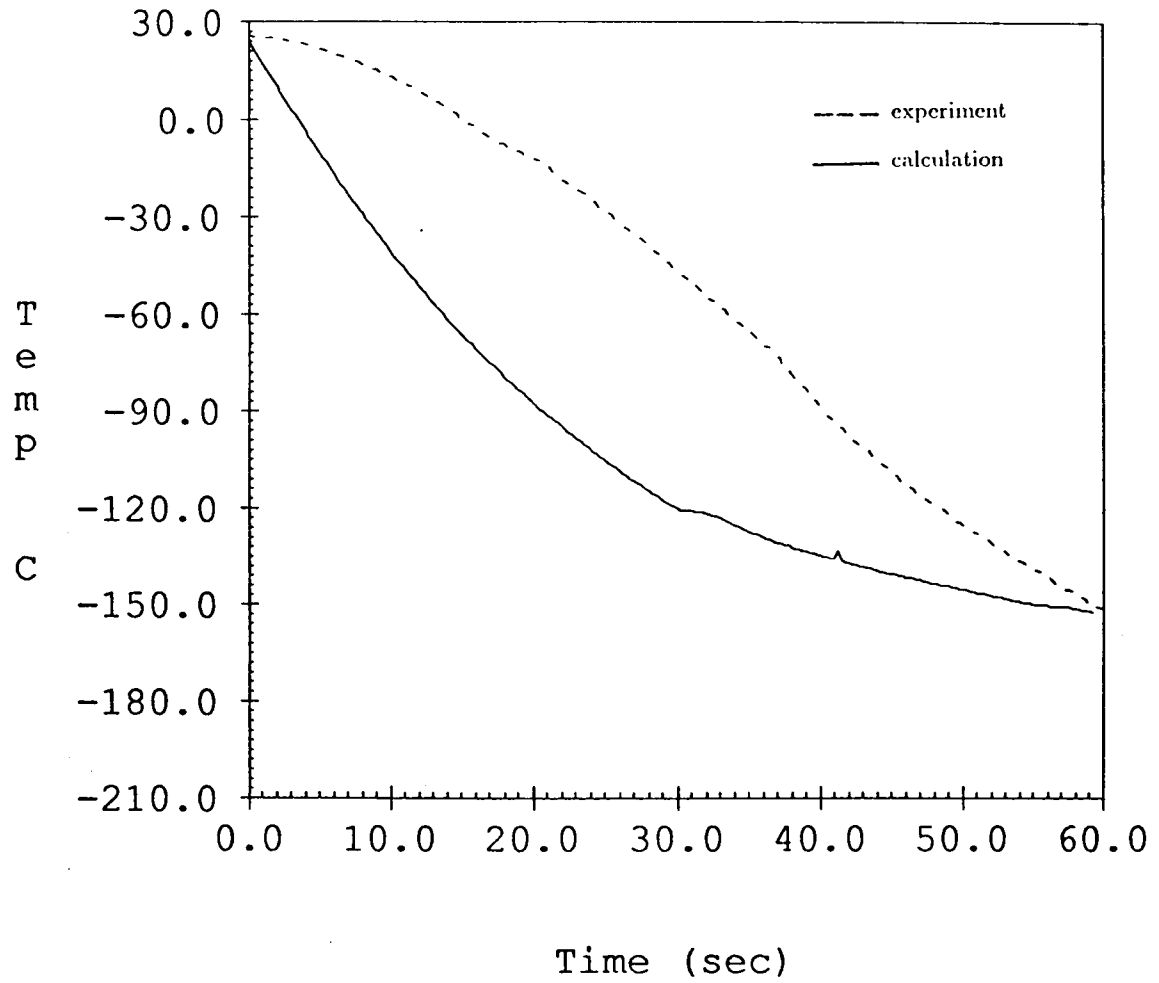

Figure 4-15. Version 2 Wall Temperature History at 11 *Ft* (Run 5 *psi*).

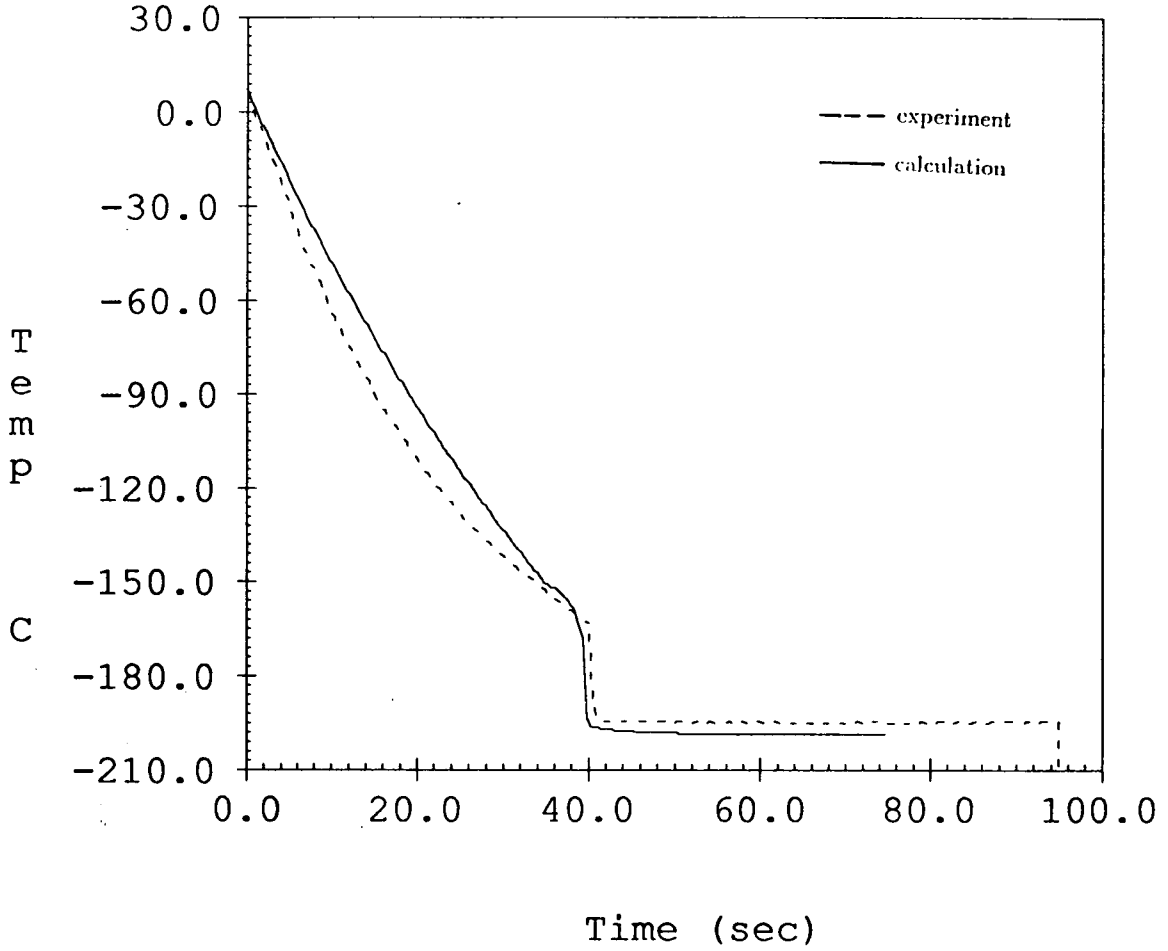

Figure 4-16. Version 2 Wall Temperature History at 1 *Ft* (Run 3 *psi*).

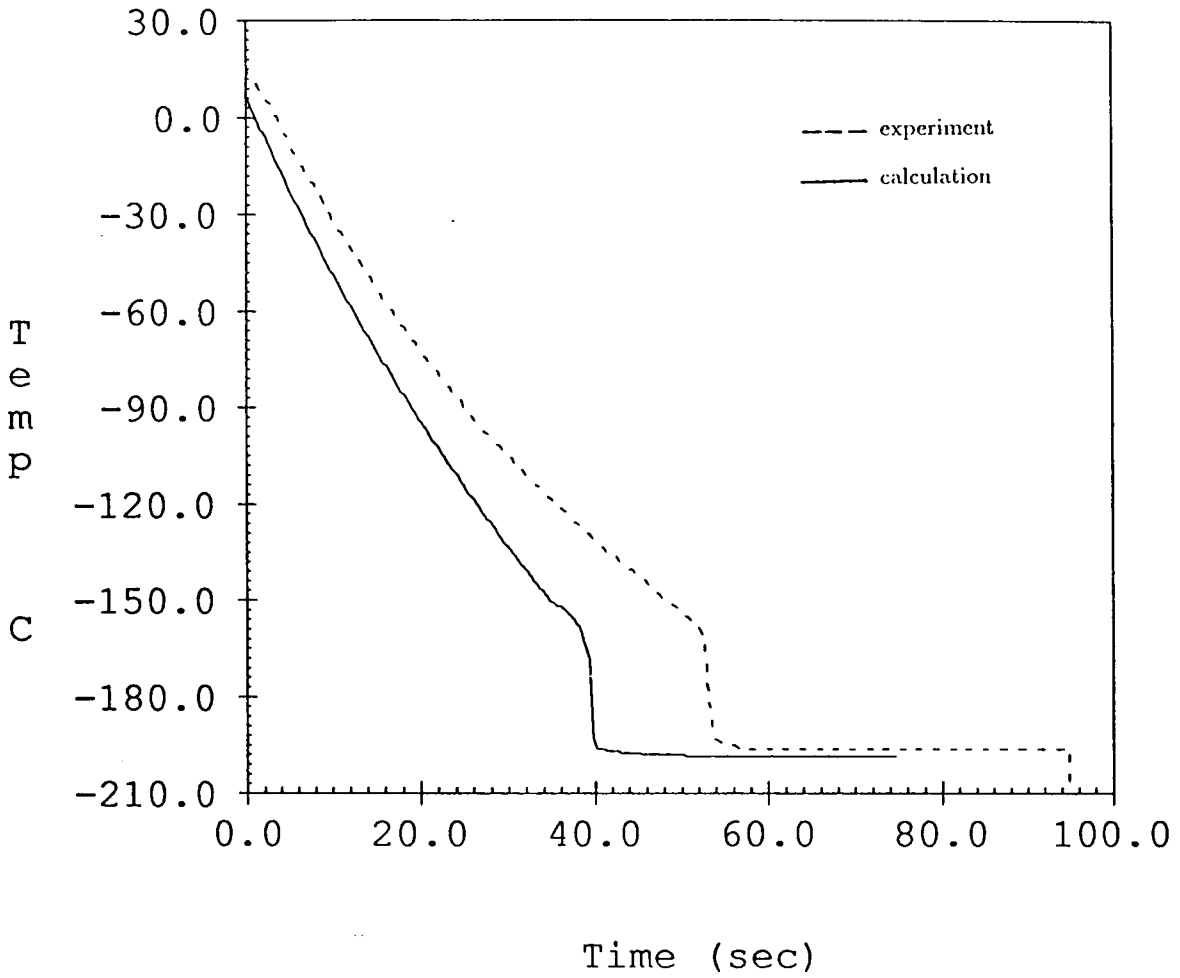

Figure 4-17. Version 2 Wall Temperature History at 3 *Ft* (Run 3 *psi*).

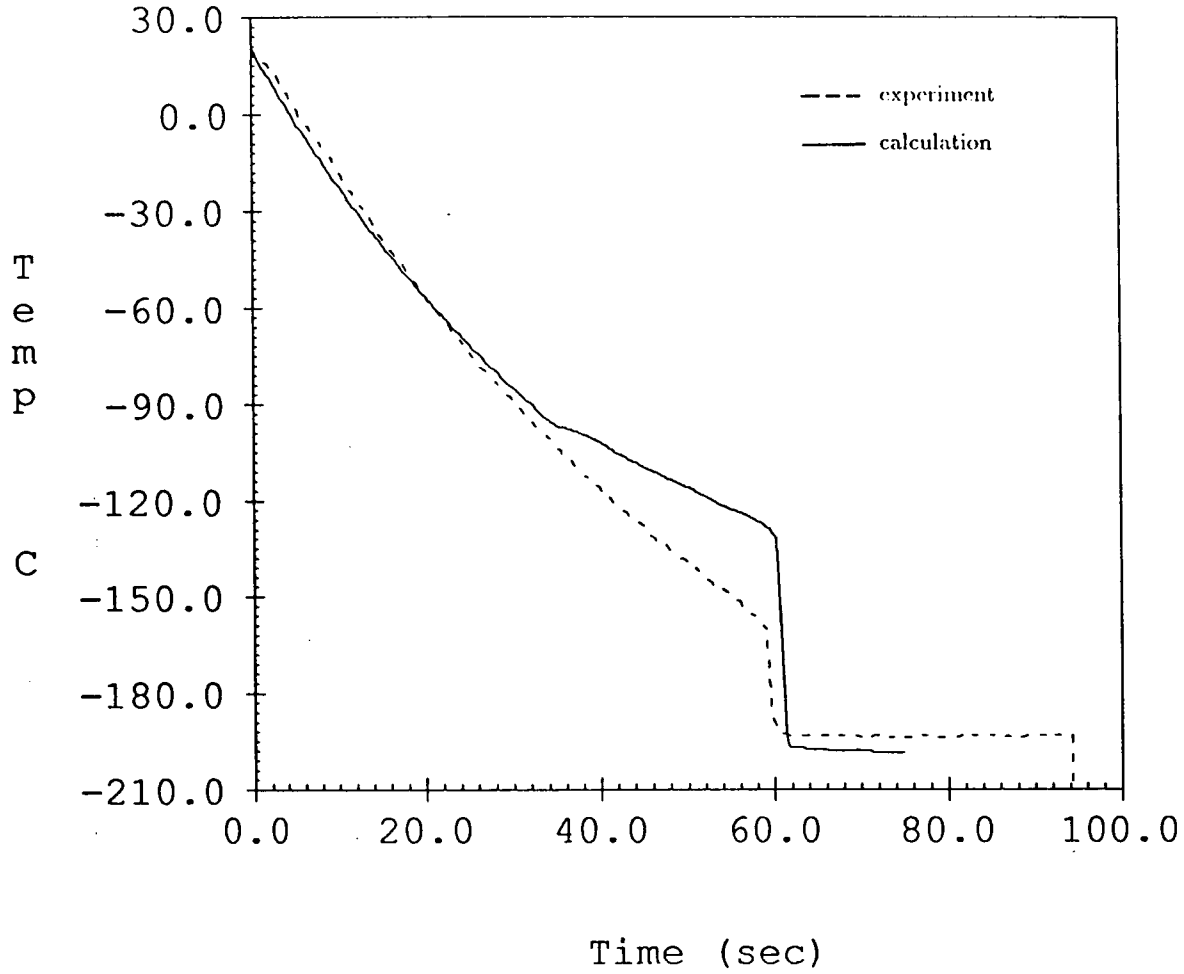

Figure 4-18. Version 2 Wall Temperature History at 5 *Ft* (Run 3 *psi*).

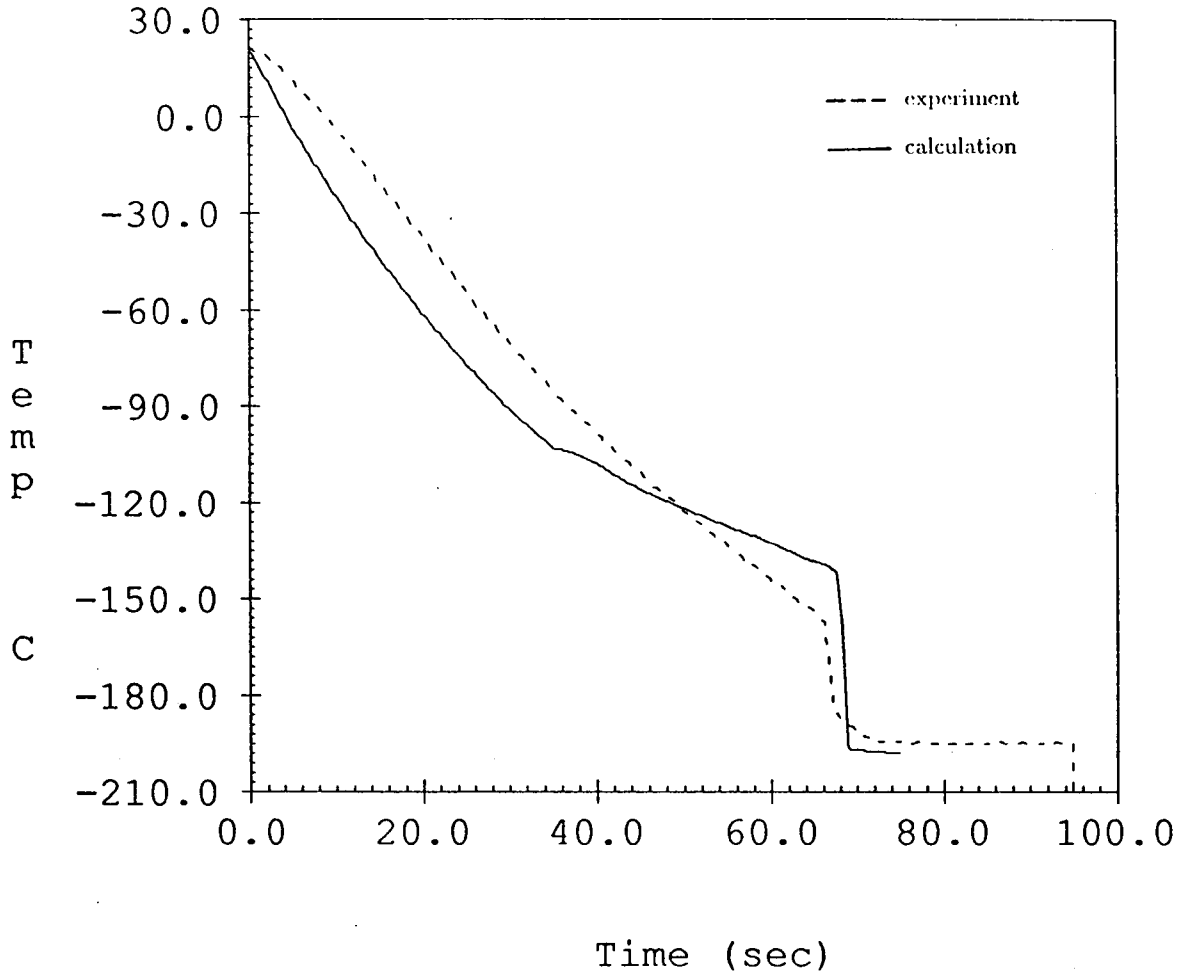

Figure 4-19. Version 2 Wall Temperature History at 7 *Ft* (Run 3 *psi*).

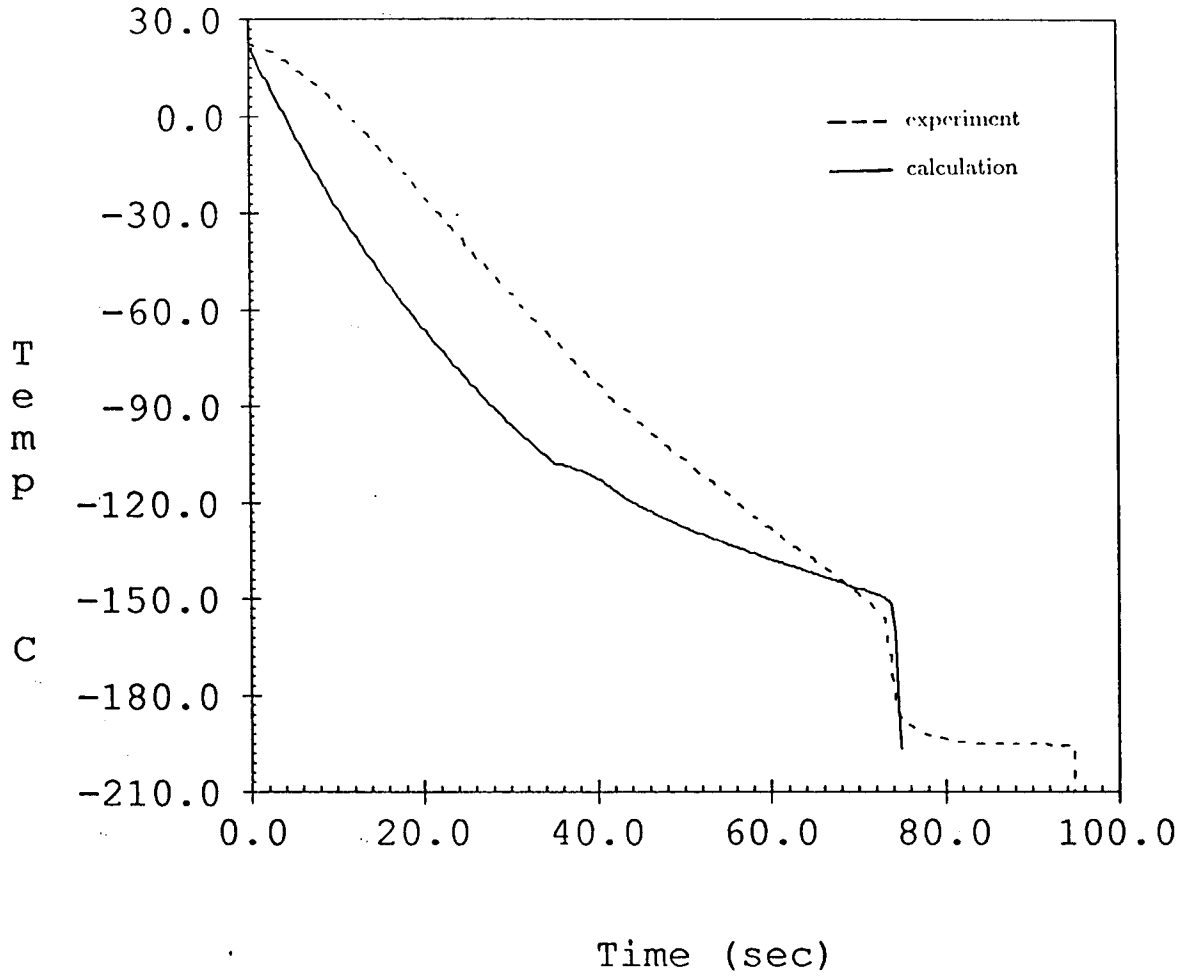

Figure 4-20. Version 2 Wall Temperature History at 9 Ft (Run 3 psi).

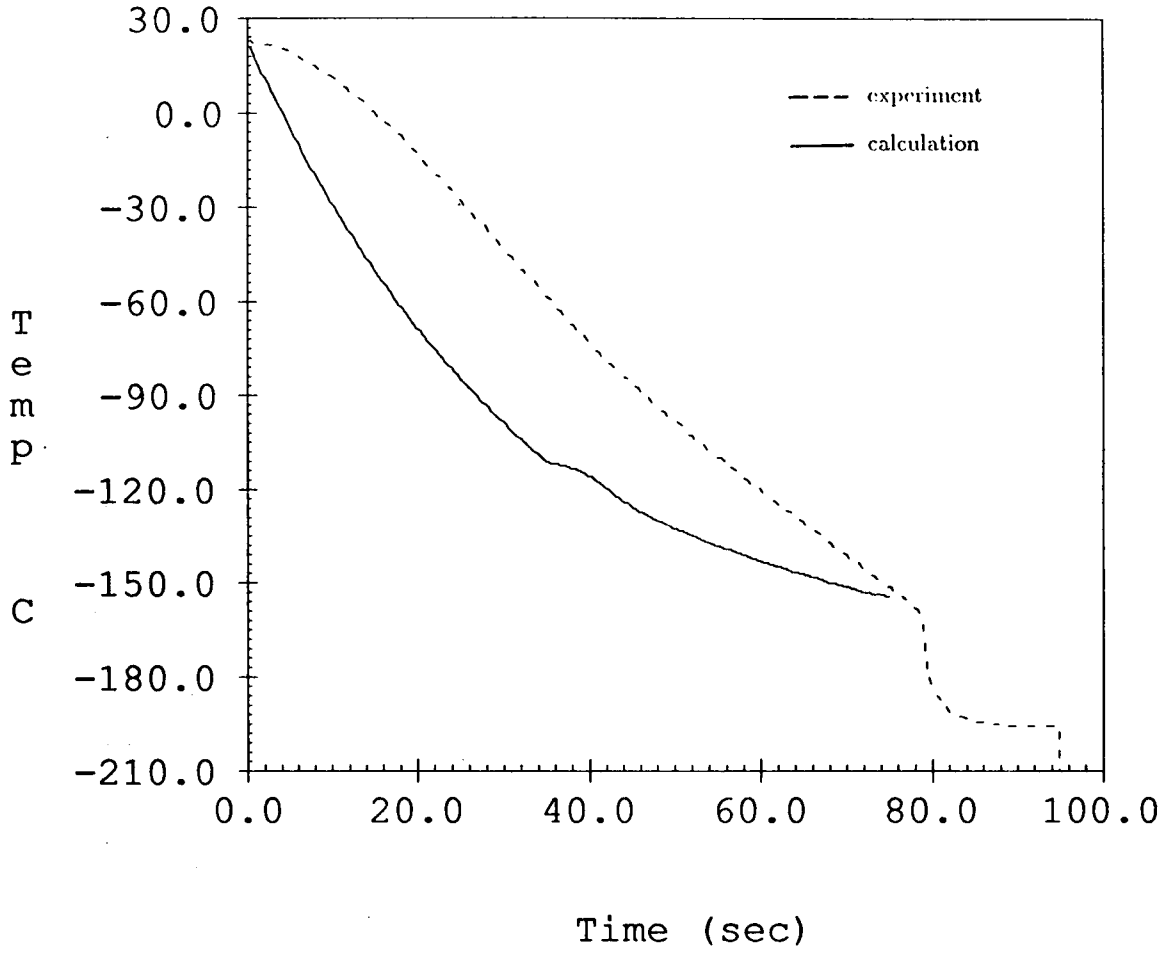

Figure 4-21. Version 2 Wall Temperature History at 11 *Ft* (Run 3 *psi*).

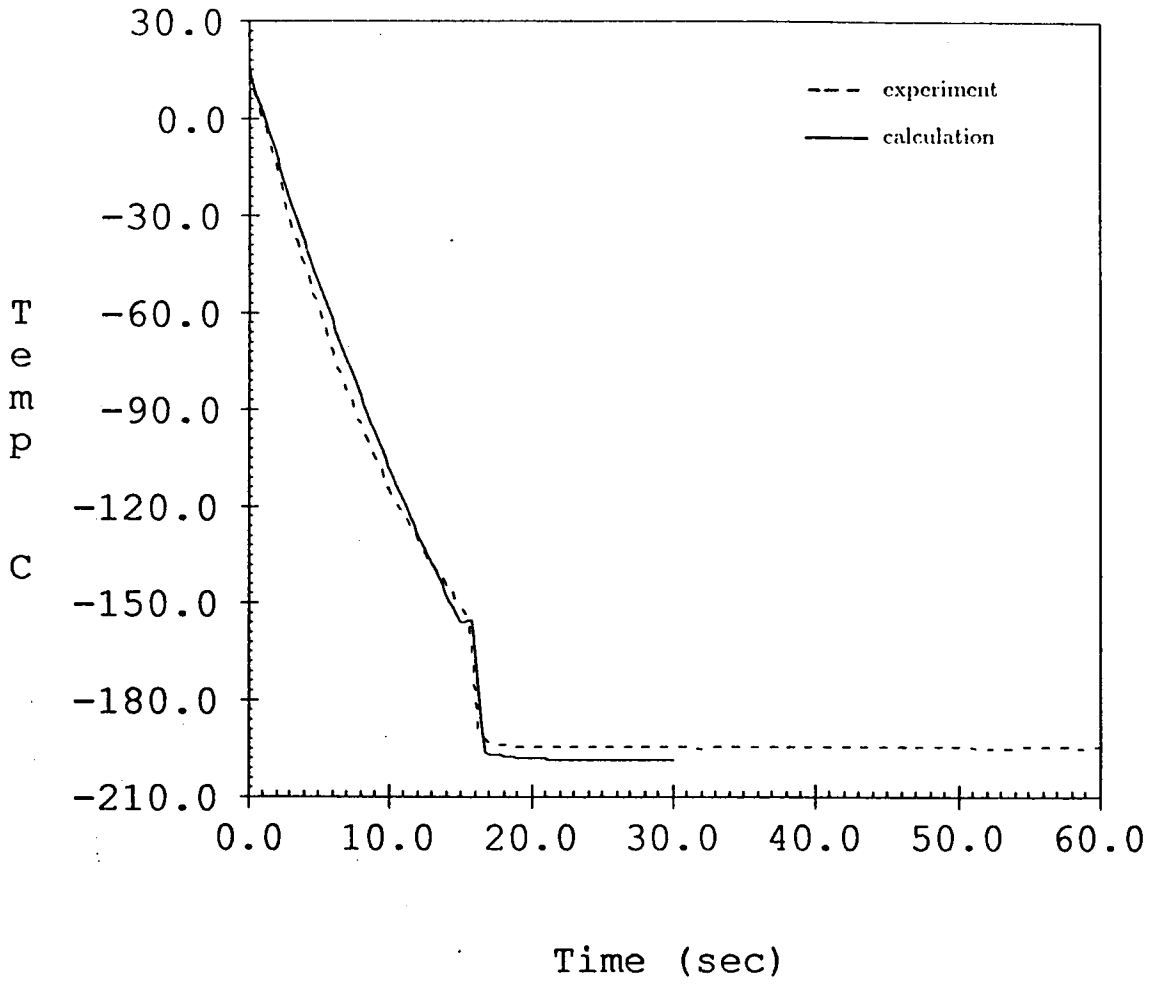

Figure 4-22. Version 2 Wall Temperature History at 1 *Ft* (Run 10 *psi*).

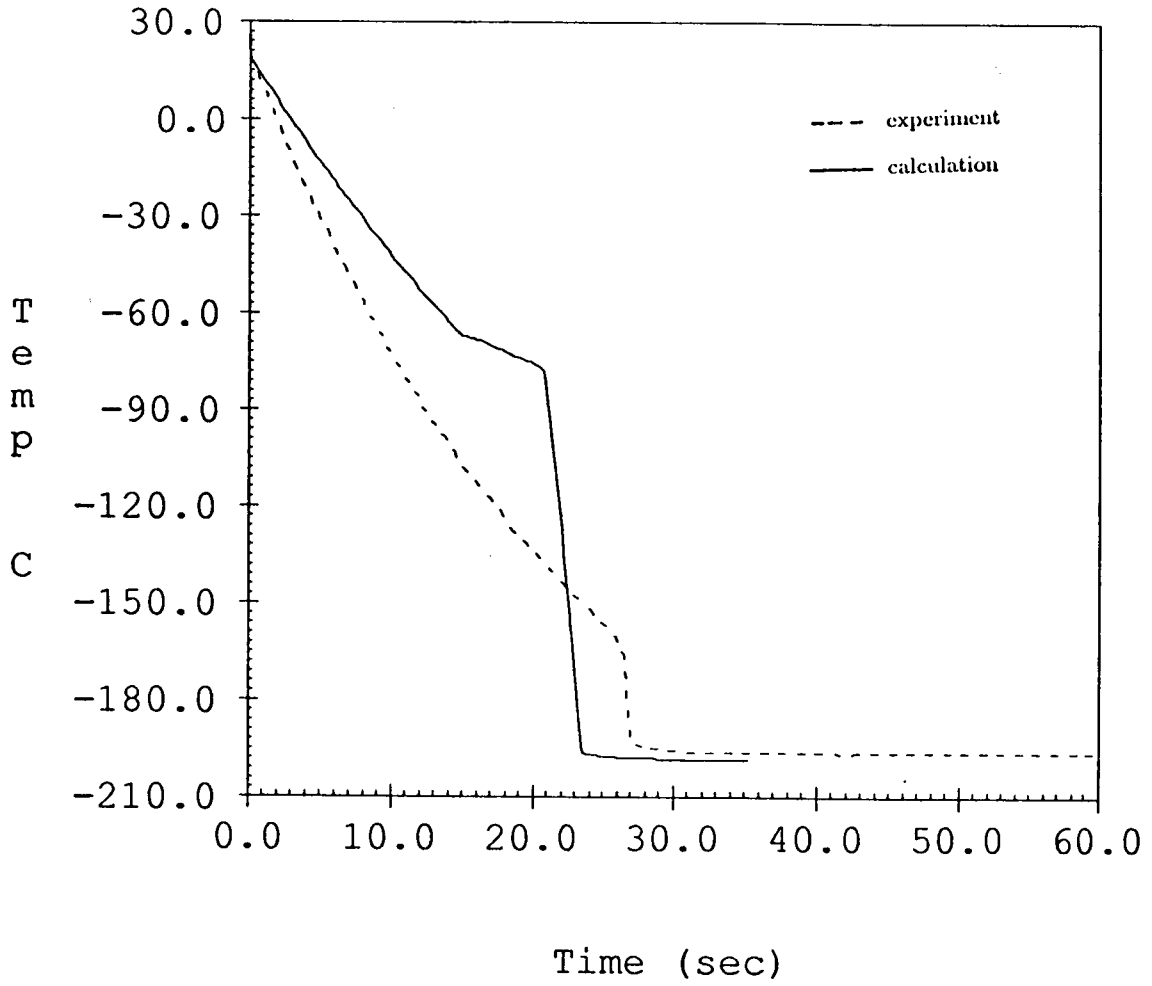

Figure 4-23. Version 2 Wall Temperature History at 3 *Ft* (Run 10 *psi*).

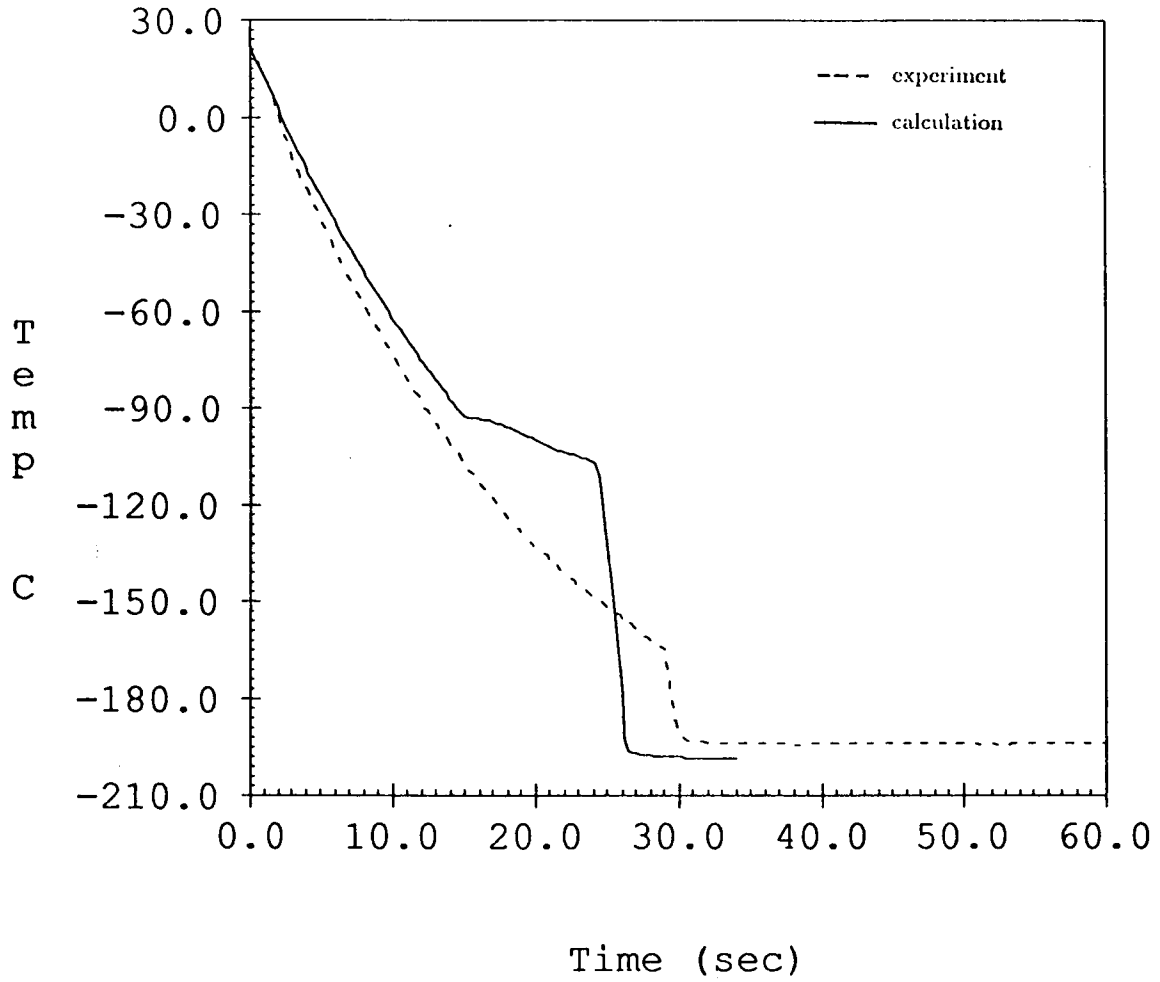

Figure 4-24. Version 2 Wall Temperature History at 5 Ft (Run 10 psi).

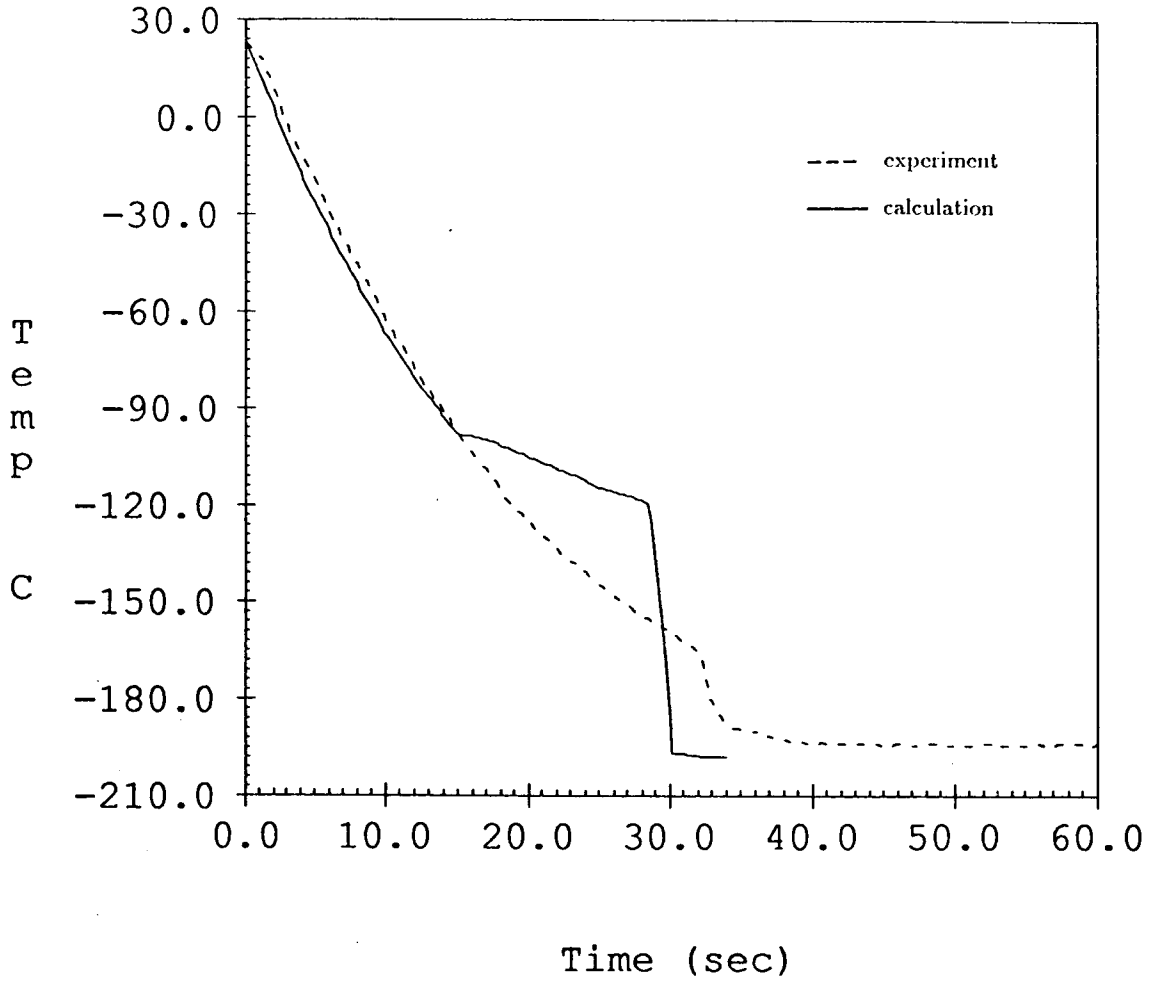

Figure 4-25. Version 2 Wall Temperature History at 7 *Ft* (Run 10 *psi*).

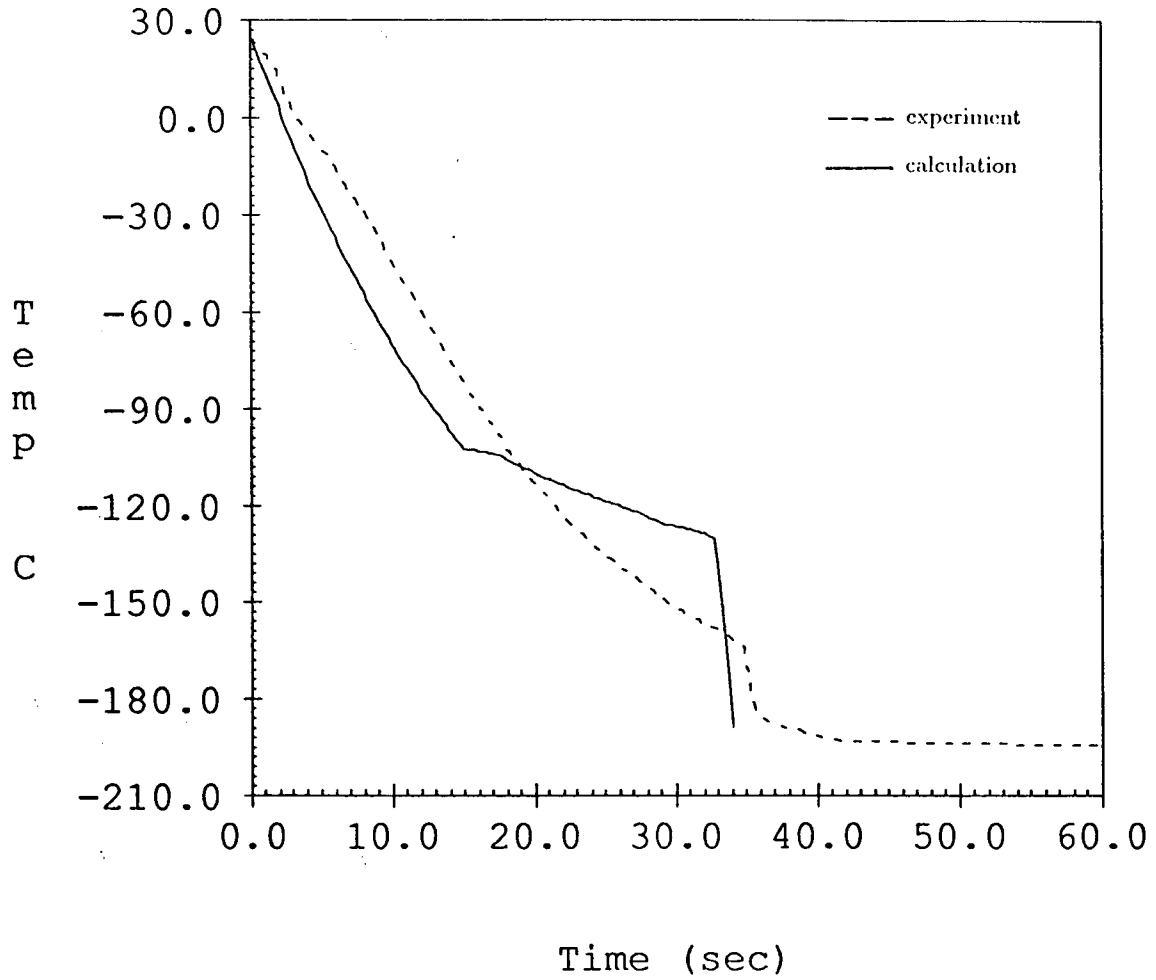

Figure 4-26. Version 2 Wall Temperature History at 9 *Ft* (Run 10 *psi*).

function is based on a laminar flow in the liquid core.

With turbulent liquid core, more heat can be transferred into the liquid core away from the liquid-vapor interface, thereby reducing the rate of vaporization at the interface. Less vapor generation is again expected to result in a thinner vapor film and increased heat transfer rates. This effect should, however, be significant only at lower positions of the test section where the liquid column is subcooled.

An important aspect of the inverted annular film boiling phenomena which could not be incorporated into the present one-dimensional two-fluid model is the possible two-dimensional motion of the liquid column. The eccentricity of the liquid core and random motion in radial and circumferential directions can lead to an extremely thin vapor film locally, and may be an important factor in enhancing the film boiling heat transfer rate, especially in regions close to the quench front. Furthermore, possible contact between the liquid and the unquenched wall surface may affect the results.

At higher elevations of the test section, the predicted wall temperature decreases faster than the measured wall temperature. This overcooling of the tube wall could be attributed to the decrease of temperature of super heated vapor due to the following reasons. Highly superheated vapor leaves the inverted annular flow regime; however, the vapor loses much of its sensible heat to liquid drops by convection and is cooled significantly. As a result, convective heat transfer from the channel wall is overpredicted further downstream, where the vapor velocity, convective heat transfer coefficient and the difference between the wall and vapor temperatures become substantially large due to vaporization of drops in the upstream region.

Convective heat transfer from superheated vapor to drops may have been overpredicted, because the predicted interfacial area or heat transfer coefficient

may be larger than it actually is. Since an equilibrium size distribution was used for the droplets in the dispersed flow regime, droplet sizes used in the calculation are most likely smaller than the actual diameters, especially in regions close to the inverted annular flow regime where large liquid fragments and ligaments rather than small drops are believed to exist.

An additional factor that should not be overlooked is the actual mechanism of wall-drop interaction heat transfer. In the present model, all of the heat transfer from the wall by this mechanism is assumed to be received by the liquid and used in either heating up of the drops or in vaporizing them. The effect of drops flowing near the hot wall surface may, instead, be to disturb the thermal boundary layer of vapor formed on the wall surface. This should increase the wall-to-vapor convection heat transfer rate well beyond the values presently calculated using a Dittus-Boelter correlation.

CHAPTER V

CONCLUSIONS AND RECOMMENDATIONS

5.1 Model for the Cooldown Process in a Vertical Tube

Based on the flow pattern observed in the past experimental studies, a model with the following regions was developed: fully liquid, inverted annular film boiling, dispersed film boiling, and fully vapor. A transient two-fluid model was developed to describe the two-phase regions. A set of mass, momentum and energy equations was solved for each phase with necessary constitutive relations that describe the wall-to-fluid and interfacial transfer of mass, momentum and energy. For the fully liquid regions, liquid velocity was considered to be constant and equal to the inlet velocity, and a transient energy equation was solved. To compute the wall temperature, a one-dimensional energy equation was formulated.

The necessary constitutive relations to solve the two-fluid equations are generally flow regime dependent and must be developed based on the correct understanding of physical mechanisms. If the mechanisms were complicated or unclear, either simple assumptions were made or a dominant mechanism was considered.

For the inverted annular flow regime, a set of six fully-transient conservation equations was solved. The difference in the pressure between the vapor and the liquid phases arising from surface tension and interfacial vaporization forces was incorporated into the momentum equations.

In the present model, the phases in the inverted annular flow regime were assumed to be completely separated with liquid flowing in the center of the flow channel and the channel wall. The wall-vapor and interfacial momentum transfer terms were modeled assuming a flow of vapor in a straight annulus with the outer

wall fixed and inner wall moving upward.

The heat transfer mechanisms considered in the inverted annular flow regime were as follows: wall-to-vapor convection, wall-to-liquid radiation and vapor-to-liquid convection. Liquid heating and vaporization heat were described by a correlation which was developed from a solution to the laminar thermal entry problem.

For the dispersed flow regime, a two-fluid model consisting of five transient conservation equations was considered. In order to describe the size dependent motion of liquid drops, an upper-limit, log-normal distribution function was used to model the drop size distribution. The maximum drop size, which corresponds to the upper limit of the log-normal function, was determined from smaller of the maximum stable diameter specified by the critical Weber number and the maximum entrainable diameter calculated from balancing the drag and body forces acting on the drops. Wall-to-fluid heat transfer was assumed to be comprised of the following mechanisms: wall-vapor convection, wall-drop interaction, wall-drop and wall-vapor radiation.

Two versions were considered. In the first version, the flow field consisted of fully liquid, inverted annular flow, dispersed flow, and fully liquid regions. The predictions were compared with the experimental data. The calculated wall temperatures for the lower elevations were higher than the experimental measurements.

In the second version, it was assumed that in the early stage of the process the tube wall was cooled by the vapor, and followed later by the fully liquid, inverted annular flow, dispersed flow, and vapor regions. This modification led to closer corrleation of the results with the experimental data.

5.2 Recommendations

The present analytical model considered the cooldown process based on the observed flow pattern. In order to enhance the understanding of the cooldown and improve the model, the following recommendations are made:

Flow visualization experiments and local measurements of parameters such as void fraction are required. Observe the development of the flow regime in each phase, particularly the transition of inverted annular flow to the dispersed flow. Determine the nature of the vapor phase in the inverted annular flow, experimentally, by finding whether this flow is turbulent or laminar and develop a proper constitutive relation for the interfacial phenomena. The effect of the eccentricity and lateral motion of the liquid column on film boiling heat transfer must be analyzed in greater detail. Existance of the liquid column contact with the wall must be verified experimentally and, in the case of such phenomena, a physical model needs to be developed for the wall-liquid heat transfer. The size distribution of drops in the dispersed flow must be measured through the experimental investigation. Finally, a mechanistic criterion for the quenching phenomena and a correlation for the quench temperature must be developed.

LIST OF REFERENCES

LIST OF REFERENCES

1. Burke, J. C., Byrnes, W. R., and Ruccia, F. E., "Pressurized Cooldown of Cryogenic Transfer Line," Advances in Cryogenic Engineering, Vol. 4, Plenum Press, New York, 1960.

2. Jacobs, R. B., "Liquid Requirements for the Cooldown of Cryogenic Equipment," Advances in Cryogenic Engineering, Vol. 8, Plenum Press, New York, 1962.

3. Drake, E. M., Ruccia, F. E., and Ruder, J. M., "Pressurized Cooldown of a Cryogenic Liquid Transfer System Containing Vertical Sections," Advances in Cryogenic Engineering, Vol. 6, 1966, pp. 323-333.

4. Steward, W. G., Smith, R. V., and Brennan, J. A., "Cooldown Transients in Cryogenic Transfer Line," Advances in Cryogenic Engineering, Vol. 14, July 1974, pp. 375-383.

5. Steward, W. G., "Transfer Line Surge," Advances in Cryogenic Engineering, 1964, Vol. 10, pp. 313-322.

6. Bronson, J. C., Edeskuty, F. J., and Hammel, E. F., "Problems in Cooldown of Cryogenic Systems," Advances in Cryogenic Engineering, Vol. 7, Plenum Press, New York, 1960.

7. Srinivasan, K., Seshagiri, V., and Krishna Murthy, M. V., "Analytical and Experimental Investigation on Cool-Down of Short Transfer Lines," Cryogenics, Vol. 14, 1974, pp. 489-494.

8. Chi, J. W. H., "Cooldown Temperatures and Cooldown Time During Mist Flow," Advances in Cryogenic Engineering, Vol. 10, Plenum Press, New York, 1965.

9. Laverty, W. F. and Rohsenow, W. M., "Film Boiling of Saturated Nitrogen Flowing in a Vertical Tube," Journal of Heat Transfer, February, 1967, pp. 90-98.

10. Forslund, R. P. and Rohsenow, W. M., "Dispersed Flow Film Boiling," ASME Journal of Heat Transfer, 1968, Vol. 90, pp. 399-407.

11. Kawaji, M. and Banerjee, S., "Application of a Multifield Model to Reflooding of a Hot Vertical Tube: Part I - Model Structure and Interfacial Phenomena," ASME Transactions, Vol. 109, February, 1987, pp. 204-211.

12. Kawaji, M. and Banerjee, S., "Application of a Multifield Model to Reflooding of a Hot Vertical Tube: Part II - Analysis of Experimental Results," ASME Transactions, Vol. 110, August, 1988, pp. 710-720.

13. Wallis, G. B., "Review - Theoretical Models of Gas-Liquid Flows", Journal of Fluids Engineering, Vol. 104, pp.279-283.

14. Wallis, G. B., "One Dimensional Two-Phase Flow," MacGraw-Hill, New York, 1969.

15. Delhaye, J. M., and Achard, J. L., "On the Averaging Operations Introduced in Two-Phase Flow Modelling," Proceedings 1st OECD/NEA Specialists Meeting on Transient Two-Phase Flow, Toronto, Vol. 1, 1976, pp. 5-84.

16. Vernier, P. & Delhaye, J. M., "General Two-Phase Flow Equations Applied to the Thermodynamics of Boiling Nuclear Reactors," Energie Primaire, 1968, Vol. 4, pp. 5-36.

17. Ishii, M., "Thermo-fluid Dynamic Theory of Two-Phase Flow," Eyrolles, Paris, 1975.

18. Wallis, G. B., "The Separated Flow Model of Two-Phase Flow," Interim Rep. EPRI NP-275, 1976.

19. Yadigaroglu, G. and Lahey, Jr., R. T., "On the Various Forms of the Conservation Equations in Two-Phase Flow," International Multiphase Flow, Vol. 2, 1976, pp. 477-494.

20. Agee, L. J., Banerjee, S., Dyffey, R. B. & Hughes, E. D., "Some Aspects of Two-Fluid Models and Their Numerical Solutions." Paper Presented at 2nd OECD/NEA Specialists Meeting on Transient Two-Phase Flow, Paris, 1978.

21. Groenveld, D. C., "Post-Dryout Heat Transfer at Reactor Operating Conditions," Presented at the Natl. Mtg. on Water Reactor Safety, Americal Nucl. Soc., Salt Lake City, UT, March 26-28, 1973.

22. Chi, J. W. H., "Slug Flow and Film Boiling of Hydrogen," J. Spacecraft, Vol. 4, 1967, p. 1329.

23. Kalinin, E. K., Koshkin, V. K., Yarkho, S. A., Berlin, I. I., Kostyuk, V. V., and Kochelaev, Yu. S., "Heat Transfer in Tubes with Rod Regime in the Case of Film Boiling of A Subcooled Liquid," Cocurrent Gas Liquid Flow, p. 497, Plenum Press, New York, 1969.

24. Kalinin, E. K., Koshkin, V. K., Yarkho, S. A., Berlin, I. I., Kochelaev, Yu. S., and Kostyuk, V. V., Korolev, A. L., and Sdobnov, G. N., "Investigation of Film Boiling in Tubes with Subcooled Nitrogen Flow," 4th Intl. Heat Trans. Conf., Paper B3.6, Paris, 1970.

25. Cumo, M., Farello, G. E. and Furrer, M., "Experimental Remarks on Sputtering Phenomena and Droplets Generation in Falling Film Rewetting," Proc. ANS/ASME/NRC Intl. Mtg. on Nucl. Reactor Thermal

Hydraulics, NUREG/CR-0014, Vol. 2, p. 1523, Saratoga Springs, NY, 1980.

26. De Jarlais, G. and Ishii, M., "Inverted Annular Flow Experimental Study," NUREG/CR-4277, April 1985.

27. Chan, K. C. and Yadigaroglu, G., "Calculation of Film Boiling Heat Transfer Above Quench Front During Reflooding," Presented at the ASME 19th National Heat Transfer Conference, Orlando, Florida, July 27-30, 1980.

28. Ellias, E., and Chambre, P., "Inverted Annular Film Boiling Heat Transfer from Vertical Surfaces," Nuclear Engineering and Design, Vol. 64, 198l, pp. 249-257.

29. Chan, A. M. C., and Banerjee, S., "Refilling and Rewetting of a Hot Horizontal Tube, Part II: Structure of a Two-Fluid Model," Journal of Heat Transfer, Vol. 103, May, 1981, pp. 287-292.

30. Lamb, H., Hydrodynamics, Sixth Edition, Cambridge University Press, 1932.

31. Ramshaw, J. D. and Trapp, J. A., "Characteristics, Stability, and Short Wavelength Phenomena in Two-Phase Flow Equation Systems," Nuclear Science and Engineering, Vol. 66, 1978, pp. 93-102.

32. Kays, W. M., Convective Heat and Mass Transfer, 2nd Edition, McGraw-Hill Book Co., 1982.

33. Kays, W. M., and Leung, E. Y., International Journal of Heat and Mass Transfer, Vol. 6, 1963, pp. 537-557.

34. Siegel, R. and Howell, J. R., Thermal Radiation Heat Transfer, McGraw Hill, 2nd Edition, 1982.

35. Carslaw, H. S. and Jaegar, J. C., Conduction of Heat in Solids, Second Edition, Oxford Press, 1959.

36. Jeromin, L. O. F., "The Status of Research in Turbulent Boundary Layers with Fluid Injection," Progress in Aeronautical Science, Vol. 10, Pergamon Press, 1970.

37. Dougall, R. S. and Rhosenow, W. M., "Film Boiling on the Inside of Vertical Tubes with Upward Flow of the Fluid at Low Qualities," Technical Report No. 9097-26, MIT, 1963.

38. Groenveld, D. D., "Post-Dryout Heat Transfer at Reactor Operation Conditions," Proc. of the Topical Meeting on Water Reactor Safety, Salt Lake City, March 26-28, 1973.

39. Groenveld, D. C. and Delmore, G. G. J., "Prediction of Thermal Non-Equilibrium in the Post-Dryout Regime," Nuclear Engineering and Design, Vol. 36. pp. 408-413, 1971.

40. Tong, A., Wong, S. and Hochreiter, L. E., "Entrained Droplet, Disributionand Velocities in Dispersed Flow Film Boiling," Paper Presented at CSNI Meeting in Pasadena, CA, 1981.

41. Ardon, K. H., and Hall, P. C., "Droplet Hydrodynamics and Heat Transfer in the Dispersed Flow Regime in Botton Flooding," Presented in the Third CSNI Specialists Meeting on Transient Two-Phase Flow, Pasadena, California, March, 198l.

42. Parker, J. D., and Grosh, R. J., "Heat Transfer to a Mist Flow," Aec R&D Report ANL629.

43. Ganic, E. N., and Rhosenow, W. M., "Dispersed Flow Heat Transfer," International Journal of Heat and Mass Transfer, Vol. 20, 1977, pp. 855-866.

44. Bhatti, M. S., "Dynamics of a Vaporizing Droplet in Laminar Entry Region of a Straight Channel," ASME Jl Heat Transfer, Vol. 99, pp. 574-579.

45. Ganic, E. N., and Rhosenow, W. M., "On the Mechanism of Liquid Drop Deposition in Two-Phase Dispersed Flow," Journal of Heat Transfer, Vol. 101, May, 1979, pp. 51-57.

46. Chen, J. C., Ozkaynak, F. T. & Sudarum, R. K., "Vapor Heat Transfer in Post-CHF Region Including the Effect of Thermodynamic Non-Equilibrium," Nucl. Engng., Vol. 5l, pp. 143-155.

47. Yao, S. C., "Convective Heat Transfer of Laminar Droplet Flow in Thermal Entrance Region of Circular Tubes," Journal of Heat Transfer, Vol. 101, August, 1979, pp. 480-483.

48. Rane, A., and Yao, S. C., "Heat Transfer of Evaporating Droplet Flow in Low Pressure Systems," The Canadian Journal of Chemical Engineering, Vol. 58, June, 1980, pp. 303-308.

49. Yao, S. C. and Rane, A., "Heat Transfer of Laminar Mist Flow in Tubes," Journal of Heat Transfer, Vol. 102, November, 1980, pp. 678-683.

50. Sun, K. H., Gonzalez-Santalo, J. M., and Tien, C. L., "Calculations of Combined Radiation and Convection Heat Transfer in Rod Bundles Under Emergency Cooling Conditions," ASME Journal of Heat Transfer, Vol. 98, pp. 414-420.

51. Young, A. C., and Spencer, M. Y., "A Mechanistic Model for the Best Estimate Analysis of Reflood Transients," Presented at the ASME 19th National Heat Transfer Conference, Orlando, Fl, July 20-30, 1980.

52. Mugele, R. A., and Evans, H. D., "Droplet Size Distribution in Sprays," Industrial and Engineering Chemistry, Vol. 43, No. 6, 1951, pp. 1317-1324.

53. Hinze, J. O., "Fundamentals of the Hydrodynamic Mechanism of Splitting in Dispersion Process," AIChE Journal, Vol. 1, 1955, pp. 289-295.

54. Lane, W. R., "Shatter of Drops in Streams of Air," Industrial and Engineering Chemistry, Vol. 43, No. 6, June 1951, pp. 1312-1316.

55. Rowe, R. N., Trans. Inst. Chem. Engrs., Vol. 39, p. 175.

56. Ishii, M., and Zuber, N., "Drag Coefficient and Relative Velocity in Bubbly, Droplet or Particulate Flow," AIChE Journal, Vol. 25, No. 5, September, 1979, pp. 843-855.

57. Ingebo, R. D., "Drag Coefficient for Droplet and Solid Spheres in Clouds Accelerating in Air Streams," NACA-Tech. Note 3762, September, 1956.

58. Lee, K., and Ryley, D. J., "Evaporization of Water Droplets in Superheated Steam," Journal of Heat Transfer, Vol. 90, ASME, November, 1968, pp. 445-451.

59. Papell, S. S., and Hendricks, R. C., "Incipience and Convective Boiling of Neon and Nitrogen," Advances in Cryogenic Engineering, Vol. 23, 1978, pp. 384-394.

60. Bergles, A. E. and Rohsenow, W. M., "Determination of Forced-Convection Surface Boiling Heat Transfer," ASME Journal of Heat Transfer, Vol. 86, 1964, p. 365.

61. Frost, W. and Dzakowic, G. S., "Extension of the Method of Predicting Incipient Boiling on Commercially Finished Surfaces," ASME-AICHE Paper 67-HT-61, August, 1967.

62. Shah, M. M., "Prediction of Heat Transfer During Boiling of Cryogenic Fluid Flowing in Tubes," Cryogenic, Vol. 24, May, 1984, pp. 231-236.

63. Klimenko, V. V., "Heat Transfer Intensity at Forced Flow Boiling of Cryogenic Liquid in Tubes," Cryogenics, Vol. 22, November, 1982, pp. 569-576.

64. Barron, Randall F., Cryogenic Systems, 2nd Edition, Oxford University Press, New York Clarendon Press, 1985.

65. Giarratano, P. J., and Smith, R. V., "Study of Forced Convection Boiling Heat Transfer Correlations for Cryogenic Fluids," Advances in Cryogenic Engineering, Vol. 11, Plenum Press, New York, 1965.

66. Chi, J. W. H., "Slug Flow and Film Boiling of Hydrogen," J. Spacecraft, Vol. 4, p. 1329, 1967.

67. Reynolds, W. C., Thermodynamic Properties in SI, Published by Stanford University, Stanford, 1979.

68. Younglove, B. A., "Thermophysical Properties of Fluids I - Argon, Ethylene, Parahydrogen, Nitrogen Trifluoride, and Oxygen," Journal of Physical and Chemical Reference Data, Vol. 11, 1982, Supplement No. 1.

69. Childs, Gregg E., Ericks, Lewis J. and Powell, Robert I., "Thermal Conductivity of Solids at Room Temperature and Below," September, 1973, Cryogenic Division, Institute for Basic Standards, National Bureau of Standards, Boulder, Colorado.

70. Powell, "Thermal Conductivity of Selected Materials," National Standard Reference Data Systems, Report PB-189 698, Washington D. C., November, 1966.

71. Kawaji, M. and Banerjee, S., "Flow Characteristics During Reflooding of Hot Vertical Tube," EPRI Report NP-2820, March, 1983.

72. McGee, T. L., "An Experimental Study of a Vertical Cooldown Line With LN2," MS Thesis, The University of Tennessee, May, 1990.

APPENDIX

APPENDIX

Phase Conservation Equations

The derivation of the phase conservation equations is relatively straightforward but there has been some disagreement on the form of the equations because incorrect averaging procedures have been used. We will, therefore, briefly outline the derivation of the volume averaged, area averaged form of the phase conservation equations starting from the generalized local instantaneous conservation equations of Delhaye & Achard [18]. The one-dimensional equations will be derived; however, exactly the same general procedure may be followed in deriving multidimensional equations.

Let V_k be the volume of phase k enclosed between the walls and the cross-sectional planes spaced a distance z apart (z can be arbitrarily small). To derive the volume averaged form of the conservation equations, we will use Gauss' theorem and Leibnitz rule. The particular forms applying to Figure A-1 are given below.

We have chosen to derive the equations in volume averaged form rather than cross-sectional averaged form because some difficulties arise in the latter form when the interface and the cross-section coincides as, e.g., when the whole interface occupies the cross-section in a refilling problem. Singularities may be introduced into cross-sectionally averaged equations which may be avoided by volume averaging. The distance z shown in Figure A-1 can be made as small as desired, so we essentially average over a thin slice.

The theorems we will use are given below.

Leibnitz Rule

$$\frac{\partial}{\partial t}\int_{V_k(z,t)} f(x,y,z,t)dV = \int_{V_k(z,t)} \frac{\partial f}{\partial t}dV + \int_{a_i} f(\vec{v}_i \cdot \vec{n}_k)dS \qquad (1)$$

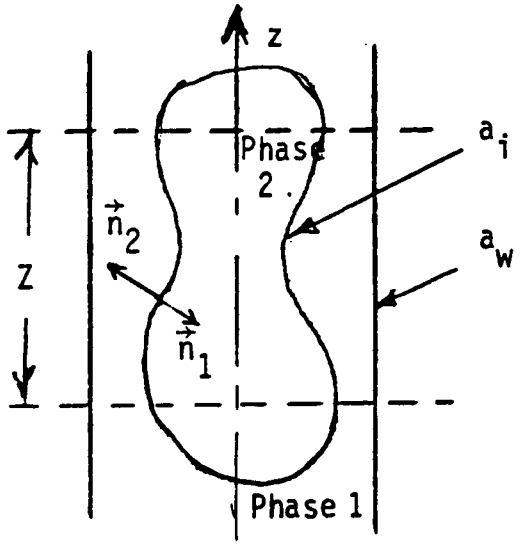

Figure A-1. Definition of Geometry.

Gauss' Theorem

$$\int_{V_k(z,t)} \nabla \cdot \vec{a} dV = \frac{\partial}{\partial z} \int_{V_k(z,t)} \vec{n}_z \cdot \vec{a} dV + \int_{a_i} \vec{n}_k \cdot \vec{a} dS \tag{2}$$

We will define averages by the following symbols

$$< f_k > = \frac{1}{V_k} \int_{V_k} f_k dV \tag{3}$$

$$< f_k >_i = \frac{1}{V} \int_{a_i} f_k dS \tag{4}$$

where

$$V = \sum V_k \tag{4a}$$

The local instantaneous form of the general conservation equation will not be derived as Truesdell and Toupin, 1960, contains a detailed discussion. If $\rho_k \psi_k$ is the quantity being conserved in the kth phase, and $\vec{j}_k$ and $\widehat{S}_k$ are the flux and source of ψ_k, then

$$\frac{\partial \rho_k \psi_k}{\partial t} + \nabla \cdot \rho_k \psi_k \vec{v}_k + \nabla \cdot \vec{j}_k - \rho_k \widehat{S}_k = 0 \tag{4b}$$

The general conservation equation may be volume averaged using Equations (1) and (2) as follows:

$$\int_{V_k} \frac{\partial \rho_k \psi_k}{\partial t} dV = \frac{\partial}{\partial t} \int_{V_k} \rho_k \psi_k dV - \int_{a_i} \rho_k \psi_k (\vec{v}_i \cdot \vec{n}_k) dS \tag{4c}$$

$$\int_{V_k} \nabla \cdot (\rho_k \psi_k \vec{v}_k + \vec{j}_k) dV = \frac{\partial}{\partial z} \int_{V_k} \vec{n}_z \cdot (\rho_k \psi_k \vec{v}_k + \vec{j}_k) dV + \int_{a_i + a_{kw}} \vec{n}_k \cdot (\rho_k \psi_k \vec{v}_k + \vec{j}_k) dS \tag{4d}$$

The usual assumption that $\vec{v}_k = 0$ at the wall (a_{kw}) has been used. The general volume averaged conservation equation is then derived as follows:

$$\frac{\partial}{\partial t} \int_{V_k} \rho_k \psi_k dV + \frac{\partial}{\partial z} \int_{V_k} \vec{n}_z \cdot (\rho_k \psi_k \vec{v}_k + \vec{j}_k) dV - \int_{V_k} \rho_k \widehat{S}_k dV$$

$$= \int_{a_i} \rho_k \psi_k \vec{n}_k \cdot (\vec{v}_i - \vec{v}_k) dS - \int_{a_i + a_{kw}} \vec{n}_{kw} \cdot \vec{j}_k dS \qquad (4\epsilon)$$

Let $\alpha = V_k/V$ = phase volume fraction. Then using equation (3) (the definition of $< \cdot >$, we have

$$\frac{\partial}{\partial t}\alpha_k < \rho_k \psi_k > + \frac{\partial}{\partial z}\alpha_k < \vec{n}_z \cdot (\rho_k \psi_k \vec{v}_k + \vec{j}_k) > - \alpha_k < \rho_k \widehat{S}_k >$$

$$= -\frac{1}{V}\int_{a_i} (\dot{m}_k \psi_k + \vec{j}_k \cdot \vec{n}_k) dS - \frac{1}{V}\int_{a_{kw}} \vec{n}_{kw} \cdot \vec{j}_k dS \qquad (5)$$

where we have written the interphase mass transfer rate as

$$\dot{m}_k = \rho_k \vec{n}_k \cdot (\vec{v}_k - \vec{v}_i) \qquad (6)$$

The forms of the conservation equations for each quantity (mass, momentum in the z direction, and energy) for each phase may now be derived.

Mass

In this case $\psi = 1, \quad \vec{j}_k = 0, \quad \widehat{S}_k = 0.$

$$\frac{\partial}{\partial t}\alpha_k < \rho_k > + \frac{\partial}{\partial z}\alpha_k < \rho_k u_k > = - < \dot{m}_k >_i = \Gamma_{mk} \qquad (7)$$

where equation (4) has been used to write the right-hand side. In general, the volume averaged interfacial mass transfer rate is not known "a priori" and a correlation must be supplied.

Momentum

In this case $\psi = \vec{v}_k, \quad \vec{j}_k = p_k \overline{\overline{I}} - \overline{\overline{\tau}}_k, \quad \widehat{S}_k = \vec{F}_k$. Taking the dot product of the conservation equation (5) with $\vec{n}_z \cdot$, we obtain the equation for conservation of z direction momentum as follows:

$$\frac{\partial}{\partial t}\alpha_k < \rho_k u_k > + \frac{\partial}{\partial z}\alpha_k < \rho_k u_k^2 > + \frac{\partial}{\partial z}\alpha_k < p_k > - \frac{\partial}{\partial z}\alpha_k < \vec{n}_z \cdot (\overline{\overline{\tau}}_k \cdot \vec{n}_z) >$$

$$-\alpha_k < \rho_k F_{z,k} >= -\frac{1}{V}\int_{a_i}\left[\dot{m}_k u_k + \vec{n}_z \cdot \vec{n}_k p_k - \vec{n}_z \cdot (\vec{n}_k \cdot \bar{\bar{\tau}}_k)\right] dS$$

$$+\frac{1}{V}\int_{a_{kw}} \vec{n}_z \cdot (\vec{n}_{kw} \cdot \bar{\bar{\tau}}_k) dS \qquad (8)$$

To derive equation (8) we have used the relationship $\vec{n}_{kw} \cdot \vec{n}_z p_k = 0$ (since $\vec{n}_{kw} \cdot \vec{n}_z = 0$ if there is no area change).

The pressure term on the right-hand side can be further simplified by using equation (2) (Gauss' Theorem) as shown below, provided we assume that $p_k = p_{ki}$ (the phase pressure at the interface).

Now

$$\int_{a_i} \vec{n}_k \cdot (\vec{n}_z p_k) dS = \int_{a_i} \vec{n}_k \cdot [\vec{n}_z (< k_k > + \Delta p_{ki})]\, dS \qquad (8a)$$

where $\Delta p_{ki} = p_{ki} - < p_k >$.

It is often possible to write the difference in bulk and interfacial pressures through a form drag term of the form

$$\Delta p_{ki} = C_k \rho_k \Delta u^n \qquad (8b)$$

where Δu is the difference between the volume averaged quantities. This is understood to be simply an empirical constitutive law. Using this form we obtain

$$\frac{1}{V}\int_{a_i} \vec{n}_k \cdot (\vec{n}_z p_k) dS = -\left[< p_k > + C_k \rho_k \Delta u^n\right] \qquad (9)$$

Substituting equation (9) into equation (8), we obtain the momentum conservation equation as

$$\frac{\partial}{\partial t}\alpha_k < \rho_k u_k > + \frac{\partial}{\partial z}\alpha < \rho_k u_k^2 > + \alpha_k \frac{\partial < p_k >}{\partial z} - \frac{\partial}{\partial z}\alpha_k < \bar{\bar{\tau}}_{zz,k} >$$

$$-C_k \rho_k u^n \frac{\partial \alpha_k}{\partial z} = \alpha_k < \rho_k F_{z,k} > - < \dot{m}_k u_k >_i + < (\dot{n}_k \cdot \bar{\tau}_z >_i + < (\vec{n}_{kw} \cdot \bar{\tau}_z) >_w \qquad (10)$$

Note that a term involving the form drag multiplied by the derivative of α_k appears in the equation. This is a purely empirical term which arises out of the relationship between bulk and interfacial pressure and is introduced at this stage to illustrate the form of the terms introduced by the retention of unequal pressures.

Energy

In this case

$$\psi_k = E_k = \left(e_k + \frac{u_k^2}{2}\right); \qquad \vec{j}_k = \vec{q}_k - (p_k \overline{\overline{I}} - \overline{\overline{\tau}}_k) \cdot \vec{v}_k; \qquad (10a)$$
$$; \qquad \widehat{S}_k = \vec{F}_k \cdot \vec{v}_k + Q_k$$

We have

$$\frac{\partial}{\partial t}\alpha_k < \rho_k E_k > + \frac{\partial}{\partial z}\alpha_k < \rho_k E_k u_k > + \frac{\partial}{\partial z}\alpha_k < q_{z,k} > + \frac{\partial}{\partial z}\alpha_k < p_k u_k > \qquad (10b)$$

$$-\frac{\partial}{\partial t}\alpha_k < \vec{n}_z \cdot (\overline{\overline{\tau}}_k \cdot \vec{v}_k) > = \alpha_k < \rho_k (\vec{F}_k \cdot \vec{v}_k + Q_k >$$

$$-\frac{1}{V}\int_{a_i} \left[\dot{m}_k E_k + \vec{n}_k \cdot (\vec{q}_k + p_k \vec{v}_k - \overline{\overline{\tau}}_k \cdot \vec{v}_k)\right] dS$$

$$-\frac{1}{V}\int_{a_{kw}} \vec{n}_{kw} \cdot \vec{q}_k dS \qquad (11)$$

The equation can be written in enthalpy form as

$$E_k = h_k + \frac{u_k^2}{2} - p_k/\rho_k \qquad (11a)$$

Now $\dot{m}_k = \rho_k(\vec{v}_k - \vec{v}_i) \cdot \vec{n}_k$ by definition, therefore

$$\vec{n}_k \cdot p_k \vec{v}_k = \frac{p_k}{\rho_k}\{\vec{n}_k \cdot (\vec{v}_k - \vec{v}_i)\rho_k\} + p_k \vec{n}_k \cdot \vec{v}_i$$
$$= \dot{m}_k \frac{p_k}{\rho_k} + p_k \vec{n}_k \cdot \vec{v}_i \qquad (11b)$$

or

$$-\frac{1}{V}\int_{a_i}(\dot{m}_k E_k + \vec{n}\cdot p\vec{v}_k)dS = -\frac{1}{V}\int_{a_i}\left[\dot{m}_k\left(h_k + \frac{u_k^2}{2}\right) + p_k(\vec{n}_k\cdot\vec{v}_i)\right] \quad (12a)$$

$$\frac{1}{V}\int_{a_i} p_k(\vec{n}_k\cdot\vec{v}_i)dS = \frac{1}{V}\int_{a_i}[< p > + C_k\rho_k\Delta u^n](\vec{n}_k\cdot\vec{v}_i)ds \quad (12b)$$

As discussed previously for the derivation of equation (9). Using Leibnitz's rule, we find

$$\frac{1}{V}\int_{a_i} p_k(\vec{n}_k\cdot\vec{v}_i)dS = [< p_k > + C_k\rho_k\Delta u^n]\frac{\partial\alpha_k}{\partial t} \quad (13)$$

Substituting equation (13) into equation (12) and then substituting equation (12) into equation (11), we obtain the form of the energy equation given below. Note again that a form drag term involving $\frac{\partial\alpha_k}{\partial t}$ has appeared in the equations to account for the difference between the bulk and interfacial pressure.

$$\frac{\partial}{\partial t}\alpha_k < \rho_k E_k > + \frac{\partial}{\partial z}\alpha_k < \rho_k E_k u_k > + \frac{\partial}{\partial z}\alpha_k < q_{z,k} > + < p_k > \frac{\partial\alpha_k}{\partial t}$$

$$+C_k\rho_k\Delta u^n\frac{\partial\alpha_k}{\partial t} + \frac{\partial}{\partial t}\alpha_k p_k u_k - \frac{\partial}{\partial z}\alpha_k < \vec{n}_z\cdot(\overline{\overline{\tau}}\cdot\vec{v}_k) >$$

$$= - < \left[\dot{m}_k\left(h_k + \frac{u_k^2}{2}\right) + \vec{n}_k\cdot\vec{q}_k - \vec{n}_k\cdot\vec{v}_k\cdot\overline{\overline{\tau}}_k\right] >_i - < (\vec{n}_{kw}\cdot\vec{q}_k) >_w$$

$$+\alpha_k < (\rho_k\vec{v}_k\cdot\vec{F}_k + Q_k) > \quad (13a)$$

The left-hand side may be written in enthalpy form.

$$\frac{\partial}{\partial t}\alpha_k < \rho_k\left(h_k + \frac{u_k^2}{2}\right) > + \frac{\partial}{\partial z}\alpha_k < \rho_k u_k\left(h_k + \frac{u_k^2}{2}\right) > - \alpha_k\frac{\alpha < p_k >}{\partial t}$$

$$+C_k\rho_k\Delta u^n\frac{\partial}{\partial t}\alpha_k + \frac{\partial}{\partial z}\alpha_k < q_{z,k} > - \frac{\partial}{\partial z}\alpha_k < \vec{n}_z\cdot(\overline{\overline{\tau}}_k\cdot\vec{v}_k) >$$

$$= - < \left[\dot{m}_k\left(h_k + \frac{u_k^2}{2}\right) + \vec{n}_k\cdot\vec{q}_k - \vec{n}_k\cdot\vec{v}_k\cdot\overline{\overline{\tau}}\right] >_i - < (\vec{n}_{kw}\cdot\vec{q}_k) >$$

$$+\alpha_k < (\rho_k\vec{v}_k\cdot\vec{F}_k + Q_k) > \quad (14)$$

VITA

Ali Hedayatpour was born in Abadan, Iran on September 23, 1952. He attended elementary schools in that city and was graduated from Marvi High School in Tehran in 1972. The following September he entered Tabriz University, and in 1976 he received a Bachelor of Science degree in Mechanical Engineering. After graduating, he joined the Iranian National Oil Company where he was employed as a design engineer until he came to the United States to pursue a graduate degree. He entered graduate school at The University of Tennessee in Chattanooga, and received a Master of Science degree in Mechanical Engineering in 1982.

In January 1984, he accepted a graduate research assistantship at The University of Tennessee Space Institute, Tullahoma where he worked on several research projects while pursuing a Doctor of Philosophy degree in Mechanical Engineering. This degree was awarded in August 1990.

The author is a member of the American Society of Mechanical Engineers, The American Institute of Aeronautics and Astronautics, and Sigma Xi. He and his wife, Marsha, presently reside in Tullahoma, Tennessee. Mr. Hedayatpour is currently employed by McDonnell Douglas Space Systems Company in Huntsville, Alabama.